A COMPUTATIONAL SIMULATION OF HEAT TRANSFER TO TURBULENT FLOW SEPARATION USING NANO FLUID IN A CONCENTRIC PIPE

OON CHEEN SEAN

DISSERTATION SUBMITTED IN FULFILMENT OF THE REQUIREMENTS FOR THE DEGREE OF MASTER OF ENGINEERING SCIENCE

FACULTY OF ENGINEERING
UNIVERSITY OF MALAYA
KUALA LUMPUR

2013

UNIVERSITI MALAYA

ORIGINAL LITERARY WORK DECLARATION

Name of Candidate: OON CHEEN SEAN

Registration/Matric No: KGA 100039

Name of Degree: MASTER OF ENGINEERING SCIENCE

Title: A COMPUTATIONAL SIMULATION OF HEAT TRANSFER TO TURBULENT FLOW SEPARATION USING NANO FLUID IN A CONCENTRIC PIPE

Field of Study: HEAT TRANSFER

I do solemnly and sincerely declare that:
(1) I am the sole author/writer of this Work;
(2) This Work is original;
(3) Any use of any work in which copyright exists was done by way of fair dealing and for permitted purposes and any excerpt or extract from, or reference to or reproduction of any copyright work has been disclosed expressly and sufficiently and the title of the work and its authorship have been acknowledged in this Work;
(4) I do not have any actual knowledge nor do I ought reasonably to know that the making of this work constitutes an infringement of any copyright work;
(5) I hereby assign all and every rights in the copyright to this Work to the University of Malaya ("UM"), who henceforth shall be owner of the copyright in this Work and that any reproduction or use in any form or by any means whatsoever is prohibited without the written consent of UM having been first had and obtained;
(6) I am fully aware that if in the course of making this Work I have infringed any copyright whether intentionally or otherwise, I may be subject to legal action or any other action as may be determined by UM.

Candidate's Signature: Date:

Subscribed and solemnly declared before,

Witness's Signature: Date:

Name:

Designation:

ABSTRACT

Backward facing step play a vital role in the design of many equipment and engineering applications where heat transfer is concerned. The investigation is mainly concentrated on turbulent fluid flows in an annular passage utilizing computational fluid dynamic package (FLUENT). Present research work is complied into two parts. The first section is planned to gather results of investigation on various numerical model parameters and compare with the experimental results obtained previously. The results were then verified by using various techniques such as mesh independent study, surface roughness study and the effect of various viscous models. The second part of the research was focused on the numerical simulation of preliminary experimental setup. The numerical simulation on heat transfer over a considerable number of parameters were carried out; including wall heat flux, fluid flow velocity, separation step height, different concentrations and various nanofluids. The increase of flow reduces the surface temperature along the pipe to a minimum point then gradually increases up to the maximum and hold for the rest of the pipe. The minimum surface temperature is obtained at flow reattachment point. The position of the minimum temperature point is dependent on the flow velocity over sudden expansion. Generally, the local Nusselt number (Nu) increases with the increase of the Reynolds number. Heat transfer coefficient of nanofluids increases with increase in the volume concentration of nanofluids and Reynolds number s. Higher temperature operation of the nanofluids y ields higher percentage increase in heat transfer rate. Finally, with the advent of computational fluid dynamic software, a fair and agreeable results were obtained for the present research.

ABSTRAK

Aliran ke belakang menghadap tetanga memainkan peranan yang penting dalam reka bentuk peralatan dan aplikasi kejuruteraan yang berkaitan dengan pemindahan haba. Penyelidikan ini tertumpu pada cecair aliran gelora di dalam saluran anulus menggunakan pakej dinamik bendalir pengiraan (FLUENT). Kerja-kerja penyelidikan dibahagikan kepada dua bahagian. Seksyen pertama dirancang untuk mengumpul hasil siasatan ke atas pelbagai parameter model berangka dan bandingkan dengan keputusan eksperimen yang diperolehi sebelum ini. Keputusan kemudian disahkan dengan menggunakan pelbagai teknik seperti jejaring kajian bebas, kajian kekasaran permukaan dan pelbagai model kelikatan. Kajian di bahagian kedua tertumpu kepada simulasi berangka untuk persediaan eksperimen. Simulasi berangka ke atas ciri-ciri pemindahan haba ke atas beberapa parameter telah dijalankan, termasuk fluks haba dinding, aliran halaju bendalir, ketinggian tannga, pelbagai kepekatan dan pelbagai bendalir nano. Peningkatan aliran mengurangkan suhu permukaan di sepanjang paip ke titik minimum kemudian meningkat semula. Suhu permukaan minimum diperolehi pada titik kesambungan aliran. Kedudukan titik suhu minimum adalah bergantung kepada halaju aliran melalui tetanga. Secara amnya, nombor Nusselt tempatan (Nu) meningkat dengan peningkatan nombor Reynolds. Pekali pemindahan haba bendalir nano meningkat dengan peningkatan dalam kepekatan nanofluids dan nombor Reynolds. Suhu operasi yang lebih tinggi bendalir nano menyebabkan peratusan peningkatan yang lebih tinggi dalam kadar pemindahan haba. Akhirnya, dengan munculnya perisian pengiraan dinamik bendalir, ia boleh memberikan keputusan yang adil dan munasabah dalam penyelidikan ini.

ACKNOWLEDGEMENT

I would like to deliver my deepest appreciation to my supervisor, Dr. Kazi Md. Salim Newaz for allowing me to complete my Master study under his guidance and supervision. It has been some grey period during the Master candidature but his enormous encouragement and supports passed me through the hard time. The positive thinking and yet realistic views of him brought confidence and energy for me to complete the research.

Great appreciation goes to the contribution of my co-supervisor Dr. Ahmad Badarudin Mohamad Badry for his commitment and cooperation during my Master study.

Thanks and appreciation to Deputy Vice Chancellor Prof. Dr. Mohd Hamdi Bin Abd Shukor and Deputy Dean Associate Prof. Ir. Dr. Abdul Aziz Bin Abdul Raman for the commitment and effort to take care of the welfare of the students.

Deepest thanks are extended to my good friends and colleagues, Mr. Tommy Chang Chee Pang, Mr. Ding lai Chet, Mr. Chan Hon Ki, Mr. Mohd Nashrul Bin Mohd Zubir, Mr. Hussein Togun and Mr. Emad Sadeghinezhad for the supports and helps when I was in need. Their willingness to help and offering valuable information are highly appreciated.

Last but not the least, my deep gratitude goes to my parents, family members, special mate of mine, friends and others for their cooperation, encouragement, constructive suggestion and full support in completion of this research from the beginning till the end.

TABLE OF CONTENTS

Title	**Page**
Title Page	i
Declaration	ii
Abstract	iii
Abstrak	iv
Acknowledgement	v
Table of Contents	vi
List of Figures	viii
List of Tables	xii
Nomenclature	xiii
Chapter 1 Introduction	1
1.1 Turbulent flow	1
1.2 Backward Facing Step	4
1.3 Application of Step Flow	6
1.4 Modeling of Step Flow	9
1.5 Step Flow with Different Fluids	11
1.6 Objective	13
Chapter 2 Literature review	14
Chapter 3 Methodology	37
3.1 Numerical simulation of air flow in an annular passage	37
3.1.1 Computational Fluid Dynamic (CFD)	42
3.1.2 Mesh Independent Study	47

3.1.3 Surface Roughness Study 47

3.2 Basefluid and Nanofluid Methodology 48

3.2.1 Thermophysical properties of nanofluids 49

Chapter 4 Results and Discussions 53

4.1 Numerical simulation of air flow in an annular passage 54

4.1.1 Mesh Independent Study 63

4.1.2 Surface Roughness 66

4.2 Numerical simulation of base fluid and nanofluids in an annular passage 67

4.2.1 Numerical simulation of base fluid and nanofluids for 0 step height 67

4.2.2 Numerical simulation of base fluid and nanofluids at 13.5 mm step height 72

Chapter 5 Conclusions 80

List of Publications and Awards 83

References 85

Appendices 90

List of Figure **Page**

Figure 1.1: Backward facing step in sudden expansion pipe. 7

Figure 1.2: Flow geometry. 8

Figure 2.1: Computational domain of the duct from Iwai *et al.* 16

Figure 2.2: Nusselt number contours on the bottom wall (*AR* = 16). 17

Figure 2.3: C_f contours on the bottom wall (*AR* = 16). 17

Figure 2.4: Velocity field with square blockage (ER = 2, *Re* = 105). 18

Figure 2.5: Variation of the surface temperature with axial distance for (q = 2098 W/m^2, *Re* = 44545). 19

Figure 2.6: Effect of *Re, Pr, k* and *b* on the local Nusselt number. 20

Figure 2.7: Computational domain in the plane with a non-uniform grid distribution. 22

Figure 2.8: Distribution of local Nusselt number in the axisymmetric abrupt expansion for *d/D* = 0.4. 22

Figure 2.9: 2–D Computational domain for *Re*=44000. 25

Figure 2.10: Streamwise velocity *Re*=5100, *x/h*=4. 26

Figure 2.11: Grip refinement: Streamwise velocity profiles for *tlen*=7% (a) x/h=1.33 (b) 2.66. 26

Figure 2.12: The effect of the Reynolds number on the reattachment length for *E*=0.001. 27

Figure 2.13: Variation of total averaged Nusselt number as function of Stuart numbers Re=380. 29

Figure 2.14: (a) Increase in nanofluid heat transfer coefficient along the tube axis for Re = 250 and q = 5000 W/m^2 for constant and variables properties, (b) heat transfer coefficient for constant properties and (c) heat transfer coefficient for temperature dependent properties. 33

Figure 2.15: Nusselt number distribution using different types of nanoparticles, *Re* = 400, *u* = 0.1. (a) Top wall and (b) Bottom wall. 35

Figure 3.1: Experiment setup conducted by Togun et al. 38

Figure 3.2: Schematic diagram of flow in the annular sudden expansion passage (Togun et al., 2011). 38

Figure 3.3: Geometry and dimensions of the model. 40

Figure 3.4: Geometry and boundary conditions are drawn by using GAMBIT. 40

Figure 3.5: Schematic diagram of the annular sudden expansion in annular pipe flow for basefluid and nanofluid. 48

Figure 3.6: Geometry of asymmetry annular test section are drawn by using GAMBIT. 49

Figure 4.1: Vector of air inside the pipe. 53

Figure 4.2: Temperature distribution along the pipe. 54

Figure 4.3: The variation of surface temperature with x/D. 54

Figure 4.4: The graph of Nusselt number versus x/D. 55

Figure 4.5. The graph of local Nusselt number/Nusselt number (Dittus-Boelter) versus x/D. 56

Figure 4.6 Variation of surface temperature versus distance (for heat flux=790 W/m^2, D/d=1.8). 57

Figure 4.7: Variation of surface temperature versus distance (for re=17050, D/d=1.8). 58

Figure 4.8: Variation of surface temperature versus distance (for Re=44545, D/d=1.8). 58

Figure 4.9: The graph of surface temperature versus distance with different step height (for *Re*=39992, *q*=2098 W/m^2). 59

Figure 4.10: The graph of local heat transfer coefficient versus distance with different step height for (*Re*=39992, *q*=2098 W/m^2). 60

Figure 4.11: The graph of Nusselt number versus distance with different step heights (for *Re*=39992, *q*=2098 W/m^2). 61

Figure 4.12: Surface temperature distribution (for *s*=18.5 mm, *q*=2098 W/m^2) *Re*=17050, 30720, 39992 and 44545 from top to bottom. 62

Figure 4.13: The graph of temperature versus distance with different viscous model (for *s*=18.5 mm, *Re*=44545 and *q*=2098 W/m^2). 63

Figure 4.14: Comparison of average temperature over various Reynolds numbers at s=18.5 mm and q=2098 W/m^2. 64

Figure 4.15: Comparison of average heat transfer coefficient over various Reynolds numbers at s=18.5 mm and q=2098 W/m^2. 65

Figure 4.16: Comparison of average Nusselt number over various Reynolds numbers at s=18.5 mm and q=2098 W/m^2. 65

Figure 4.17: Graphical representation of temperature versus distance for various surface roughnesses. 66

Figure 4.18: Graph of average temperature versus roughness height for different materials. 67

Figure 4.19: Temperature variation along the test section with wall heat flux of 49 050 W/m^2 (0 step height). 68

Figure 4.20: Graph of temperature versus distance for water at various Reynolds numbers (at heat flux=49050 and step height=0). 69

Figure 4.21: Graph of heat transfer coefficeint versus distance for water at various Reynolds numbers (at heat flux=49050 and step height=0). 69

Figure 4.22: Graph of Nusselt number versus distance for water at various Reynolds numbers (at heat flux=49050 and step height=0). 70

Figure 4.23: Graph of Temperature versus distance for water Al_2O_3 nanofluids with different concentrations (at heat flux of 49050W/m2 and step height=0). 71

Figure 4.24: Graph of heat transfer coefficient versus distance for water Al_2O_3 nanofluids with different concentration (heat flux of 49050W/m2, step height=0). 71

Figure 4.25: Graph of nusselt number versus distance for water Al_2O_3 nanofluids with different concentrations (at heat flux of 49050W/m2 and step height=0). 72

Figure 4.26: Temperature variation along the test section with wall heat flux of 49 050 W/m^2 (at 13.5 mm step height). 72

Figure 4.27: Graphical representation of temperature versus distance for water at various Reynolds numbers (at heat flux=49050). 74

Figure 4.28: Graphical representation of Heat Transfer Coefficient versus distance at different Reynolds numbers at heat flux of 49050 W/m^2. 74

Figure 4.29: Variation of Nusselt Number as a function of distance at different Reynolds numbers at heat flux of 49050 W/m^2. 75

Figure 4.30: Temperature variation as a function of versus distance for water Al_2O_3 nanofluids at different concentrations and at heat flux of 49050W/m^2. 76

Figure 4.31: Graphical representation of Heat Transfer Coefficient as a function of distance for water Al_2O_3 nanofluids at different concentrations and at heat flux of 49050W/m^2. 76

Figure 4.32: Nusselt Number variation with distance for water Al_2O_3 nanofluids at different concentrations and at heat flux of 49050W/m^2. 77

Figure 4.33: Average Nusselt number as a function of Reynolds number at different step heights. 77

Figure 4.34: Graphical presentation of temperature versus distance for different types of nanofluids at 1% nano particles concentration (at heat flux of 49050 W/m^2). 78

List of Tables **Page**

Table 2.1: Thermophysical properties of the nanofluids. 35

Table 3.1: Dimensions of experimental setup. 39

Table 3.2: Experimental parameters. 39

Table 3.3: Dimensions of the entrance section and test section. 40

Table 3.4: Computaional conditions. 44

Table 3.5: Number of mesh with different interval size. 47

Table 3.6: Roughness height of the commercially available test specimens (Kazi et al., 2010). 48

Table 3.7: Dimensions of the model. 49

Table 3.8: Dimensions of the entrance section and test section. 49

Table 3.9: Thermophysical properties of nano particles. 50

Table 3.10: Thermophysical properties of water-Al_2O_3 nanofluids at different concentration. 51

Table 3.11: Thermophysical properties of nanofluids with 1% volumetric concentration. 52

Nomenclature

ρ	Density of Air (kg/m^3)
h_x	Local heat transfer coefficient (W/m^2.K)
u	Velocity components in the x direction (m/s)
v	Velocity components in the y direction (m/s)
q_c	Convection heat flux (W/m^2)
T_{sx}	Local surface temperature (K)
Re_d	Reynolds number based on hydraulic diameter
T_{bx}	Local bulk air temperature (K)
ρ_f	Density of fluid (kg/m^3)
d	Diameter of the pipe (m)
U	Velocity of the fluid (m/s)
Kf	Thermal conductivity (W/m.K)
D_h	Hydraulic diameter of the annular pipe (m)
Nu_d	Nusselt numbers evaluated from Dittus Boelter correlation
μ_f	Dynamic viscosity of the fluid at film temperature (kg/m.s)
Pr	Prandtl number
ρ_{nf}	Density of nanofluid (kg/m^3)
ρ_{bf}	Density of basefluid (kg/m^3)
ρ_p	Density of nanoparticle (kg/m^3)
Cp_{nf}	Specific heat of nanofluid (kJ/kg.K)
Cp_{bf}	Specific heat of basefluid (kJ/kg.K)
Cp_p	Specific heat of nanoparticle (kJ/kg.K)
μ_{nf}	Dynamic viscosity of the nanofluid (kg/m.s)

μ_{bf} Dynamic viscosity of the basefluid (kg/m.s)

ϕ Concentration of nanofluid

k_{nf} Thermal conductivity of nanofluid (W/m.K)

k_{bf} Thermal conductivity of basefluid (W/m.K)

k_p Thermal conductivity of nanoparticle (W/m.K)

CHAPTER 1: Introduction

1.1 Turbulent Flow

Turbulent flow separation occurs in many flow situations in nature. Different pressure gradients generated are due to changes in the geometry of the flow path and alteration of boundaries introduce by the flow separation. The results of recirculation flows with separation causes high pressure losses, enhances turbulence and increases mass and heat transfer rate. All kinds of the separated fluid flows are extensively used in industrial applications even though there are still lack of knowledge on the information of the flow around the recirculation zone (Tihon et al.). Separation is a phenomenon which appears under a variety of flow conditions and encountered in many engineering problems. The performance of fluid machinery in industrial flows is greatly influenced by its occurrence. So, to control flow separation, many investigations by numerous authors have been conducted in fluids engineering. Flow separation on a boundary surface occurs when the flow stream lines (the closest stream line to the boundary surface) breaks or separates away from the boundary surface and then the flow reattached at a different point. If the boundary surface is a finite dimension, then flow separation is expected due to the flow diverges over the downstream edge and the fluid flows away from the surface such as air flow across an airfoil. The separation of fluid flow is represented by viscous flow. This has got scientific importance as well as practical. From the classical concept, viscosity induces flow separation, it is recognized as boundary layer separation (Armaly et al., 1983a).

Turbulence is a phenomenon that occurs frequently in nature. It has been the subject of study for over 100 years. In present days, the prediction and control of

turbulent flows have become increasingly important, especially for particle-laden turbulent flows, due to their frequent occurrence in technological applications involving industrial systems, energy conversion systems and geophysical applications. Describing and predicting the turbulent characteristics of particle-laden flows is therefore an important research topic in applied fluid mechanics.

Many works has been carried out concerning the flow development through heat exchangers mainly on the comparison of the effects of tube geometry. Comparative studies have been carried out between tubes having elliptic and circular cross section on the basis of pressure loss and heat transfer performance. In most cases better results for staggered banks of finned elliptic tubes submitted to a cross-flow free stream were reported by (Missirlis et al., 2005)

Heat transfer in separated flows is frequently encountered in various engineering applications. Some examples include combustors, heat exchangers, axial and centrifugal compressor blades, gas turbines blades, and microelectronic circuit boards. It is well known that heat transfer characteristics experience large variation within separated regions. Thus, it is very essential to understand the mechanisms of heat transfer in such regions in order to enhance heat transfer. An innovative technique for improving heat transfer by using ultra fine solid particles in the fluids has been used extensively during the last decade (Abu-Nada, 2008).

Turbulent flow over a backward-facing step is frequently employed for benchmarking the performance of turbulence models for separated and reattaching flows. If a turbulence model can reproduce this flow correctly, then the possibilities that

the model is equally successful with other types of turbulent flows would be high. Separated and reattaching flows are encountered in a host of practical engineering situations. The flow separation and subsequent reattachment processes generate extremely complex flow characteristics. Among others, the separated flow, which then reattaches in the downstream locations, gives rise to flow unsteadiness, pressure fluctuations, noise, etc. Also, flow separation tends to enhance mixing. It is, therefore, desirable to develop a new turbulence model for separated and reattaching flows, and an accurate prediction poses a significant and challenging task (Ahn et al., 1997).

Flow separation and reattachment are of great importance in such fields as aeronautical, mechanical, civil, and chemical engineering, and in the environment, because their frequent occurrence may affect fundamental flow characteristics and result in a drastic change in the performance of fluid machinery and heat transfer devices. Hence, any modem computational fluid dynamics code should be tested in a flow problem with separation and reattachment. In particular, the accuracy of numerical schemes and turbulence models should be thoroughly evaluated. Among a number of flows with separation and reattachment, the flow over a backward-facing step is one of those with the simplest geometries; however, when it is turbulent, the flow structure is very complex, and much remains to be explored (Kasagi and Matsunaga, 1995).

Flow fields with regions of recirculation that also have heat transfer and a particulate phase are interesting relevant to combustion processes that form the foundation of combustion unit design, as well as other chemically reacting processes. The flow structure for such problems have the fundamental features of flow separation and subsequent reattachment; heat transfer and associated thermal effects,

such as buoyancy; and inertial effects associated with the particulate drag (Barton, 1997).

1.2 Backward Facing Step

A widely known case is the backward facing step flow. Indeed it provides an excellent test flow for studying the basic physical phenomena of separation and reattachment. This geometry is of particular interest because separation is imposed at the step edge and one can focus attention on the study of reattachment process, while in many real engineering flows separation and reattachment are interacting and then occurring at variable distances. The backward facing step (BFS) flow has been extensively studied, but many aspects of the flow structure and the dynamics of this geometrically simple turbulent flow remain incompletely explained.

The principal flow features of turbulent BFS flow are described as follows: a turbulent boundary layer of thickness, which develops on a surface, encounters a backward facing step of height. The sudden change in surface geometry causes the boundary layer to separate at the sharp step edge. The resulting flow behaves downstream, essentially like a free shear layer, with high speed flow on the upper side and low speed flow on the lower side. Some distance downstream, the shear layer impinges on the surface and then forms a closed recirculation region containing turbulent, moving fluid. A small counter-rotating “corner eddy” developing below the mean recirculating flow may also exist in this region. The instantaneous location of reattachment occurs over a region located all around the time averaged reattachment point and it is found to vary slightly in time about its mean position. At the downstream

of reattachment, the boundary layer begins to redevelop undergoing a relaxation towards a standard turbulent boundary layer state.

Some of the earlier studies have been focused on understanding the parameters which affect the reattachment process in this flow from the point of consideration of suppression and control of the separation process. Other studies put a major emphasis on observation and analysis of such a flow field. The effect of the Reynolds number, as one of the important parameters, has been studied by (Terekhov and Pakhomov, 2009) and (Kurtbaş, 2008).

Up to now, no systematic and extensive study has been made about the influence of turbulence on the step flow with various kinds of fluids. In this regard, the precise aim of the present work is to get new information on the influence of the turbulent flow on the recirculation region and particularly on its spatial extension. The incoming flow considered in the present case is a developed turbulent flow. The intension of the present work is to show that considering a fully developed flow instead of a standard boundary layer, may considerably modify the flow patern in the wall region of the step. In a step flow, the outer free shear layer induces mass entrainment of fluid and the free boundary is characterized by the presence of large eddies. The phenomena observed in the present flow after a backward facing step is also encountered in many industrial processes involving fluid separation. The study of more academic configurations in a laboratory model is thus of particular interest for the understanding and the control of these phenomena.

Furthermore, the turbulent fluid flow in presence of step is a basic flow of fundamental interest for turbulence research (Launder and Rodi, 1983) and (Wygnanski

et al., 1992). The fully developed flow is similar to a classical turbulent boundary layer while the outer layer is like a free jet. Consequently, the turbulent fluid flow presents two major sources of turbulence production: one of them is located in the inner wall shear layer and characterized by small scale eddies, and the other flow characterized by strong entrainment of fluid by large eddies. The external turbulent large eddies produce real changes in the dynamics of the flow over a backward facing step. One of the important properties to observe is the reattachment length, because it indicates the rate of mixing in the separated shear layer which is very sensitive to the incoming flow parameters cited above.

The turbulent backward facing step flow is an excellent test case for the validation of turbulence models. The flow includes three typical zones of different types: a separated shear layer when the incoming jet reaches the step edge, a recirculating flow region extending down to the stagnation point followed by a relaxation region. These different regions are often used to test the validity and the degree of universality of one point statistical turbulence closures which have been tuned against simple academic homogeneous and non homogeneous flows.

1.3 Application of Step Flow

Step flow in the form of backward facing play a vital role in the design of many equipment and engineering applications where heat transfer is concerned. The noted heat transfer applications are combustion engines, heat exchangers, environmental control systems, cooling systems for electronic devices, chemical process instrument and cooling channels in turbine blades. Mixing of low and high thermal fluid happens in the reattachment flow region of the considered instrument which affects the heat

transfer characteristic. Due to this phenomena, convection over forward and backward step geometries have been investigated by researches (Abu-Mulaweh, 2003). Fig. 1.1 illustrates the backward facing step in a sudden expanded pipe.

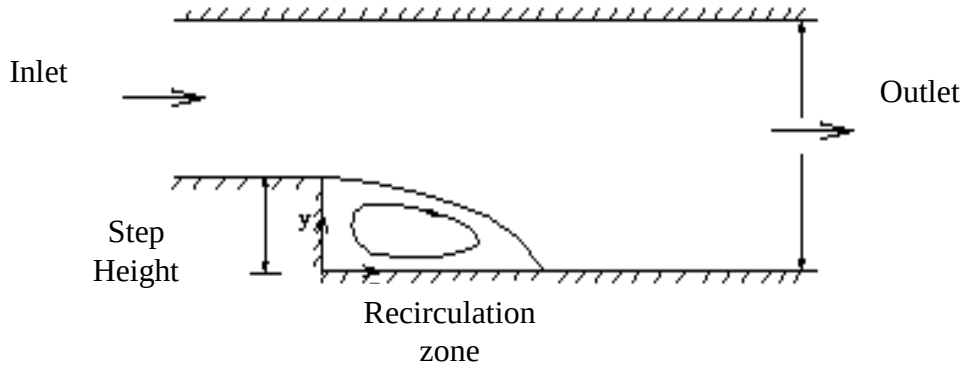

Figure 1.1: Backward facing step in sudden expansion pipe.

In industries, rotating cylindrical surface in annular passage is commonly used. Thus, the knowledge of this type of flow passage has got special attention. The simplest representation of this geometry is an annulus space between two concentric-shape surfaces (Murata and Iwamoto, 2011). Study of separation and reattachment flow was conducted first in late 1950's. With the development of advanced instrumentations and numerical codes, the investigations made are more facilitated to study complex three dimensional flows in the recirculation area. The works were further extended to vertical, horizontal, inclined etc. cases for different fluids, geometrical shapes and boundary conditions (Al-aswadi et al., 2010). Large percentage of the research on separation flow is performed on duct and circular pipe flow on the other hand little is published about heat transfer and flow phenomena in annular passage. Such knowledge is critical for optimizing the performance of physical heat exchanging systems in parallel and counter flow heat exchangers. Purpose of the present research is to compute the heat transfer rate to turbulent air flow in concentric pipe, and also to investigate the effect of flow

separation due to sudden enlargement in the flow passage. Heat transfer rate along the walls expected to differ for the long and short stall condition in any given flow situation as shown in Figure 1.2 (Khoeini et al., 2012).

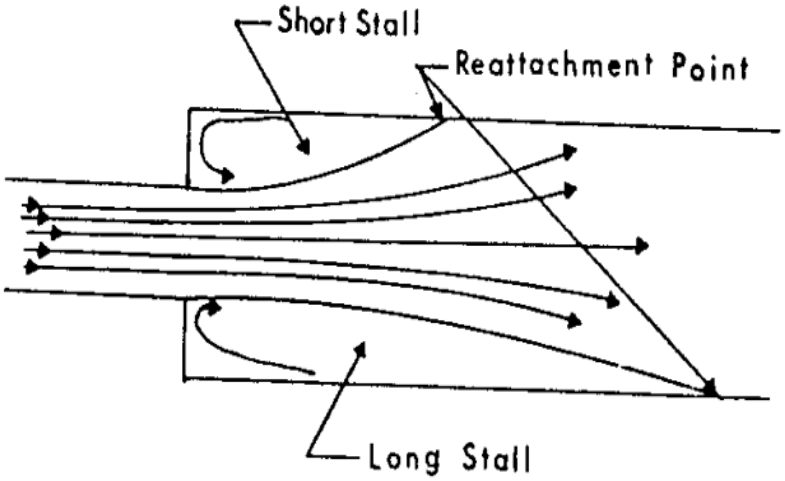

Figure 1.2: Flow geometry.

In general, this phenomena is encountered in some engineering application such as, in wide angle diffusers, airfoils with large angle of attack and with sudden increases in area in channels, heat exchangers, combustors, nuclear reactor cooling channels in power plant, gas turbine electronic circuiting and the throttling action in house hold water faucets.

The fluid flows over forward and backward steps can be found in many engineering systems are good examples. A great deal of mixing of high and low fluid energy occurs in the recirculation region has a considerable effect on the flow and heat transfer performance of these devices. For example, the maximum convective heat transfer coefficient and minimum wall shear stress take place in the neighborhood of reattaching flow region, while the minimum heat transfer occurs at the corner. Therefore, the

studies on separated flows both theoretically and experimentally have been conducted extensively during the past decade, and the fluid flow over backward step received most of the attention. Although this geometry is very simple, but the heat transfer and fluid flow over this type of step contain most of complexities. Consequently, it has been used in the benchmark investigations. In the benchmark problem, a steady-state two-dimensional mixed convection turbulent flow in a horizontal channel with a backward-facing step was solved. By now, plenty of papers were contributed in which the benchmark problem was solved numerically by different methods.

Fluid flows in channels with flow separation and reattachment of the boundary layers are encountered in many flow problems. Typical examples are the flows in heat exchangers and ducts. Among this type of flow problems, a backward-facing step can be regarded as having the simplest geometry while retaining rich flow physics manifested by flow separation and flow reattachment in the channel depending on the Reynolds number and the geometrical parameters such as the step height and the channel height.

1.4 Modeling of Step Flow

A review of research on laminar mixed convection flow over forward and backward-facing steps was done by (Abu-Mulaweh, 2003).In that work, a comprehensive review of such flows those have been reported in several studies in the open literature was presented. The purpose was to give a detailed summary of the effect of several parameters such as step height, Reynolds number, Prandtl number and the buoyancy force on the flow and thermal fields downstream of the step. Several

correlation equations were also summarized in that review. There are several works in which the turbulent flows with heat transfer over forward- and backward-facing steps were studied theoretically. The governing equations for the thermodynamically consistent rate-dependent turbulent model were briefly reviewed by (Chowdhury and Ahmadi, 1992). The requirements of the model were incorporated in a computer code (STARPIC-RATE) which is the advanced version of TEACH code. The model leaded to an anisotropic effective viscosity and was capable of predicting the expected turbulent stresses. The computational model was used to simulate the mean turbulent flow fields behind a plane backwardfacing step in a channel, and good results were obtained.

A new turbulent model for predicting flow and heat transfer in separating and reattaching flows was introduced by (Abe et al., 1994, Abe et al., 1995). The model was modified from the latest low-Reynolds number k–ε model. After investigating the characteristics of various time scales for the heat transfer model, they adopted a composite time scale which gives weight to a shorter scale among the velocity- and temperature-field time scales. The model predicted quite successfully the separating and reattaching turbulent flows with heat transfer at the downstream of a backward-facing step. In a recent study, (Yılmaz and Öztop, 2006) examined the turbulence forced convection heat transfer over double forward facing step in 2006. The Navier–Stokes and energy equations were solved numerically by CFD techniques. The solutions were obtained using the commercial FLUENT code which uses the finite volume method. Effects of step heights, step lengths and the Reynolds number on heat transfer and fluid flow were investigated. Results showed that the second step can be used as a control device for both heat transfer and fluid flow. There are many publications in literature that experimentally studied the effects of sudden contraction and expansion on

characteristics of flow and heat transfer in turbulent condition. Laser-Doppler velocimeter and cold wire anemometer were used to measure simultaneously the time-mean turbulent velocity and temperature distributions and their turbulent fluctuation intensities. Results revealed that the maximum local Nusselt number appears in the vicinity of the reattachment region and it is approximately twice for the case of backward-facing step and two and a half times for the case of forward-facing step, than that of the flat plate value at similar flow and thermal conditions.

1.5 Step Flow with Different Fluids

Conventional heat transfer fluids such as water or ethylene glycol is used in cooling or heating applications are characterized by poor thermal properties. In the past years, many different techniques were utilized to improve the heat transfer rate in order to reach a satisfactory level of thermal efficiency. The heat transfer rate can passively be enhanced by changing flow geometry, boundary conditions or by improving thermophysical properties for example, increasing fluid thermal conductivity.

One way to enhance fluid thermal conductivity is to add small solid particles in the fluid. The first effort to show the possibility of increasing thermal conductivity of a solid–liquid mixture by more volume fraction of solid particles was conducted back in 1870s (Bianco et al., 2011). Particles of micrometer or millimetre in dimensions were use in the experiments. Those particles were the cause of numerous problems, such as abrasion, clogging, high pressure drop and poor suspension stability. Therefore, a new class of fluid for improving thermal conductivity and avoiding adverse effects due to the presence of particles is required.

To meet these important requirements, a new kind of fluids, called nanofluids have been developed. Nanofluids are liquid suspensions of nano-sized particles. These particles have attracted significant attention since anomalously large enhancement in effective thermal conductivity at low particles concentration were reported by (Keblinski et al., 2002). Because of their unique features, nanofluids have attracted attention as a new generation of fluids in building heating, heat exchangers, technological plants, automotive cooling applications and many other diversified applications. By employing nanofluids it is possible to reduce the dimensions of heat transfer equipment, due to the increase in the heat transfer efficiency from the improved thermophysical properties of the working fluid.

Large portion of the research on separation flow is performed on duct and circular pipe flow on the other hand, little is published about heat transfer and turbulent flow phenomena in annular passage. Such knowledge is critical for optimizing the performance of physical heat exchanging systems in parallel and counter flow heat exchangers. The objective of the present research is to compute the heat transfer rate to turbulent air flow in concentric pipe, and also to investigate the effect of flow separation due to sudden enlargement in the flow passage. Heat transfer rate along the walls expected to differ for the long and short stall condition in any given flow situation (Oon et al., 2012).

1.6 Objective

-To study numerically the effect of backward facing step in an annular passage flow separation on heat transfer for the two dimensional axisymmetric turbulent flow.

-To determine the influence of variable parameters such as wall heat flux, fluid flow velocity, separation step height and various fluids on heat transfer characteristic.

-To investigate performance of heat exchangers based on parameters from the simulations.

CHAPTER 2: Literature Review

The separation of fluid flow is one of important investigation of viscous flow. This study is worthy, not only for scientific knowledge but also for practical applications. As per classical concept, flow separation is due to viscosity. Therefore, it is often expressed as “boundary layer separation". The event of flow separation and subsequent reattachment due to a sudden expansion or compression in the flow passages, such as backward-facing steps play an important role in the design of a wide variety of engineering applications where heating or cooling is required. These heat transfer applications appear in cooling systems for electronic equipment, combustion chambers, chemical processes and energy systems equipment, environmental control systems, high performance heat exchangers, and cooling passages in turbine blades. A great deal of mixing of high and low energy fluid occurs in the reattachment of flow region of these devices, thus affecting their heat transfer performance. Due to this, the problem of laminar and turbulent flow over backward-facing and forward-facing step geometries in forced, natural, and mixed convection have been investigated.

The turbulent flow in a sudden pipe expansion is an important internal flow phenomenon with separation which falls in the general class of complex shear flows. Such flow geometry is of common occurrence in industrial piping systems and aerospace application. A dominant feature of such a flow is the existence of a recirculation region characterized by low mean velocities but high turbulence intensities. This feature is also shared by other fully –separated internal flows such as those over single and double backward – facing steps and in confined –jet mixing (ejectors). In hydraulics also, recirculation regions appear in many situations, as for

example, in harbors, bays, in the flow around obstacles and sluice gates, and in cooling ponds (especially when equipped with baffles).

Many industrial problems involve separating and reattaching flows in channels, usually combined with recirculation bubbles. Heat exchanger flows, for instance, often bear such kind of behaviors. But despite the complexity of the flow topology,the entire behavior of most fluid flows is described by the so-called Navier–Stokes equations. Since in most cases, these equations do not provide the known analytical solutions, many numerical methods have been developed over the years to solve them. The space discretization can be based on, the finite element formulation or more usually, the finite volume method.

The separation of the boundary layer from the solid boundary surface does not occur in straight pipes or ducts .This is because there is a steady static pressure loss in the direction of flow. It does occur however tees, Y junction, bends and gradual enlargements and its effects on pressure losses. (Tihon et al.) studied backward facing step experimentally and numerically at Reynold number lower than 2000. Expansion ratio of 1.43, 2, 2.5 and 4 is used in the investigations. 2D model is used to perform numerical simulation using Fluent software. The experiment and numerical simulation result shows that increasing of the expansion ratio will make backward facing flow structure more complex.

(Ko, 1999) studied numerically the two-dimensional, incompressible turbulent flows in a near-wall Reynolds Stress Model (NRSM) for backward-facing step flows. Three numerical results are compared with Direct Numerical Simulation and experimental data. They found that the development of the boundary layer at the

downstream of the reattachment point satisfied the NRSM when Reynolds number is low. However, in high Reynolds number, weak separation bubble and slow developing boundary layer occurred in NRSM.

(Iwai et al., 2000) studied the effect of the duct in three-dimensional numerical simulation of backward-facing step flow at Reynolds number between 125 to 375 as shown in figure 2.1. Interest quantities were at the Nusselt number and the skin friction at the bottom wall. They found that an aspect ratio of as large as AR = 16 was required to obtain a 2D region near the centerline at Re = 250 as shown in figure 2.2. For the constant aspect ratio, AR = 16, the 2D region becomes wider with the decrease of Re number as shown in figure 2.3. They also found that maximum Nusselt number on the bottom wall occurs at two positions near the side walls, symmetrical with the duct centerline. Increase of AR and Re number will lead to maximum increase of the Nusselt number.

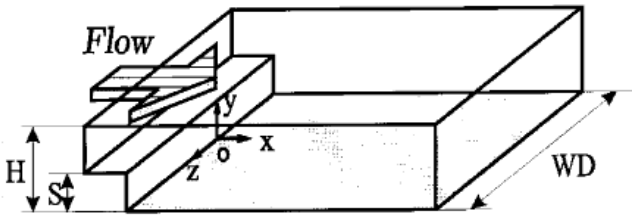

Figure 2.1: Computational domain of the duct from Iwai *et al.*

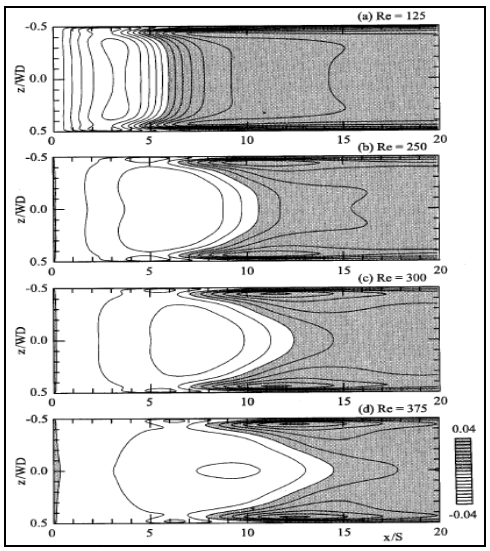

Figure 2.2: Nusselt number contours on the bottom wall (*AR* = 16)

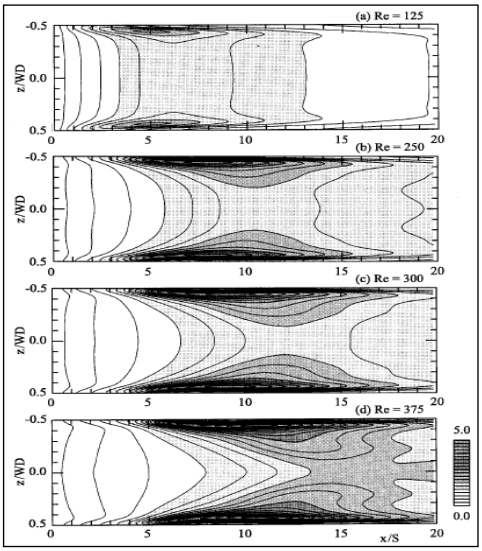

Figure 2.3: C_f contours on the bottom wall (*AR* = 16)

(Kim and Baik, 2004) developed a three-dimensional computational fluid dynamics model with renormalization group (RNG) *k*-ε turbulence scheme to study the effects of ambient wind direction on flow and dispersion around a group of buildings. Three flow patterns have been studied numerically such as a portal vortex generated behind the east wall of the upwind building is symmetric about the center of the street canyon, a portal vortex generated behind the east wall of the upwind building with its horizontal axis is not perpendicular to the ambient wind direction and the footprints of a portal vortex are located behind both the east and north walls of the upwind building. In their investigation, they stated the numerical models that are suitable for simulation of urban flow; large-eddy simulation (LES) and Reynolds-averaged Navier-Stokes equation (RANS). LES is less applied as it requires expensive computing times and RANS is considered as it widely applied in urban flow and diffusion search. The three-dimensional CFD model with RNG *k*-ε turbulence is compared with standard *k*-ε turbulent. They found that the changes in ambient wind direction can highly affect mean flow circulation and spatial distribution of passive pollutants.

(Barton, 1997) studied different types of laminar flows which consist of particle-laden flow, particle-laden flow with heat transfer, single-phase flow with heat transfer, particle-laden flow with heat transfer and related thermal properties for a backward-facing step geometry. Eulerian-Lagrangian approach is used in the modeling and the thermal properties measured are buoyancy and the thermophoresis effect. In the investigation, the flow particle tends to generate stronger upper and lower recirculation regions as the particles increase the inertia of the free-stream by overshooting the streamlines at the expansion. Also, as the particles are gaining momentum, the increases in inertia in free stream causes stronger recirculation. Finally, higher heat capacities of the particles successfully augmented the heat capacity of the liquid and further reduce the temperature in the flowing mixture.

(Chen et al., 2006a) investigate numerically 2 dimensional backward facing steps using low Reynolds number, incompressible and steady flowing fluid. The lattice Boltzmann method is utilized in this simulation. A square blockage is placed behind the sudden expansion to enhance the heat transfer and uniformity of the fluid flow. It was found that the numerical simulation of temperature field and velocity do agree with the experimental and numerical results. Figure 2.4 shows the velocity field with square blockage.

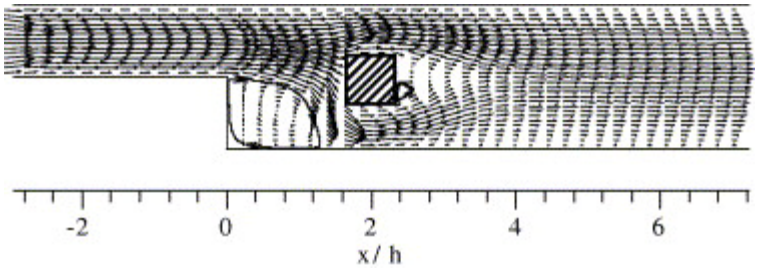

Figure 2.4: Velocity field with square blockage (ER = 2, *Re* = 105).

(Koutmos and Mavridis, 1997) reported a computational study on unsteady separated flow for different geometries. Time dependent Nevier Stroke equation was used in the study by using 2 dimensional model. The simulation is performed by using standard K-epsilon model and Large eddy simulation (LES). The numerical investigation on backward facing step is executed under low and high Reynolds number. It was found that the time dependent formulation is better than the steady state standard k-epsilon model.

(Togun et al., 2011) studied experimentally the effect of step height on heat transfer to outward expanded air flow stream in a concentric annular passage. The experiment was done with *Re* number range from 17050 to 44545, heat flux from 719 W/m^2 to 2098 W/m^2 and step heights, s = 0, 6mm, 14.5mm, and 18.5mm. They found that the increase of flow and step height reduces the surface temperature until the lowest temperature is achieved where reattachment point is located then it increases (figure 2.5). The local heat transfer coefficient (h_x) increases with *Re* number for all cases with or without step height.

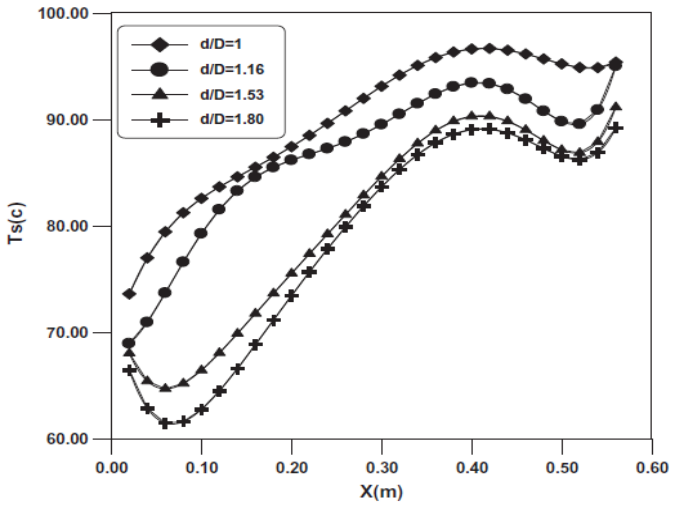

Figure 2.5: Variation of the surface temperature with axial distance for (q = 2098 W/m^2, *Re* = 44545).

(Kolaczkowski et al., 2007) in thier study, offers how to select either a two-dimensional (2–D), or a three-dimensional model (3–D). They found that the model with symmetry could be assumed in the tangential direction (axisymmetric option in FLUENT) and the model with parallel plates, where the gap between the plates is very much smaller than the width of the plates, could use 2–D model. A model of gas flow in circular tube, and in a square channel require 3–D model. 3–D requires more computational resource and it is more complex than 2–D.

(Rajesh Kanna and Manab Kumar, 2006) studied the conjugate heat transfer characteristic in backward-facing step flow. They studied the effect of Reynolds number *Re*, Prandtl number *Pr*, thermal conductivity ratio, *k* and thickness of the slab *b* on the local Nusselt number by using Alternating Direction Implicit (ADI) discretization method with centered space. High thermal gradients are observed near the reattachment location in the solid region shown in figure 2.6. The peak Nu occurs at the downstream to the reattachment location and at the same location considered for the k values.

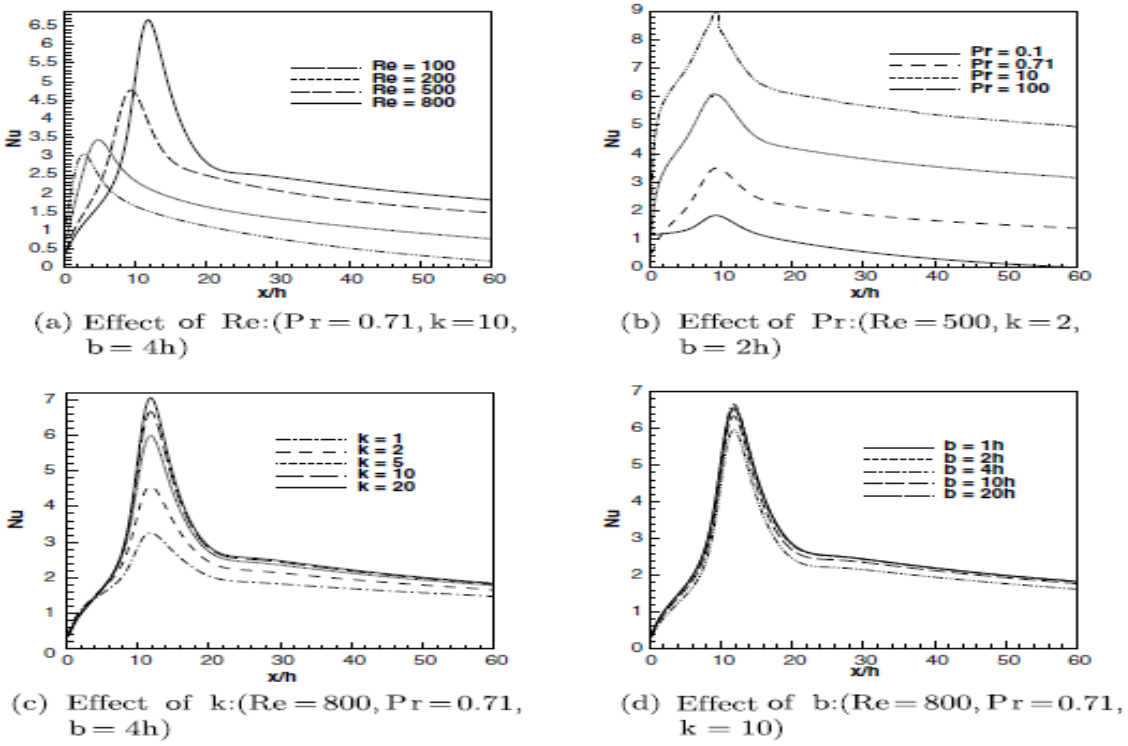

(a) Effect of Re:(Pr = 0.71, k = 10, b = 4h)

(b) Effect of Pr:(Re = 500, k = 2, b = 2h)

(c) Effect of k:(Re = 800, Pr = 0.71, b = 4h)

(d) Effect of b:(Re = 800, Pr = 0.71, k = 10)

Figure 2.6: Effect of *Re, Pr, k* and *b* on the local Nusselt number.

(Wu et al., 2002) experimentally investigated the mixed convection heat transfer through vertical annular passage by using water instead of air (Kim et al., 2002) as flowing fluid. Inner surface was heated uniformly to determine the condition of turbulence, buoyancy-influence and heat transfer to upward and downward flow. They found that by increasing buoyancy influence, heat transfer and turbulence production intensity enhances. They also found that the effect of buoyancy in annular tube is weaker than that in the circular tube. When heating is applied, laminar flow is changed to turbulent flow due to the presence of strong buoyancy influence which causes effective heat transfer enhancement.

(Rouizi et al., 2009) studied numerically the effect of reducing size of the model on 2–D steady incompressible laminar flows. The objective is to build low-order model that will fit the original ones. Case of backward-facing step is considered as its geometry could be simply meshed. Identification technique was derived from the Modal Identification Method. It can be concluded that a reduced order of model can satisfy the tests based on computation with other Reynolds number.

(Lee et al., 2011) conducted experiment and numerically studied the heat transfer and fluid flow properties in circular tube at a uniform wall temperature. Areas of interest are separated, recirculated and reattached regions produced by an axisymmetric abrupt expansion and contraction. Diameter ratio of d/D = 0.4 and Reynolds numbers range from 4,300 – 44,500 are applied. In experimental investigation, balance-type isothermal heat flux gage was used to measure local heat transfer coefficients. In numerical investigation, a model of two-equation turbulence was used. The model shown in figure 2.7 is designed by using the Reynolds-averaged Navier-Stokes equations, and energy equation for steady, incompressible,

axissymmetric and turbulent flow. SIMPLE algorithm was used and second-order upwind technique was applied to the convective fluxes in the momentum. They found that a minimum Nusselt number occurs at about 1 step height from the abrupt expansion step shown in figure 2.8, and the value is up to 1.4 times as high as the fully developed value. They also found that the reattachment point has strong relationship with the downstream Reynolds number, which later agreed with the location of maximum Nusselt number.

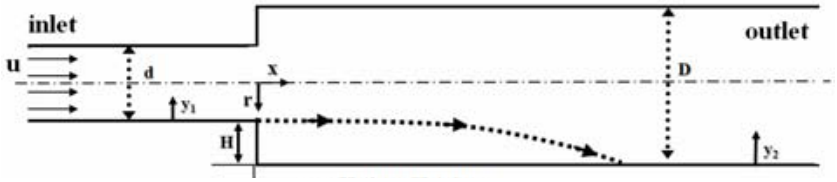

Figure 2.7: Computational domain in the plane with a non-uniform grid distribution.

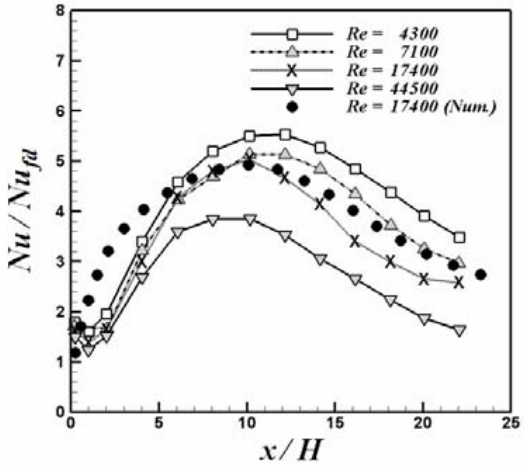

Figure 2.8: Distribution of local Nusselt number in the axisymmetric abrupt expansion for $d/D = 0.4$.

(Goldstein et al., 1970) studied experimentally the laminar air-flow in a downstream-facing step. The observer were interested in visual observations of smoke filaments in the viscous layer qualitative velocity fluctuation measurements and mean velocity profiles. Step height varies from 0.36 to 1.02 cm, free steam velocity varies as 0.61 – 2.44 m/s and 0.16 – 0.51 cm in boundary layer displacement thickness at the step. They found that the laminar reattachment length depends on Reynolds number and

boundary layer. The shape of the velocity profile at reattachment is found to be similar to the shape of a laminar boundary layer profile at separation and the boundary layer profiles downstream of reattachment are similar to those in a laminar boundary layer developing toward separation except that they are traversed in the reverse sense.

(Zhang, 2003) investigated turbulent flows in constricted conduits with low Reynolds number. A model of three-dimensional complex conduits was designed, with variation of renormalization (RNG) k-epsilon and k-omega, to allow incompressible laminar-to-turbulent fluid flow through it and comparison has been made for different RNG cases. They found that, both k-epsilon and k-omega model increases the flow instabilities after tubular constrictions, thus fail to the behavior of laminar flow at low Reynolds numbers. The low-Reynolds-number (LRN) k-epsilon model is unable to simulate the transition to turbulent flow and it requires high computational resources due to the slower convergence. LRN k-epsilon model is adopted well in complex 3–D tubular flows and able to reproduce the laminar, transition and fully turbulent flows and even could predict the maximum turbulence fluctuations quite well. It can be concluded that the LRN k-omega model is suitable for simulation of laminar-transitional-turbulent flows in the constricted tube.

(Furuichi et al., 2004) investigated experimentally in a large-scale structure of backward-facing step flow by using an advanced multi-point LDV. The advanced multi-point LDV has a 1–bit FFT where it is specialized in the time resolution and measurement in the near wall area. LDV system was used to measure the spatio-temporal velocity fields around the separated shear layer and reattachment region of two-dimensional backward facing step. The channel of water, 2300mm length and expansion ratio, ER=1.5 was used, with Reynolds number fixed as 5000 and turbulent

intensity of 0.6%. They found that the moving path of the vortex shedding from separated shear layer to the reattachment region shows two patterns, one is moving to near the wall region and the other is moving in the middle of the step height at the reattachment region. They also found that the turbulence due to reattachment phenomenon moves from reattachment region to separated shear layer by recirculation flow. They proposed a self-excitation motion to be a model of large-scale fluctuation.

(Uruba et al., 2007) investigated experimentally on a backward facing step in a flow through a narrow channel by means of suction or blowing. The flow is set to Reynolds number 50000 and the intensity of the suction/blowing coefficient was maintained at -0.035 to 0.035. Preliminary results show that both suction and blowing can cut down the length of the separation zone to around one third of its result. The 3D vortex structures close to the step are easily affected by suction compared to blowing.

(Chun and Sung, 1996) studied experimentally the effect of local forcing on flow structures over a backward-facing step, with a sinusoidal velocity fluctuation which was applied through a thin-slit near separation line. The experiment was carried out with Reynolds number varied from 13,000 to 33,000, forcing amplitude, A_o from 0 to 0.07 and forcing frequency, St_H from 0 to 5.0. They found that the forcing frequency was higher than the critical value and the reattachment length was larger than that of the unforced flow. They also found that the most effective forcing frequency to minimize the reduction of the reattachment length is close to the vortex shedding frequency of the unforced flow.

(Armaly et al., 1983b) investigate the backward facing step experimentally and numerically in a 2 dimensional channel. The range of Reynold number used in the

investigation starting from 70 to 8000. The aspect ratio (1:36) was selected to ensure the fully developed flow. It was shown experimentally that the downstream of the step remain 2 dimensional for low and high Reynolds numbers only. The performed investigation also had included numerical prediction for comparisons. It was reported that as long as the flow maintained its 2 dimensional status in the experiments, both numerical and experiment results shown good and fair agreement.

(Tota, 2009) studied a turbulent flow over a backward-facing step simulated by FLOW-3D. A model of Renormalization-group (RNG) *k*-ε was used with two Reynolds numbers involved, Re_h=5100 and Re_h=44000. The numerical results were compared *with* the experimental results and showed good agreement. The study observed the dependency of the turbulent mixing length parameter, *tlen* in the RNG model. The model was designed in two dimensional as shown in figure 2.9 where the third-order upstream advection scheme and GMRES iterative solver were used to solve momentum and Poisson's equation for pressure respectively. They found that with the increase of the value of *tlen* the velocity profiles move close to the experimental results as shown in figure 2.10. They also found the reattachment length for *tlen*=7% is the nearest to the experimental result whereas *tlen*=3.5% indicates incorrect result. The streamwise velocity profiles showed better result after grid refinement applied as shown in figure 2. 11. It can be said that with increase of the value of *tlen* the turbulent dissipation decreases. In brief, it was found that there is a value of *tlen* beyond which mean flow parameters are not affected.

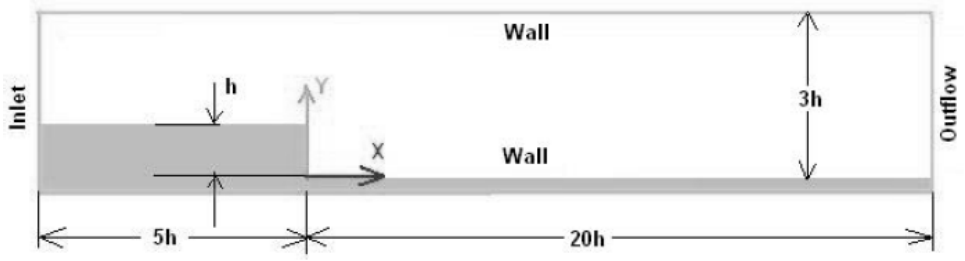

Figure 2.9: 2–D Computational domain for *Re*=44000.

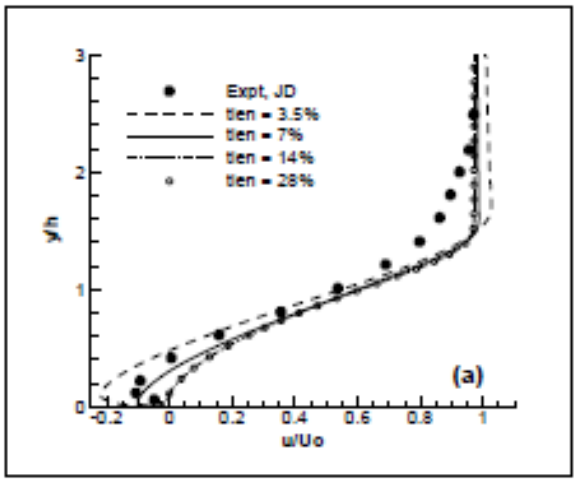

Figure 2.10: Streamwise velocity *Re*=5100, *x/h*=4.

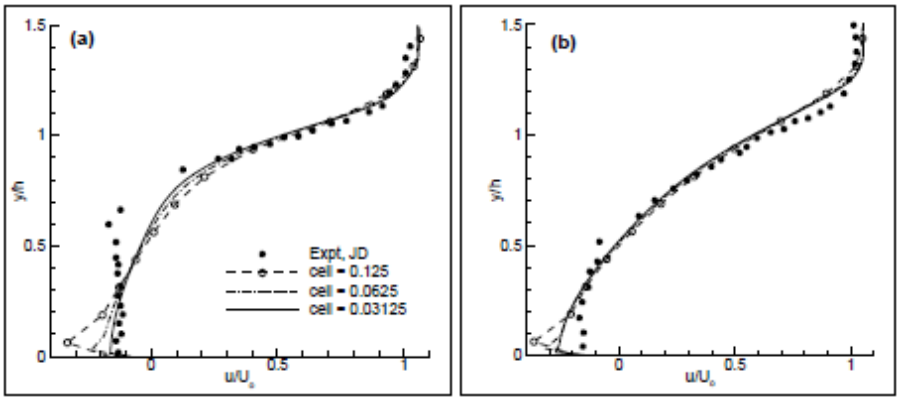

Figure 2.11: Grip refinement: Streamwise velocity profiles for *tlen*=7% (a) x/h=1.33 (b) 2.66.

(Yamamoto et al., 1979) studied the heat transfer characteristics in external flows over rectangular cavities where the bottom walls were heated at a uniform heat flux while the other two cavity walls were insulated. They observed that the effects of the reattachment of separated flow and vortex flow in the cavity on heat transfer were unexpectedly large. It also found that heat transfer did no always decrease monotonically with an increase of aspect (depth-width) ratio, in the flow range of laminar or turbulent.

(Hsu and Chou, 1997) studied numerically hydrodynamic properties of viscoelastic fluid on a backward-facing step. The study was performed with two-dimensional, incompressible laminar flow of a second-grade viscoelastic fluid. They also studied the "overshoot" phenomena, where the development of the main recirculation zone experiences enlargement first and later shrinkage. The combination of the line-Gauss-Seidel (LGS) method and alternating direction implicit (ADI) was applied. They found that, smaller elastic number causing larger main recirculation zone and longer reattachment length under same Reynolds number. They revealed that the "overshoot" phenomena is absence in the flow for Newtonian fluids. The secondary recirculation zone appears at a steady state at *Re*=75 and elastic number, *E*=0.001, and disappears before reaching a steady state for smaller Reynolds and elastic number flow as shown in figure 2.12.

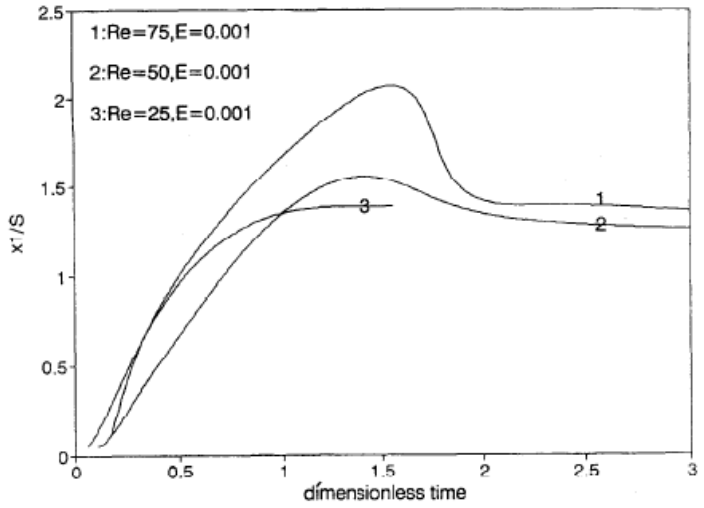

Figure 2.12: The effect of the Reynolds number on the reattachment length for *E*=0.001.

(Nait Bouda et al., 2008) studied numerically and experimentally a turbulent wall jet flow over a backward-facing step. Laser Doppler anemometry was applied to provide better understanding of turbulent flow. As for numerical investigation, two-

dimensional Reynolds Averaged Navier-Stokes (RANS) equation was implemented. They found that the comparison between experiment and numerical results showed a good agreement for the mean and turbulent flow fields. However, in the external region where the turbulent intensity is highly counted, there appears some disagreement due to the effect of large eddies and slow external motion. The numerical results revealed two bubbles existence in the recirculation zone. The flow relaxation is found to form more quickly in the external region rather than internal region.

(Abbassi and Ben Nassrallah, 2007) studied numerically the laminar flow of magnethydrodynamic (MHD) in backward-facing step. The simulations are performed for Reynolds number less than *Re*=380, Stuart number, *N*, the ratio of electromagnetic force to inertia force, from 0 to 0.2 and Prandtl number, *Pr* from 0.02 to 7. They found that Nusselt number, $\overline{Nu}$ increases with the increase of Stuart number, *N* as shown in figure 2.13. For low Prandtl numbers, heat transfer is not practically dependant by magnetic field, but depends essentially by diffusion mode. In downstream region, out of the recirculation zone, the basic flow is damped by magnetic effects, while acceleration of the flow occurs in near walls.

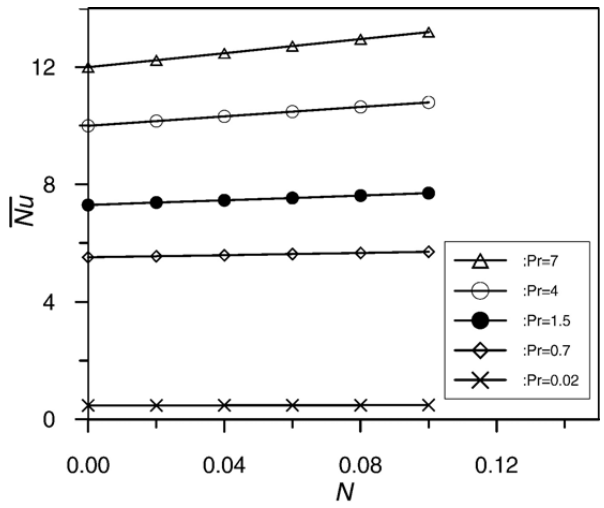

Figure 2.13: Variation of total averaged Nusselt number as function of Stuart numbers Re=380.

(Mohammed et al., 2011) studied the microchannel heat sink (MCHS) made out of different geometries; one of them is with step. 3 dimensional numerical simulation is used to solve the conjugate heat transfer governing equations by utilizing Finite Volume Method. Finite-volume method (FVM) was used to convert the governing equations to algebraic equations accomplished by using hybrid differencing scheme. The SIMPLE algorithm was used to enforce mass conservation and to obtain pressure field. Water is used as working fluid in the simulation and the performance is evaluated based on pressure drop, wall shear stress, friction factor, heat transfer coefficient and temperature profile. The step MCHS is the best channel for the hydraulic performance with moderate degradation of heat transfer compared to conventional straight MCHS.

(Yang et al., 2005) has investigated numerically the homogenous shear flow and backward-facing step flow with a few linear and non-linear turbulence models. Two linear models were used in the investigation, such as the standard k–ε model and non-equilibrium model whereas the non-linear models involves are three quadratic models from Speziale, Shih, Zhu and Lumley and Huang and also the cubic model of Craft, Launder and Suga. They found that, under fully developed turbulent flow over backward-facing step, the non-linear models offers better agreement than linear models. This is mainly due to the contributions of those non-linear terms representing the anisotropy of the normal Reynolds stresses.

(Kumar and Dhiman, 2012) numerically studied backward-facing step of laminar forced convection flow on a circular cylinder for the Reynolds number range 1-200 and Prandtl number of 0.71. The simulation is conducted using FLUENT and investigation on the flow and thermal fields are being focused on no temperature

dependency. The geometry has been done by GAMBIT consisting of both uniform and non-uniform grid distribution. The QUICK scheme has been used for momentum and thermal energy equations and SIMPLE scheme is used for pressure and velocity equations. It can be found that the insertion of a circular cylinder at a correct position is really helpful in controlling the velocity field of the backward-facing flow.

(Bsebsu and Bede, 2002) studied theoretically the heat transfer characteristics of down flow in the single-phase forced-convection with narrow vertical annuli sub-channels (WWR-M2 channel) using THMOD2 code. The main objective of this study is to investigate in the turbulent flow region, the applicability of existing heat transfer equations in the narrow vertical annuli channel, which is modeling and simulating sub-channel of 3 mm spacing (gap) and 600 mm in active length in the fuel elements for thermal hydraulic analysis tasks of the WWR-M2 research reactor or any other type. As a result, it was revealed that by use of equivalent hydraulic diameter, existing correlations are applicable to a WWR-M2 channel as narrow as 3 mm in gap for turbulent flow though the precision and Reynolds number are different among the heat transfer correlations. A new heat transfer equation for sub-channels of WWR-M2 channel heated at one side or both sides has been proposed.

(Ota and Kon, 1979) studied the heat transfer measurements in the separated, reattached and redeveloped regions of the two dimensional airflow on a flat plate with blunt leading edge. The test plate (20 mm thick, 100 mm wide and 400 mm long) was made from a stainless steel sheet (0.05 mm thick and 100 mm wide), Bakelite and plywood. Heating of the plate was done by mean of electric current to both sides of the plate causing an axisymmetric of flow and temperature fields involved. Heat flux was

controlled with sliders and the temperatures on the heating surface were measured with 0.07 mm copper – constant thermocouple soldered on the back of the stainless steel sheet. The experiments were carried out under the condition of constant heat flux. The flow reattachment occurs at about four plate thickness downstream from the leading edge and the heat transfer coefficient becomes maximum at that point. This behavior is dependent on the Reynolds number which ranged from 2720 to 17900 in this investigation. It was found that the heat transfer coefficient increases sharply near the leading edge.

(Aung et al., 1985) presented theoretical results concerning hydrodynamics and heat transfer to laminar flow passed through a backward step. Computations were carried out using the stream function vortices forms of the elliptic partial differential equations to calculate temperature profiles and local Stanton numbers .The available results indicate that the shear layer and reattachment length, when normalized by the step height increases with Reynolds number in the range of 25 <Re < 850.

(Q.Li, 2002) investigated experimentally the convective heat transfer and flow characteristics in a tube with a constant heat flux at the wall. From data collected on nanofluids composed of water and Cu, TiO_2 and Al_2O_3 particles, they proposed empirical correlations for the Nusselt number in both laminar and turbulent flows.

(D.Wen, 2004) investigated the heat transfer performance of water - Al_2O_3 mixture under laminar flow regime in a copper tube with 4.5 mm inner diameter. They found that the convective heat transfer coefficient increases with increasing Reynolds number and particles concentration. Furthermore, the improvement of the heat transfer coefficient was large in the entrance region of the horizontal heated tube.

(Y.Yang, 2005) measured the convective heat transfer coefficient of nanofluids composed of transmission fluids and graphitic-based nanoparticles. Results from the above experimental works have shown that the presence of nanoparticles produces a clear increase of heat transfer. The nanofluids give a higher heat transfer coefficient than the base fluid irrespective of Reynolds number, and such enhancement becomes more significant with an increase of particle concentration.

(R.BenMansour, 2009) studied numerically the conjugate heat transfer to laminar mixed convection flow of Al_2O_3-water nanofluid in a uniformly heated inclined tube. They found that the presence of nanoparticles intensifies the buoyancy-induced secondary flow, especially in the developing region. Their results also show an augmentation of the heat transfer coefficient and a decrease of the wall friction when using nanofluids.

(S.Z.Heris, 2006) investigated experimentally the convective heat transfer coefficient of Al_2O_3-water and CuO-water nanofluids for laminar flow in an annular tube under a constant wall temperature boundary condition. Their results have shown that the heat transfer coefficient increases with an increasing Peclet number and increasing particle volume concentrations while Al_2O_3-water nanofluid have shown larger heat transfer enhancement than CuO-water nanofluid.

(Bianco et al., 2009) investigated numerically the heat transfer of nanofluids in circular tubes. Forced convection flow of water and aluminium oxide nano particle mixture is subjected to uniform surface temperature and constant heat flux at surface of the tube. It was found that the convective heat transfer coefficients to nanofluids are higher than that of the base fluid. The result also shows the heat transfer enhancement with higher particle concentration of nanofluids but wall shear stress increases as well. It was reported in this case that increment in Reynolds number enhances the heat

transfer. Figure 2.14 shows nanofluid heat transfer coefficient along tube axis for constant and variables properties, heat transfer coefficient for constant properties and heat transfer coefficient for temperature dependent properties.

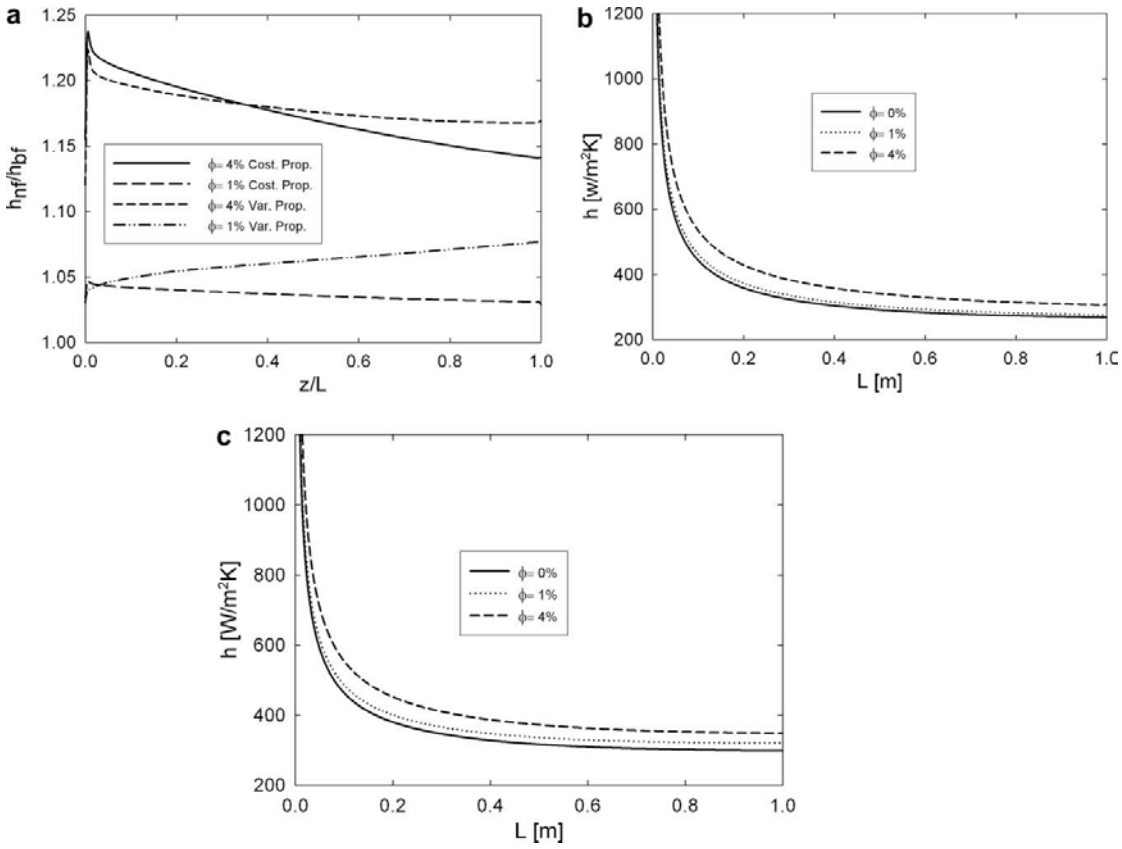

Figure 2.14: (a) Increase in nanofluid heat transfer coefficient along the tube axis for Re = 250 and q = 5000 W/m^2 for constant and variables properties, (b) heat transfer coefficient for constant properties and (c) heat transfer coefficient for temperature dependent properties.

The first work on nanofluids convective heat transfer inside a circular tube was presented by Pak and Cho (Pak and Cho, 1998). They have investigated on the turbulent convection of Al_2O_3 and TiO_2 nanofluids, and obtained an increase of Nusselt number with increase of particles concentration and finally proposed a new correlation of Nusselt number.

(Eiyad, 2008) studied numerically the heat transfer over a backward-facing step using nanofluids made of water and Cu, Ag, Al_2O_3, CuO, and TiO_2. The expansion ratio was 2.0 and Reynolds number ranges from 200 to 600. The range of nanoparticles

volume fraction was $0 \leq$ volume fraction ≤ 0.2 and the Prandtl number of the base fluid (water) was kept constant at 6.2. The flow was assumed Newtonian, two-dimensional, steady, incompressible, and the base fluid and the nanoparticles were assumed in thermal equilibrium and no slip occurred. The SIMPLE algorithm was used and second-order central difference is applied in the diffusion of momentum and energy equations. A second-order upwind differencing scheme is also applied in terms of convective flow. They found that Nusselt number inside the recirculation zone is highly dependent on the thermophysical properties of the nanoparticles, and independent of Reynolds number. Nevertheless, outside the recirculation zone, Nusselt number depends mainly on both Reynolds number and thermophysical properties of the nanofluids as shown in table 2.1. They also found that outside the recirculation zones, nanoparticles having higher thermal conductivity enhance Nusselt number value. As in the primary and secondary recirculation zones, nanoparticles having low thermal conductivity have better enhancement of heat transfer. The behavior of heat transfer is shown in figure 2.15.

Table 2.1: Thermophysical properties of the nanofluids.

Property	Fluid phase (Water)	Cu	Ag	CuO	Al_2O_3	TiO_2
c_p (J/kg K)	4179	385	235	535.6	765	686.2
ρ (kg/m^3)	997.1	8933	10500	6500	3970	4250
k (W/m K)	0.613	400	429	20	40	8.9538
$\alpha \times 10^7$ (m^2/s)	1.47	1163.1	1738.6	57.45	131.7	30.7

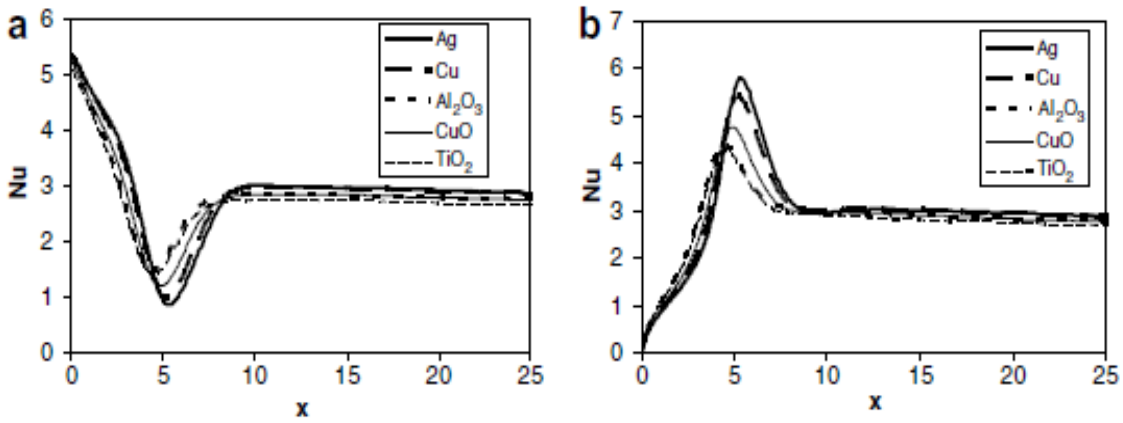

Figure 2.15: Nusselt number distribution using different types of nanoparticles, *Re* = 400, *u* = 0.1. (a) Top wall and (b) Bottom wall.

Nowadays there is a marked increase in research activities in this heat transfer area, as reviewed in (Murshed et al., 2008), (Kakaç and Pramuanjaroenkij, 2009) and (Das et al., 2006a). A good amount of nanofluids researches is dedicated to the investigation of thermophysical properties, while a relatively smaller amount of them is focused on nanofluids convection heat transfer (Murshed et al., 2008), (Das et al., 2006b) and (Pak and Cho, 1998).

To use nanofluids in heat transfer devices, their higher thermal conductivity is an encouraging feature, though not a definitive evidence of their applicability. To have a conclusive picture about the utilization of nanofluids in heat transfer applications, it is necessary to show their superior performances under convective conditions. In the last years, different researcher (Pak and Cho, 1998), (Xuan and Li, 2003), (Wen and Ding, 2004), (Zeinali Heris et al., 2007), (Zeinali Heris et al., 2006), (Williams et al., 2008), (Rea et al., 2009), (Hwang et al., 2009) and (Duangthongsuk and Wongwises, 2009) have focused on the experimental investigation, in both laminar (Wen and Ding, 2004), (Zeinali Heris et al., 2007), (Zeinali Heris et al., 2006), (Rea et al., 2009) and (Hwang et al., 2009) and turbulent regimes (Pak and Cho, 1998), (Xuan and Li,

2003), (Williams et al., 2008) and (Duangthongsuk and Wongwises, 2009), of nanofluids convection.

CHAPTER 3: Methodology

Present research work is complied into two parts. The first section is planned to gather results of investigation on various numerical model parameters and compare with the experimental results obtained previously. The results were then being verified by using different techniques like mesh independent study, surface roughness study and the effect of various viscous models. The second part of the research was focused on the numerical simulation of preliminary experimental setup by using the acquired knowledge. The numerical simulations were conducted by using computational fluid dynamic package (Fluent). The numerical simulation on heat transfer characteristics over a considerable number of parameters were carried out; including wall heat flux, fluid flow velocity, separation step height and various working fluids.

3.1 Numerical simulation of air flow in an annular passage

An experiment was conducted before the numerical simulations to verify the accuracy and reliability of numerical simulation results. Figure 3.1 shows the experimental setup conducted by (Togun et al., 2011). The experimental investigation was focused on the effect of separation flow on the local and average convection heat transfer. The experimental set-up consists of concentric tubes to form annular passage with a sudden reduction in passage cross-section created by the variations of outer tube diameter at the annular entrance section. The outer tube of test section was made of aluminium having 83 mm inside diameter and 600 mm heated length, which was subjected to a constant wall heat flux boundary condition. The investigation was performed in a Re range of 17050 – 44545 which fall in turbulence flow region and many industrial applications adopted turbulent flow in cooling and heating processes.

The heat flux is varied from 719 W/m^2 to 2098 W/m^2 and the enhancement of step heights were, s = 0 (without step), 6 mm, 14.5 mm and 18.5 mm, which refer to d/D = 1, 1.16, 1.53 and 1.80, respectively. The schematic drawing of the annular sudden expansion pipe flow is presented graphically in Figure 3.2 and the dimensions of experimental setup are summarized in table 3.1.

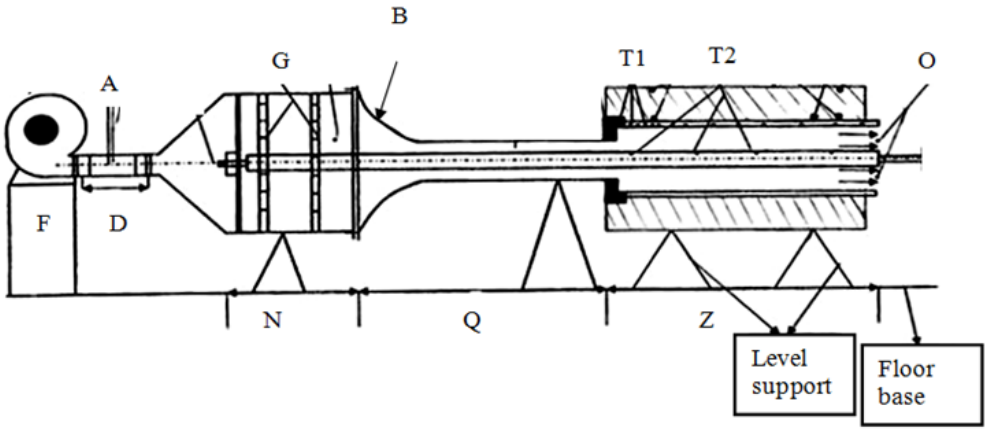

1. Centrifugal fan/ pumping equipment (F),
2. Delivery section (D),
3. Settling chamber (N)
4. Entrance section (Q)
5. Test section (Z).
6. Centrifugal fan/pumping unit (F)
7. Flowmeter (A)
8. Gauze flow straighteners (G)
9. Bell moth end delivery (B).
10. Circular concentric tube annular passage (Q and Z)
11. Outlet passage (O).

Figure 3.1: Experiment setup conducted by Togun et al.

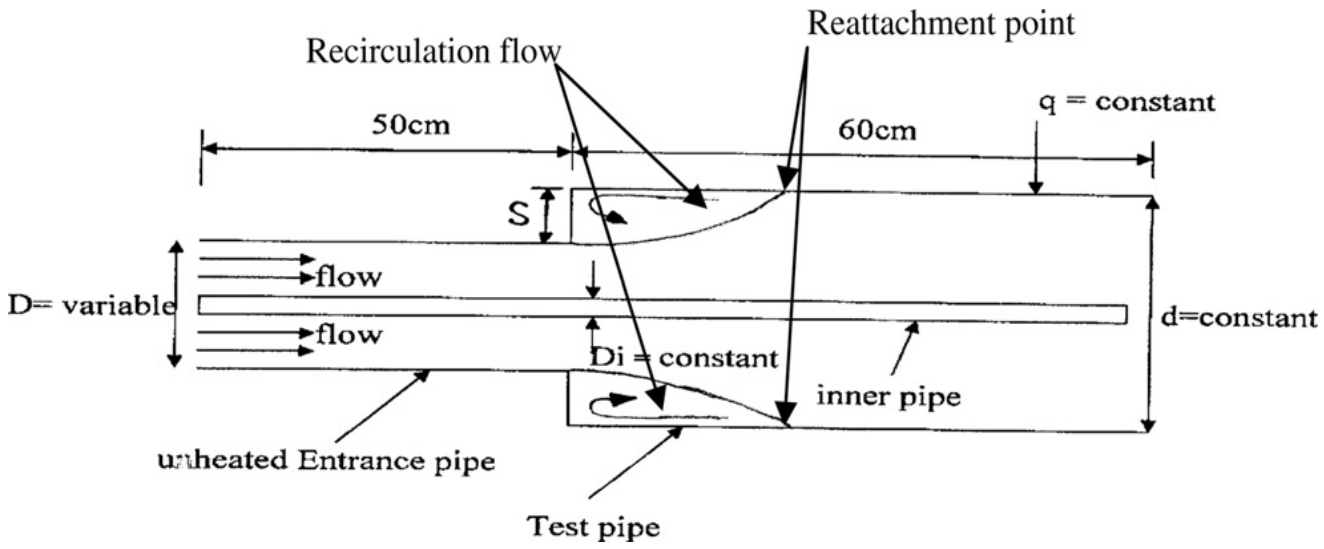

Figure 3.2: Schematic diagram of flow in the annular sudden expansion passage (Togun et al., 2011).

Table 3.1: Dimensions of experimental setup.

Inner tube	Diameter of entrance section	Diameter at test section
D_i=22 mm	D=(83, 71, 54, 46) mm	d=83 mm
L=1500 mm	L=500 mm	L=600 mm

The inner or outer surface temperatures of the annular pipes with sudden expansion can be influenced by many parameters, such as flow velocity, surface heat flux, and the step heights. The fluid utilized to conduct heat transfer in these experiments is air. The inlet and outlet diameter of the pipe are 46 and 83 mm respectively, the inner tube diameter of the annular pipe is 22 mm. In the simulations, 4 different cases were considered in an annular passage. The surface heat flux of the annular pipe is selected as 2098 W/m^2 with variable Reynolds numbers between 17,050 to 44,545 and D/d = 1.8 which is corresponding to 18.5 mm of step height. The numerical simulation parameters are summarized in table 3.2. Only Reynolds number of 17,050 and heat flux equal to 2098W/m^2 are considered experimentally to verify the numerical results.

Table 3.2: Experimental parameters.

Variable Parameter	**Value**	
Inlet dimension	0.012	m
Outlet dimension	0.0305	m
Reynolds number 1, Re_1	17,050	
Reynolds number 2, Re_2	30,720	
Reynolds number 3, Re_3	39,993	
Reynolds number 4, Re_4	45,545	

The geometry invention of the tube has been designed by using GAMBIT 2.2.30. The geometry of the tube was designed based on the exact experimental tube dimensions (Togun et al., 2011) (figure 3.3 and figure 3.4). As the geometry of the tube is symmetrical the geometry was designed by half (axissymetric), using 2–D model, as suggested in (Kolaczkowski et al., 2007). Table 3.2 and table 3.3 show the dimensions of the model drawn in GAMBIT. Models are designed with four different step heights, *s*=0, 6mm, 14.5mm and18.5mm.

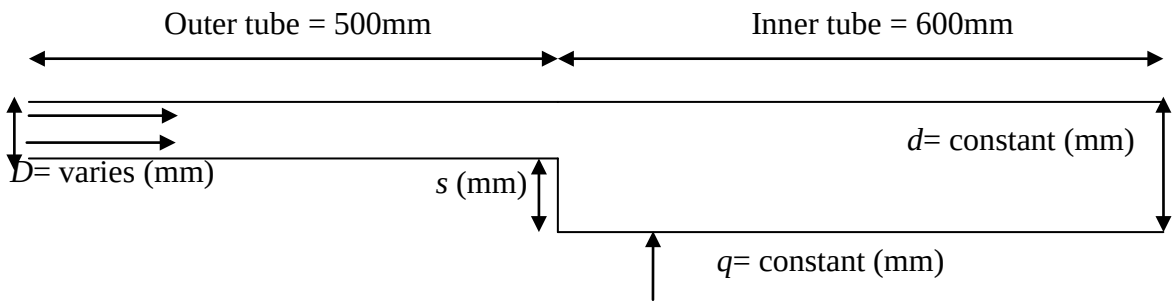

Figure 3.3: Geometry and dimensions of the model.

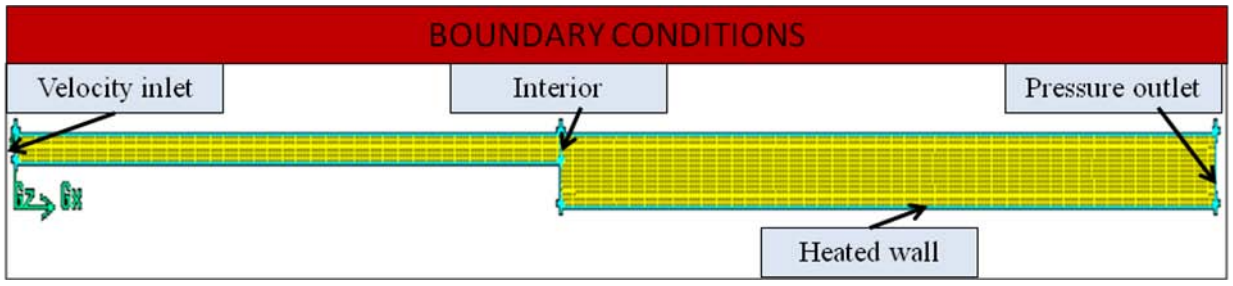

Figure 3.4: Geometry and boundary conditions are drawn by using GAMBIT.

Table 3.3: Dimensions of the entrance section and test section.

Step height, *s* (mm)	Diameter at entrance section, D (mm)	Diameter at test section, d (mm)
0	30.5	30.5
6.0	24.5	30.5
14.5	16.0	30.5
18.5	12.0	30.5

Flow Chart of Methodology

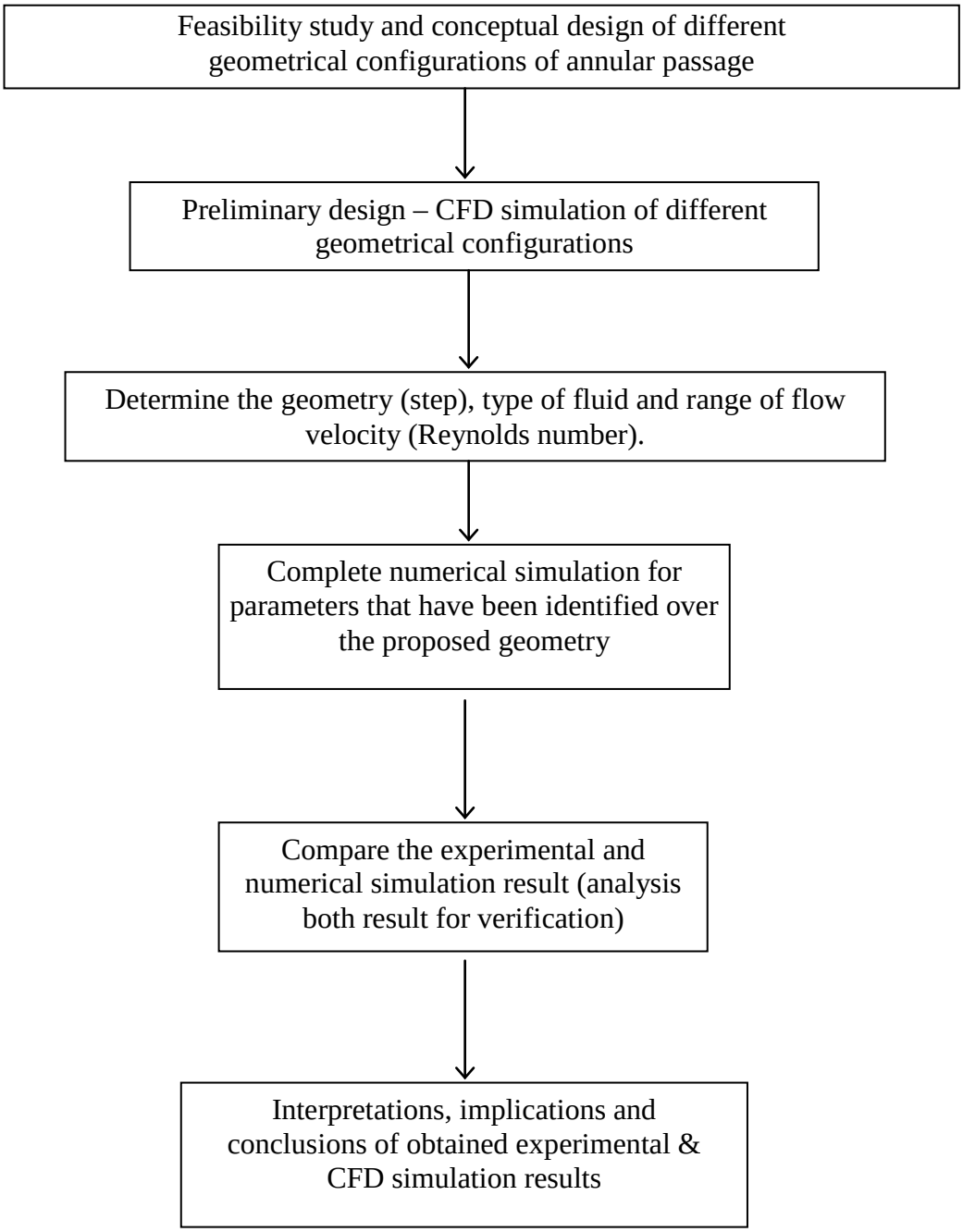

3.1.1 Computational Fluid Dynamic (CFD)

Fluid flow in a physical domain is governed by the laws of conservation of mass and momentum. These conservation laws, for steady flows in a closed conduit two-dimensional domain can be stated as follows.

Continuity equation:

$$\frac{\partial}{\partial x}(\rho u)+\frac{\partial}{\partial y}(\rho v)=0 \qquad (1)$$

Momentum conservation equations:

$$\frac{\partial}{\partial x}(\rho uu)+\frac{\partial}{\partial y}(\rho uv)=-\frac{\partial p}{\partial x}+\mu\left(\frac{\partial^2 u}{\partial x^2}+\frac{\partial^2 u}{\partial y^2}\right) \qquad (2)$$

$$\frac{\partial}{\partial x}(\rho vu)+\frac{\partial}{\partial y}(\rho vv)=-\frac{\partial p}{\partial y}+\mu\left(\frac{\partial^2 v}{\partial x^2}+\frac{\partial^2 v}{\partial y^2}\right) \qquad (3)$$

where u and v are the velocity components in the x and y directions. These equations are discretised by using the finite volume scheme.

Flow-solver formulates the principle of mass, momentum and energy conservation in partial differential equation forms on the basis of two dimensional Navier-Stokes equations. Navier-Stokes equations are discretized along with cells in the computational domain by finite volume method.

In all of the above references, the step in backward facing cases is vertical to the stepped wall. In these geometries, there is a sudden expansion or contraction in the

flowing fluid passage. But, there are several applications in which the flow geometry with sudden expansion, such as turbine blade cooling, combustion chambers, transition duct connection and atmospheric flow over fences and hills. There are few works in analyzing fluid flow with heat transfer over steps in turbulent fully developed fluid flow. The three-dimensional convection flow over an inclined backward facing step in a rectangular duct was studied by (Chen et al., 2006b) considering the wall were heated at constant heat flux condition. Numerical solution of the governing equations for laminar flow was performed by utilizing SIMPLE Algorithm for the pressure calculations. Thereby, the present work deals with the numerical solution of the governing equations to determine the fluid flow and temperature distributions of a forced convection turbulent flow over a forward inclined step, and the effects of inclined angle and the step length on the fluid flow and heat transfer are thoroughly explored. Due to complex fluid flow, the Navier-strokes, energy and continuity equations are transformed into the computational domain. The finite difference forms of the transformed equations are obtained from finite volume method and solved by the SIMPLE Algorithm.

Numerical simulation in this project was aimed to investigate typically, the heat transfer Nusselt number and understanding the flow phenomena of the sudden expansion in annular pipe. The diagram of the concentric pipe is drawn and meshed by using Gambit software. The mesh of the simulation domain consisted of 920 cells. As the geometry of the annular pipe is symmetrical, only the lower half is drawn and simulated. Following Lee et al., a finite volume based flow solver of computational fluid dynamics software (FLUENT) 6.3 is selected in the present investigation. The iteration of the standard K-epsilon viscous model is based on energy and Reynolds averaged Navier Stokes equations. The viscous model also provides good solutions for steady, near wall treatment, axisymmetric, incompressible and turbulent flow. The

second order upwind is used to solve the field variables at the finite volume cell faces for computing the solution. A SIMPLE algorithm is used to establish coupling between velocity and pressure. According to (Rahgoshay et al., 2012), the SIMPLE algorithm links the mass conservation and momentum equations through pressure corrections. Due to the computational robustness and efficiency in iterating the coupled parameters and higher order differencing schemes, this algorithm was selected over others. A balance between computing cost as well as accuracy is achieved by this method in numerical differentiation of the convective terms, with the linear upwind differencing scheme. table 3.4 shows the computational conditions of the numerical simulation.

Table 3.4: Computaional conditions.

Computational conditions			
Density	1.23 kg/m^3	Interpolating scheme (turbulence)	2nd Order Upwind
Viscosity	1.7894 x 10^{-5} kg/m.s	Residual error	1 x 10^{-4}
Pressure	101,325 Pa	Inlet Boundary Type	Velocity Inlet
Space /Time	2D /Unsteady, 2nd-Order Implicit	Reference Frame	Absolute
Viscous Model	*k* and ε	Reynolds number	See Table I
CFD algorithm	SIMPLE	Outlet Boundary Type	Pressure outlet
Interpolating scheme (momentum)	2nd Order Upwind		

The properties of air were set to the standard atmosphere values at sea level, pressure 101, 325 Pa, temperature of 300 K, thermal conductivity 0.03 W/m.K and specific heat, Cp 1.005 kJ/kg.K. The flow solver used was steady state and pressure based which associates both the momentum and mass conservation equation. Unsteady assumption is selected for most cases where convergence can be obtained. Simulations were performed until the residual values were less than 1 x 10^{-4}.

The analysis of the backward-facing step flow was performed by using FLUENT 6.3.26. Four different Reynolds numbers are tested in the simulation, *Re*=17050, 30720, 39992 and 44545, producing fully developed turbulent unsteady flow and heat flux applied to the inner tube varies from q=719 W/m^2, 968 W/m^2, 1458 W/m^2 and 2098 W/m^2. Pressure based solver with 2nd –order implicit unsteady formulation, with standard k-epsilon (Yakhot and C.G., 1992) equation were applied in defining the model.

Second order upwind is applied in solving the momentum, turbulent kinetic energy, turbulent dissipation rate and energy discretizations (Lee et al., 2011). A coupling between pressure and velocity is established through the SIMPLE algorithm. The boundary condition of the inlet is defined as velocity inlet, whereas for outlet it is pressure outlet with turbulent intensity of 7% and turbulent length scale 0.06 m. Fluid material is air having density of 1.225 kg/m^3, C_p=1006.43 J/kg-K, thermal conductivity 0.0242 (W/m-K) and viscosity 1.7894x10^{-5}(kg/m-s). Gravity influence is neglected.

The Reynolds number (Re_d) can be obtained by the following Eq. (4):

$$Re_d = \frac{\rho_f \cdot U \cdot D_h}{\mu_f} \qquad (4)$$

where ρ_f is the density of the fluid, U is the velocity of the fluid, D_h is the hydraulic diameter of the annular pipe and μ_f is the dynamic viscosity of the fluid at film temperature.

The local heat transfer coefficients are calculated using convection heat flux as shown by Eq. (5):

$$h_x = \frac{q_c}{(T_{sx} - T_{bx})} \qquad (5)$$

where q_c is the convection heat flux, T_{sx} is the local surface temperature and T_{bx} is the local bulk air temperature.

The local Nusselt number (*Nu*) can be evaluated by Eq. (6):

$$Nu = \frac{h_x \cdot d}{K_f} \qquad (6)$$

where d is the diameter of the pipe and K_f is the thermal conductivity.

Using the equations 4-6, the experimental data for expansion ratio D/d=1.8, Heat flux q=2098 and reynold number Re=17050 to 44545 were reduced. By using equation 5, the local heat transfer coefficient was calculated and subsequently local nusselt number was evaluated from equation 6. Nusselt number for turbulent fully develop flow was then calculated from Dittus-Boelter's correlation (7). The previously calculated local Nusselt numbers were divided by nusselt numbers evaluated from Dittus Boelter correlation to obtain the ratio Nu/Nu_d (Kreith and Bohn, 2001).

$$Nu_d = 0.023\ Re^{0.8}\ Pr^{0.4} \qquad (7)$$

3.1.2 Mesh Independent Study

Mesh independent study was considered to authenticate the results of numerical data obtained from software GAMBIT and FLUENT. The computational domain was being meshed by using GAMBIT software. Three different types of mesh have been created for mesh independent study as shown in Table 3.5.

Table 3.5: Number of mesh with different interval size.

Step Height (mm)	**Interval size 4**	**Interval size 4.5**	**Interval size 5**
0	2216	1701	1320
6	1962	1354	1220
14.5	1708	1371	1020
18.5	1581	1261	920
Average Mesh	2076	1422	1120

3.1.3 Surface Roughness Study

Study of the effect of surface roughness on heat transfer was taken into consideration. The surface of the heated wall is set to the surface roughness data measured by Kazi et al. for different material specimens commercially available. Then the models are simulated with same parameters and conditions to study the effect of surface roughness. Table 3.6 shows roughness height for different specimens.

Table 3.6: Roughness height of the commercially available test specimens (Kazi et al., 2010).

Specimen	Roughness Height, μm
Polycarbonate	0.25
SS 316	0.88
Brass	2.3
Aluminium	2.9

3.2 Basefluid and Nanofluid Methodology

A preliminary study on backward facing step of basefluid (water), different nanofluids and different concentration of nanofluid were conducted using CFD. The schematic drawing of the annular sudden expansion pipe flow is presented graphically in Figure 3.5. Figure 3.6 shows the geometry of asymmetry annular test section drawn in GAMBIT. The inner or outer surface temperature of the annular pipe with sudden expansion can be influenced by many parameters, such as flow velocity, surface heat flux, and the step heights. The inlet 33 mm, 39 mm, 52 mm and 60mm, then the outlet of the tube is 60 mm. The diameter of the inner tube is 20 mm. Table 3.7 and table 3.8 show the dimension of the annular test section with different step heights.

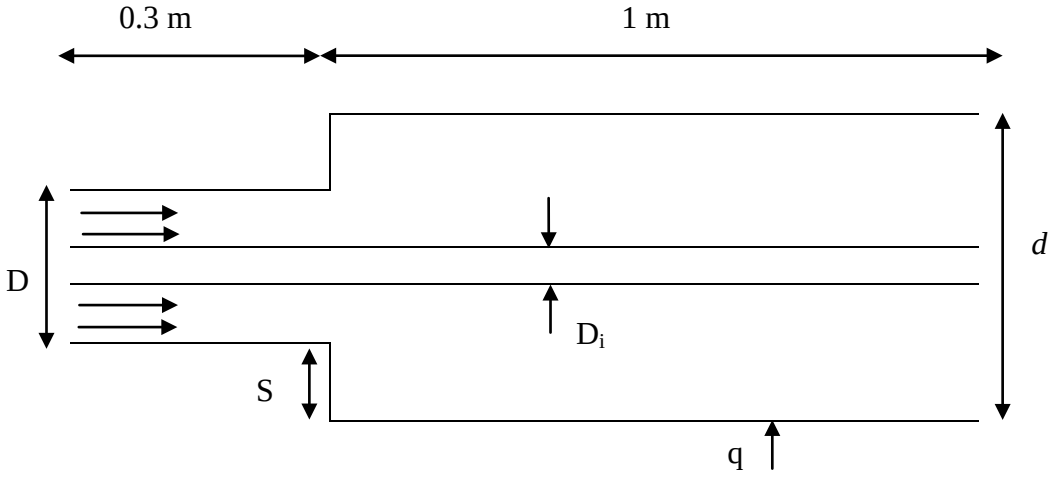

Figure 3.5: Schematic diagram of the annular sudden expansion in annular pipe flow for basefluid and nanofluid.

Table 3.7: Dimensions of the model.

Inner tube	Outer tube at entrance section	Outer tube at test section
D_i=20 mm	D=(60, 52, 39, 33) mm	d=60 mm
L=1300 mm	L=300 mm	L=1000 mm

Figure 3.6: Geometry of asymmetry annular test section are drawn by using GAMBIT.

Table 3.8: Dimensions of the entrance section and test section

Step height, s (mm)	Entrance of the tube before expansion, d (mm)	Outlet of the tube after expansion, D (mm)
0	20	20
4	16	20
10.5	9.5	20
13.5	6.5	20

3.2.1 Thermophysical properties of nanofluids

The numerical data for nanofluid densities were studied by (Brinkman, 1952), the temperature independent values based on nanoparticle volume fraction were calculated using equation (8):

$$\rho_{nf} = (1 - \emptyset)\rho_{bf} + \emptyset\rho_p \qquad (8)$$

Similarly, it has been suggested that the effective specific heat can be calculated by using equation (9).

$$Cp_{nf} = (1 - \emptyset)Cp_{bf} + \emptyset Cp_p \qquad (9)$$

In this study, dynamic viscosity, μ was considered dependent only on concentration of nano particles in the basefluid, Ø and the temperature dependency was neglected.

$$\frac{\mu_{nf}}{\mu_{bf}} = 123\emptyset^2 + 7.3\emptyset + 1 \qquad (10)$$

For the nanaofluids thermal conductivity determination, the same criteria used by (Khanafer et al., 2003) was introduced. This equation is applicable for the two-phase mixture containing micro-sized particles. In the absence of any convenient formula for the calculations of the stagnant thermal conductivity of nanofluids, equation (11) may approximately apply to obtain a reasonable estimation (Wasp et al., 1977):

$$\frac{k_{\mathrm{nf}}}{k_{\mathrm{f}}} = \frac{k_{\mathrm{s}} + 2k_{\mathrm{f}} - 2\varphi(k_{\mathrm{f}} - k_{\mathrm{s}})}{k_{\mathrm{s}} + 2k_{\mathrm{f}} + \varphi(k_{\mathrm{f}} - k_{\mathrm{s}})} \qquad (11)$$

where ρ is density, C_p is specific heat, k is thermal conductivity and μ is dynamic viscosity. Table 3.9 shows the thermophysical properties of nano particles that were used to calculate the thermophysical properties of different nanofluids.

Table 3.9: Thermophysical properties of nano particles.

Property	**Fluid phase (water)**	**Nanoparticles**				
		Cu	**Ag**	**CuO**	**Al_2O_3**	**TiO_2**
Cp (J/kg-K)	4182	385	235	535.6	765	686.2
ρ (kg/m3)	998.2	8933	10500	6500	3970	4250
k (W/m-K)	0.597	400	429	20	40	8.9538

Table 3.10 shows the thermophysical properties of water-Al_2O_3 nanofluids at different concentration. Using the present formulation, several assumptions were made, such as the flow is consider as single phase model, the concentration of nanofluid is assume to be constant during the testing and the effect of temperature to the thermophysical properties is negligible. The thermophysical properties were calculated using equations 8, 9, 10 and 11. The data were used to run the simulation in order to investigate the effect of concentration on the behavior and characteristics of water-Al_2O_3 nanofluid flowing through various steps height and Reynolds numbers.

Table 3.10: Thermophysical properties of water-Al_2O_3 nanofluids at different concentration.

Fluid	**Volume concentration (%)**	**Viscosity, kg/m-s (μ)**	**Density, kg/m^3 (ρ)**	**Specific heat, J/kg-K (C_p)**	**Thermal conductivity W/m-K (K)**
H_2O (water)	0%	1.003×10^{-3}	998.2	4182	0.6
Al_2O_3 - water	1%	1.0886×10^{-3}	1027.9	4147.8	0.6143
Al_2O_3 - water	2%	1.1988×10^{-3}	1057.6	4113.7	0.6319
Al_2O_3 - water	3%	1.3337×10^{-3}	1087.4	4079.5	0.6499
Al_2O_3 - water	4%	1.4933×10^{-3}	1117.1	4045.3	0.6682

The analysis was also conducted by using different types of nanofluids eg: water based Cu, CuO, Ag, TiO_2 and Al_2O_3. The comparison was done in 1% volumetric concentration of different nanofluids. The value of the thermophysical properties of the fluids were calculated by using equations 8, 9, 10 and 11 and presented in table 3.11.

Table 3.11: Thermophysical properties of nanofluids with 1% volumetric concentration.

Type of fluid	**Density, kg/m^3 (ρ)**	**Viscosity, kg/m-s (μ)**	**Thermal conductivity W/m-K (K)**	**Specific heat J/kg-K (C_p)**
Cu - water	1077.5	1.0886×10^{-3}	0.6150	4144
CuO - water	1053.2	1.0886×10^{-3}	0.6135	4145.5
Ag- water	1093.2	1.0886×10^{-3}	0.6150	4142.5
TiO_2 - water	1030.7	1.0886×10^{-3}	0.6119	4147
Al_2O_3 - water	1027.9	1.0886×10^{-3}	0.6143	4147.8

The analysis on the backward-facing step flow was employed using FLUENT 6.3.26. Four different Reynolds numbers *Re*=17050, 30720, 39992 and 44545 were simulated in the investigation. Heat flux applied at the test section were q=49050 W/m^2. The analysis was also conducted for different volume fraction range between $0\% \leq \varphi \leq 4\%$. The properties calculated were defined in FLUENT's materials database. The boundary conditions of the model were defined according to the setting utilized for the flow separation using air. The working fluids used in the simulation are base fluid (water) and different nanofluids (with variable thermophysical properties that have been defined in FLUENT' material database). Gravity influence is neglected.

CHAPTER 4: Results and Discussions

Generally, the presence of backward facing step in the pipe flow shows reduction of temperature on the inner surface of the pipe. Due to the turbulent flow, the heat transfer is augmented in some areas. The lowest temperature is obtained at the end of flow recirculation zone where the flow reattachment happens after the flow separated at the beginning of the step. The Vector of fluid flow is shown in figure 4.1. After flow reattachment the fully developed turbulent flow carries the heat though the rest of the pipe and exhaust as hot air. Figure 4.2 shows the temperature distribution along the pipe where the colours ranging from blue to red indicate low temperature to high temperature.

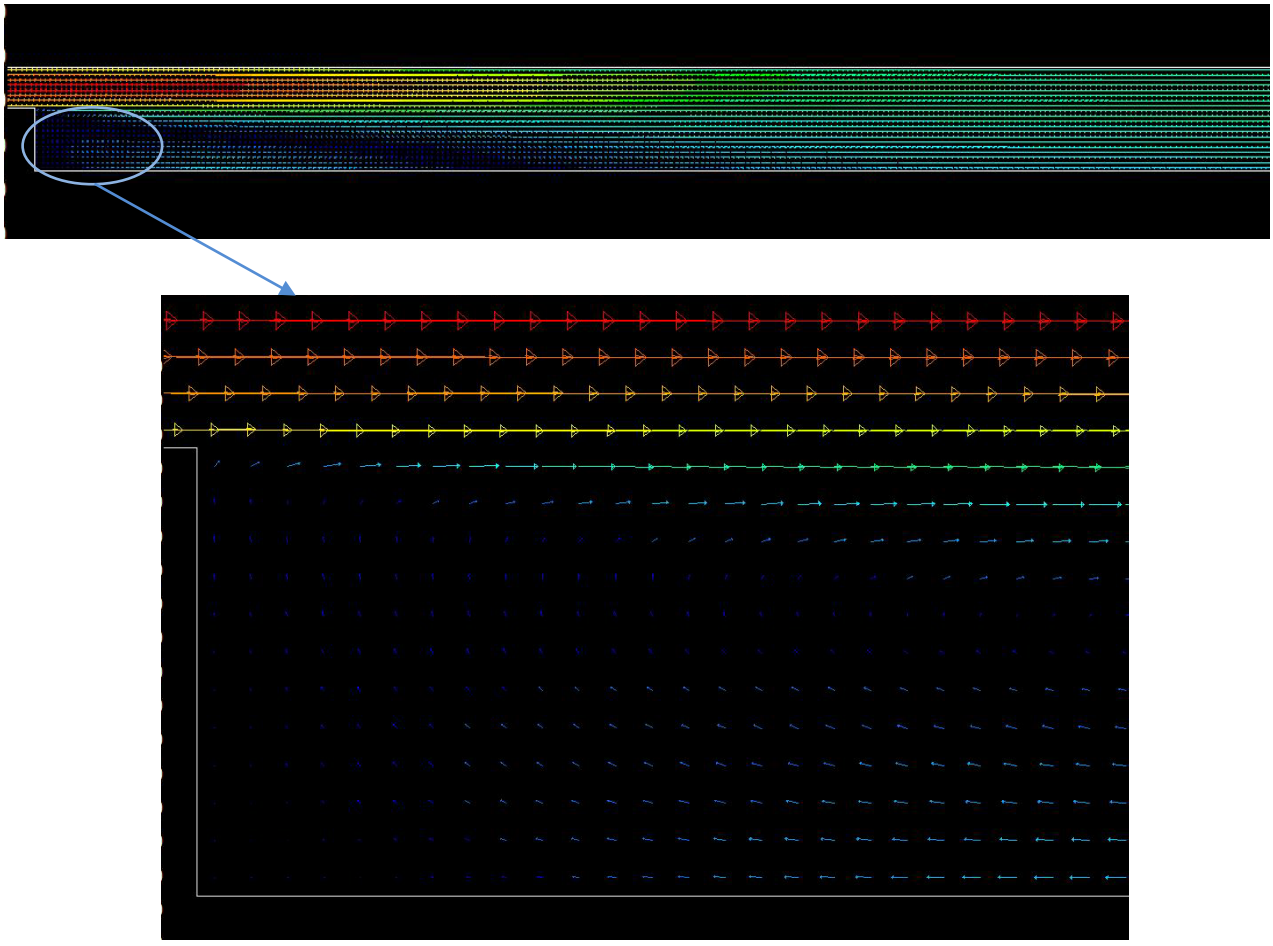

Figure 4.1: Vector of air inside the pipe.

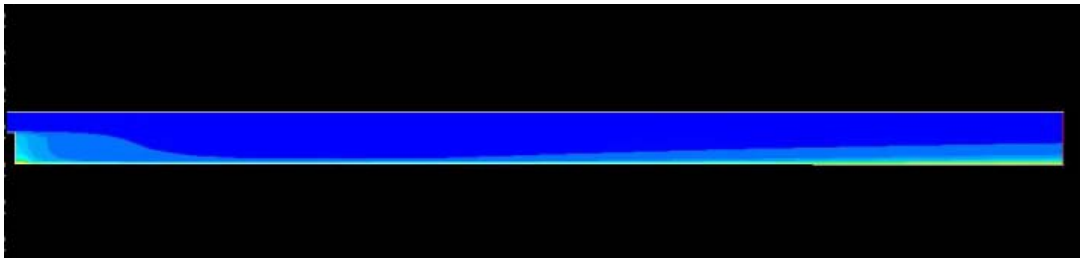

Figure 4.2: Temperature distribution along the pipe.

4.1 Numerical simulation of air flow in an annular passage

In the simulation process, 4 different cases were considered for flow through an annular passage. The surface heat fluxes from the annular pipe is selected at 2098 W/m^2 with a variable Reynolds number between 17,050 to 44,545 in a given geometry. The average temperature at Re=17,505 for both numerical and experimental results are 371.77 K and 372.19 K respectively, where the percentage of deviation error is less than 1 %. The temperature versus x/D graph is shown in figure 4.3.

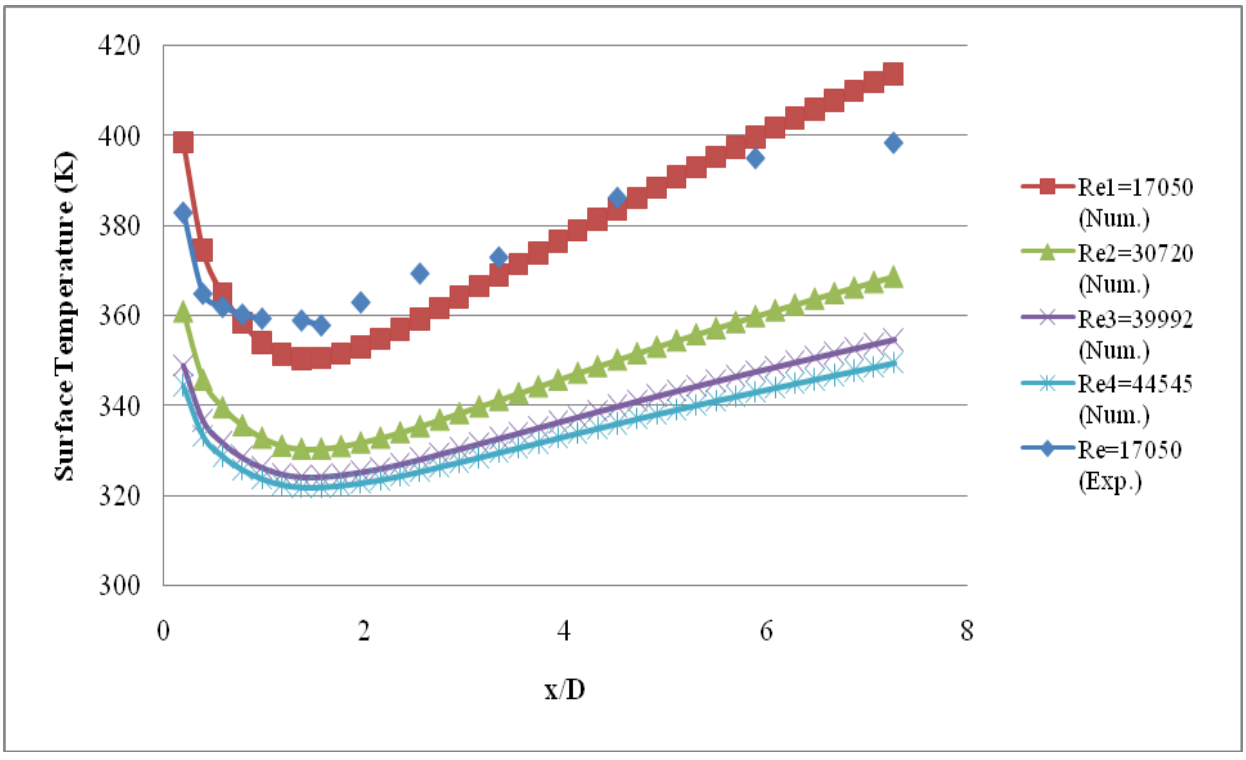

Figure 4.3: The variation of surface temperature with x/D.

The evaluated Nusselt numbers for the specific Reynolds numbers are plotted in figure 4.4. The noticeable trend of the results is the sudden increase in the local Nusselt number when the fluid flows to the end of the recirculation zone. In a study conducted by Charwat et al. [10], the obtained result is identical to the present observation due to the intervallic vortex shedding followed by the reattachment at the corner area of the recirculation zone. Also, the process of fresh fluid intervallic “filling” and “emptying” the recirculation zone may contribute to the dramatic increase in Nusselt number. Lastly, the numerically simulated Nusselt number varationswith x/D at Reynolds number 17,505 are in reasonable agreement with experimental results representing location and magnitude of the highest Nusselt number. Observed difference of both average Nusselt numbers difference are less than 10 %.

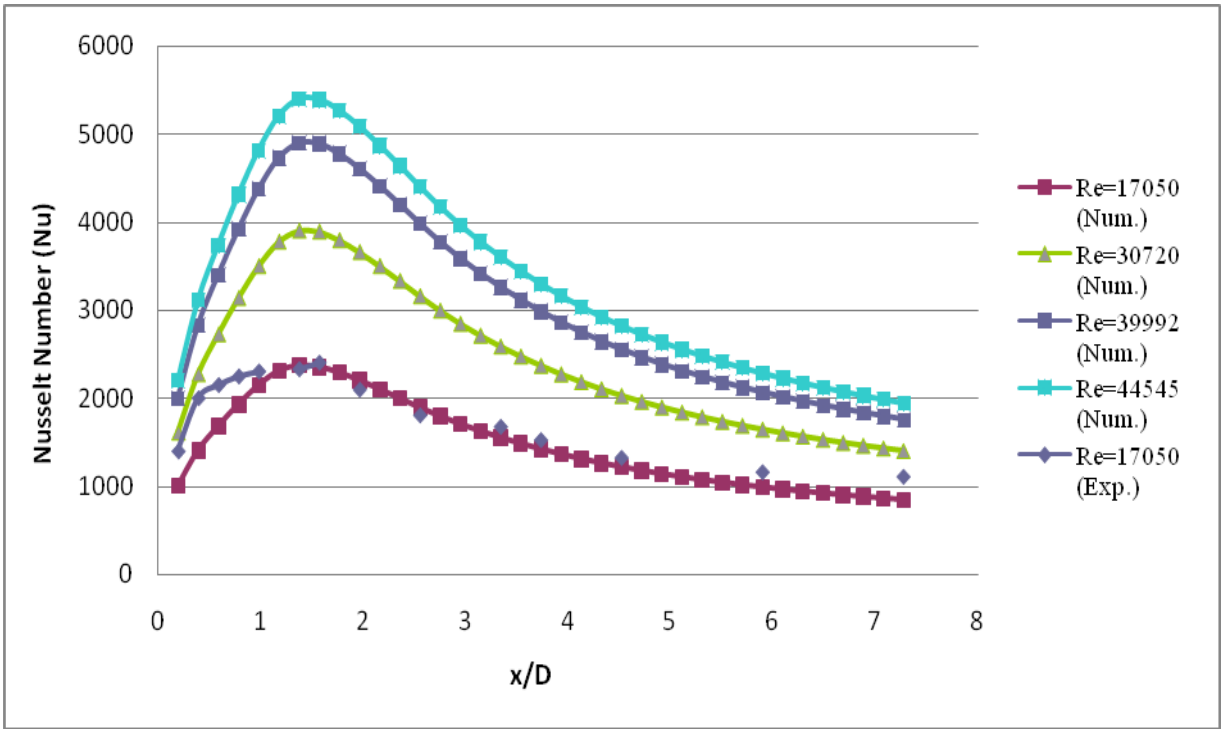

Figure 4.4: The graph of Nusselt number versus x/D.

The variation of local Nusselt number ratio (Nu/Nu_d) with x/D for heat flux q=2098 W/m^2 and expansion ratio D/d=1.8 are presented in figure 4.5. The local Nusselt number ratio increases to a maximum magnitude then decrease towards the end

of the test pipe. The maximum value of local Nusselt number ratio appears between 1 and 2 of x/D for four Reynolds numbers. The highest peak of local Nusselt number appears in the range of 34.8 to 36.5. The highest local Nusselt number obtained at Re=44545 which is 4.9% higher than that obtained at turbulent fully developed flow at Reynolds number Re=17050. The augmentation of heat transfer observed with increase of Reynolds number where the value of local Nusselt number enhances due to induced eddies. The region of heat transfer augmentation is found in the distance of four outer diameters from the expansion.

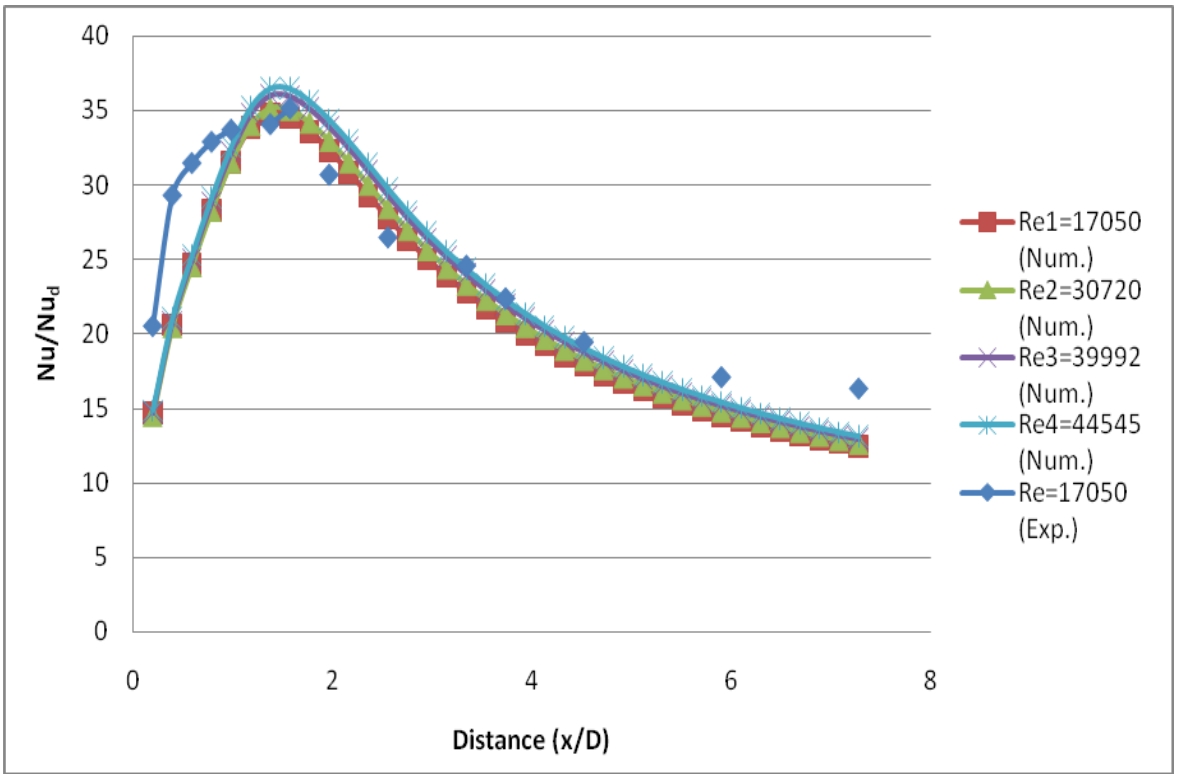

Figure 4.5. The graph of local Nusselt number/Nusselt number (Dittus-Boelter) versus x/D.

Figure 4.6 shows the variation of the surface temperature versus distance for different Reynolds number at heat flux 790 W/m^2 and a step height equal to (18.5), i.e. (d/D = 1.8). Figure 4.6 shows that the surface temperature variation decreases with the increase of Reynolds number for the same heat flux and step height. Figure 4.7 and figure 4.8 shows the effect of variation of heat flux on the simulation surface

temperature at Reynolds number 17050 and 44545 respectively with step height equal to (18.5), i.e. (D/d = 1.8). The general shape shows a reduction of surface temperature at the test section inlet directly behind the step (x = 0). The minimum magnitude of temperature is obtained at a specific axial position where the flow reattachment takes place after the separation region due to turbulence augmented heat transfer. Then the temperature gradually increases along the pipe with the reduction of heat transfer rate. It is noted that the distance increases with the surface temperature with distance increases with the increase of heat flux. Thus an optimization analysis of heat exchanger could be taken as an extension of present investigation.

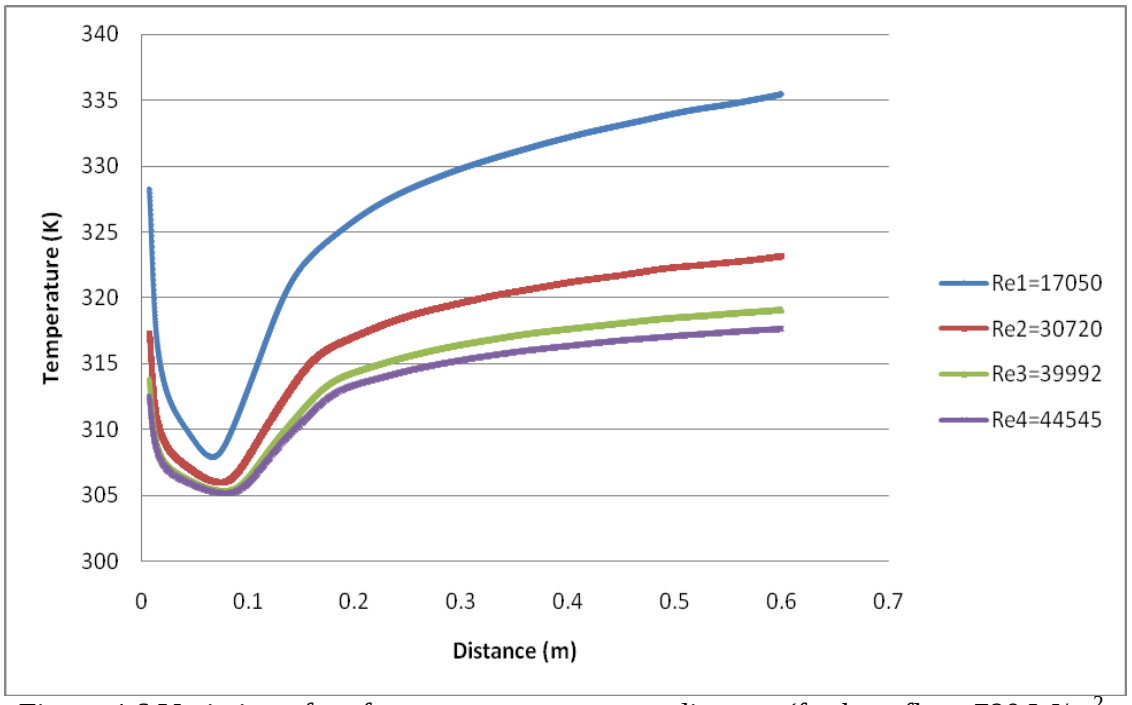

Figure 4.6 Variation of surface temperature versus distance (for heat flux=790 W/m^2, D/d=1.8).

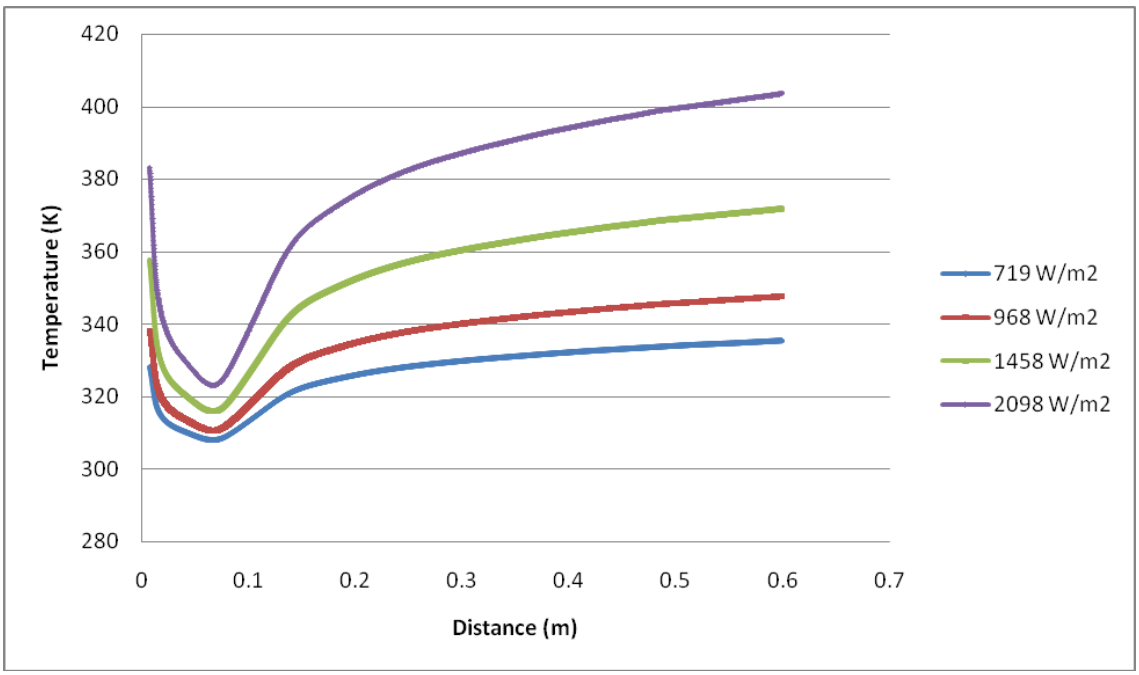

Figure 4.7: Variation of surface temperature versus distance (for re=17050, D/d=1.8).

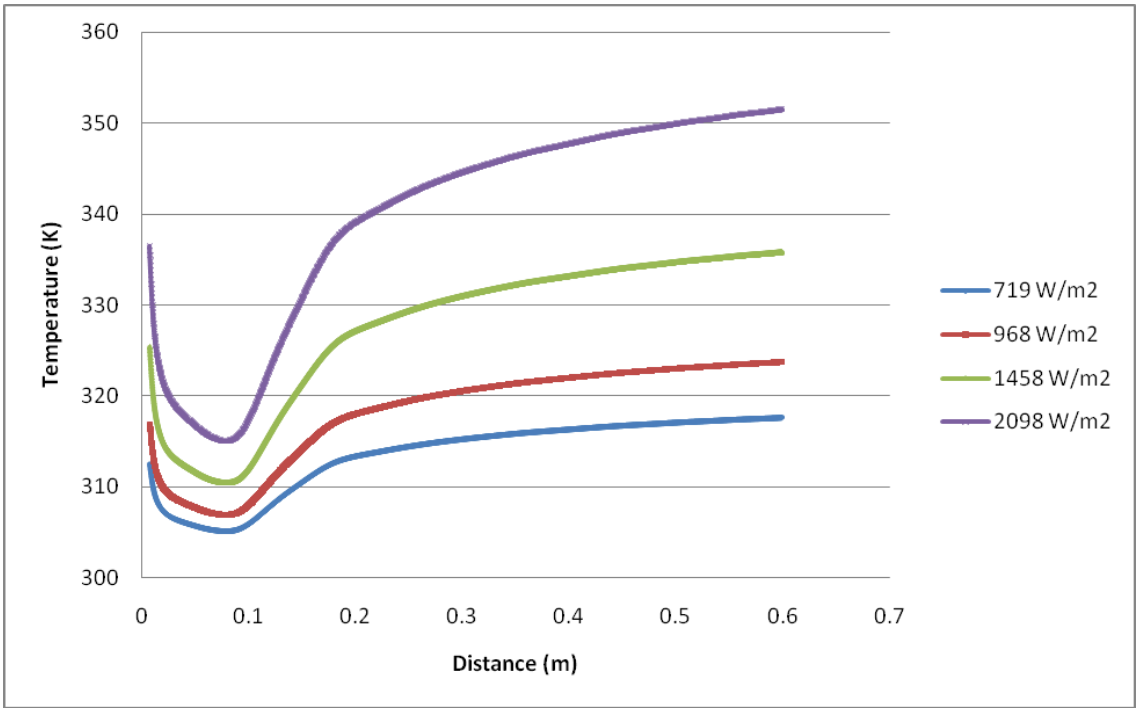

Figure 4.8: Variation of surface temperature versus distance (for Re=44545, D/d=1.8).

Figure 4.9 shows the variation of surface temperature as a function of distance with different step heights for *Re*=39992 and *q*=2098 W/m^2. The entire graph did not share a common profile, at *s*=0 and 6 mm, it appears as linear shapes slightly rise of with surface temperature until the end of the test pipe. On the other hand, in case of

s=14.5 mm and 18.5 mm, the curve shows a minimum surface temperature indicating the presence of reattachment point. For *s*=0 and 6 mm, the reattachment point could not be specified as the surface temperature is not having a sudden drop, whereas for *s*=14.5 mm and 18.5 mm, the reattachment point appears at 0.542 m, where the minimum surface temperature is obtained. The error of average surface temperature between experimental and numerical is 1.26 % referring to good numerical approach for estimating temperature profile. However, for the step heights of 0 and 6 mm, the results shows almost no fluctuation due to the step heights is too small to induce backward facing steps.

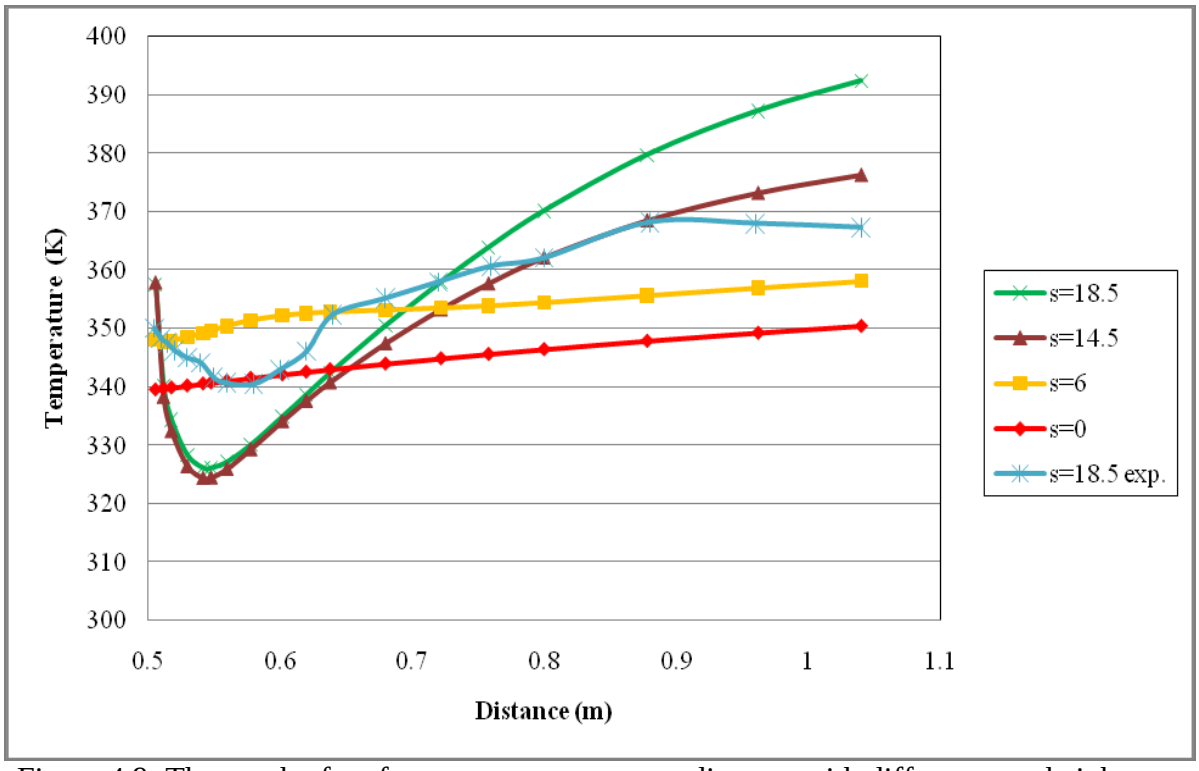

Figure 4.9: The graph of surface temperature versus distance with different step height (for *Re*=39992, *q*=2098 W/m^2).

Figure 4.10 representing the local heat transfer coefficient versus distance with different step height for the case of *Re*=39992 and *q*=2098 W/m^2. The entire graph did not share a common profile, where *s*=0 and 6 mm are maintained, It appears as profile, with heat transfer coefficient slightly decreasing until the end of the test pipe. But for

the step height of s=14.5 mm and 18.5 mm, the h_x increases up to a maximum point (reattachment point), and then decrease slowly. For s=14.5 mm and 18.5 mm, the h_x appears to be similar and overlapping each other, while at s=0 it illustrates higher h_x than s=6 mm. Thus, it opens an avenue for optimization of heat exchangers.

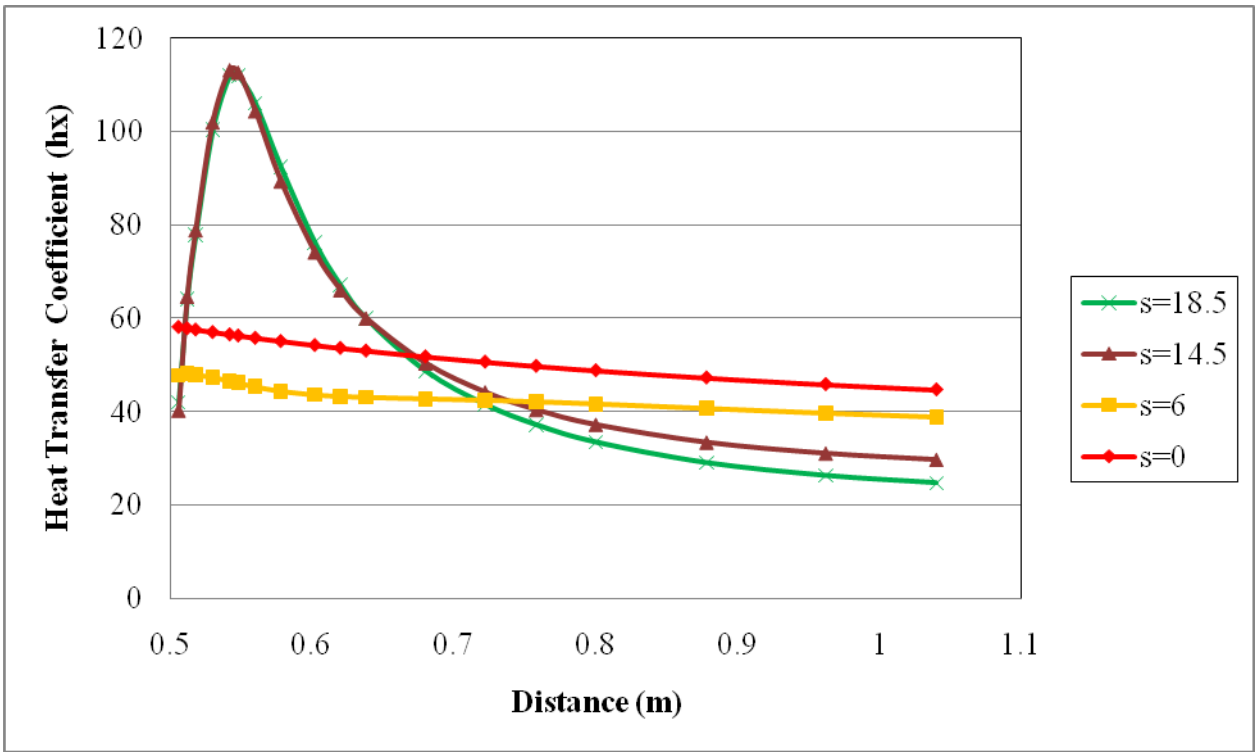

Figure 4.10: The graph of local heat transfer coefficient versus distance with different step height for (Re=39992, q=2098 W/m^2).

Figure 4.11 the graph of Nusselt number versus distance with different step heights at Re=39992 and q=2098 W/m^2. The entire graph did not share a common profile, for s=0 and 6 mm, it appears as linear curve, and for s=14.5 mm and 18.5 mm, the Nusselt number increases up to a maximum point (reattachment point), and then decreases slowly. For s=14.5 mm and 18.5 mm, the Nusselt number appears to be overlapping each other, while at s=0 it illustrates higher Nusselt number than at s=6 mm. It can be concluded that, the effect on Nusselt number is not significant in all cases when the step heights are varied with ultimately opens up an avenue of optimization of heat exchangers.

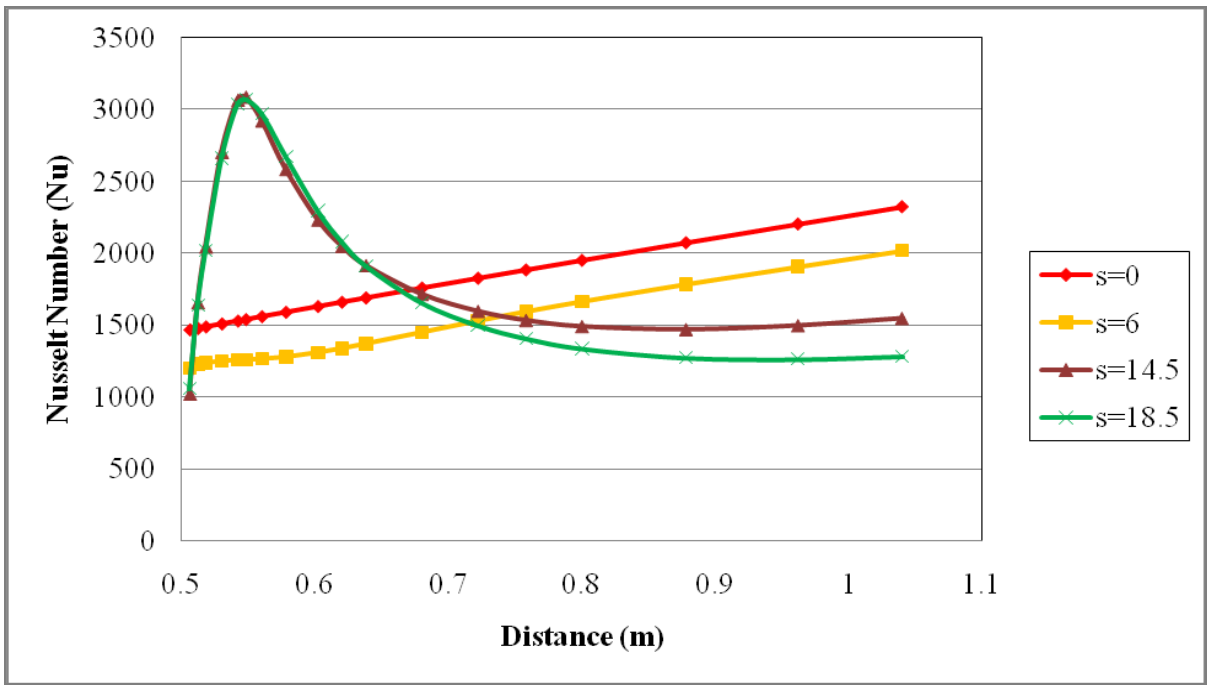

Figure 4.11: The graph of Nusselt number versus distance with different step heights (for *Re*=39992, *q*=2098 W/m^2).

Figure 4.12 represents the surface temperature distribution for different Reynolds numbers of *Re*=17050, 30720, 39992 and 44545 for *s*=18.5 mm and *q*=2098 W/m^2. The reattachment region shows the lowest surface temperature at 300 K for all Reynolds numbers. The reattachment length simulated is about 0.042 m from the expansion for all Reynolds numbers. After the fluid passes reattachment region, the surface temperature increases gradually and the higher temperature is located near the heated wall approximately at 350 K. The highest temperature is located at the outlet of the test pipe which is around 383 K.

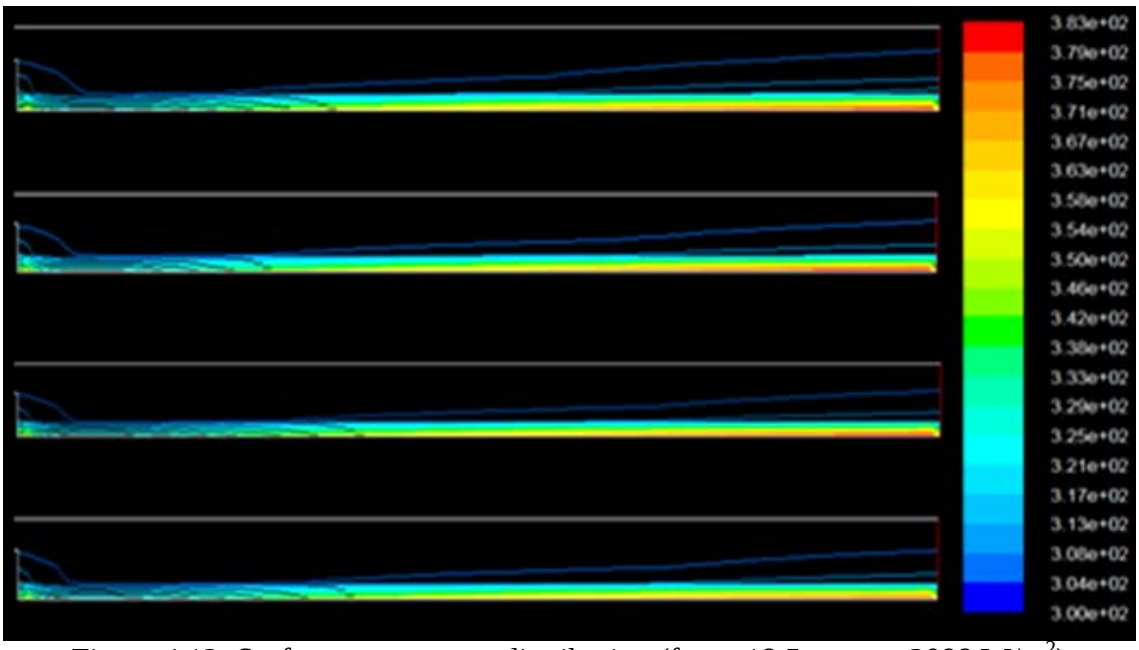

Figure 4.12: Surface temperature distribution (for s=18.5 mm, q=2098 W/m^2) Re=17050, 30720, 39992 and 44545 from top to bottom.

Figure 4.13 shows the temperature versus distance graph obtained by using different viscous models (for s=18.5 mm, Re=44545 and q=2098 W/m^2). Comparison between three types of k–ε models; standard, RNG, and realizable are being made. Reattachment point at 0.55 m was obtained by experiment investigation. Standard, RNG and realizable k–ε models showed the position of reattachment point at 0.542 m, 0.56 m, and 0.578 m respectively. Standard model obtained the nearest reattachment point in comparison of the experimental result and the other models. In averaging surface temperature, the standard model has offered the lowest error of 2.8 % in comparison to experimental results with RNG and realizable models which achieved the errors of 4.95 % and 7.41 % respectively. Therefore, standard k–ε model is offering more precise result in predicting reattachment point and surface temperature compared to other k–ε models. It was suggested that Standard k–ε model is reliable in predicting turbulent flow in this sudden expansion case.

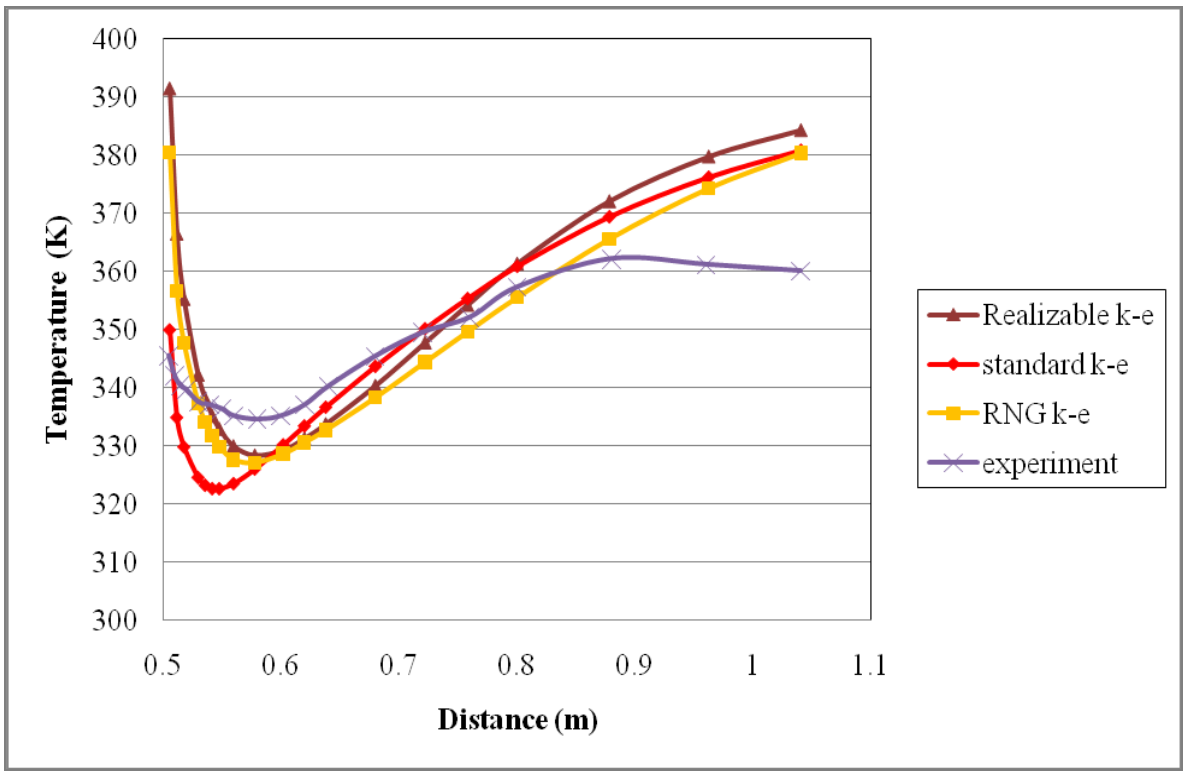

Figure 4.13: The graph of temperature versus distance with different viscous model (for s=18.5 mm, Re=44545 and q=2098 W/m^2).

4.1.1 Mesh Independent Study

The mesh independent study shows that with the reduction of meshing interval sized from 5 to 4.5, the different average temperature is about 10 K at Re=17050. On the other hand, the reduction of meshing interval size from 4.5 to 4 show only 0.5 K reduction in average temperature for the same case. It is concluded that the meshing is good enough for the simulations. Figure 4.14 shows the comparison of average surface temperature for various interval sizes at s=18.5 mm and q=2098 W/m^2. For interval size=4.5, the data is 2.14 % deviated from the interval size 5 at Reynolds number=17050, whereas for the interval size of 4.5 and 5, it shows errors of less than 0.1 %. Interval size of 4 offers less deviation compared to other interval sizes, such as the interval size of 5 which contributes larger error. For the reduction of interval size

from 4.5 to 4, the number of meshing element will increase. The result shows the meshing is good enough to validate the mesh independent study.

Average heat transfer coefficient is being compared for different interval sizes in figure 4.15. Interval size of 4.5 shows the smallest difference among all the numerical data. Interval size of 4 and 5 show errors of 2.44 % and 9.76 % respectively compare to interval size of 4.5 at Reynolds number=39992. Same trend is applied for the Reynolds number of 30720 and 44545. Finally, the deviation of numerical data for Reynolds number=17050 is not significant for three interval sizes. It can be conclude that the interval size of 4 and 4.5 are preferable meshing for heat transfer coefficient investigation in present case. Figure 4.16 shows the comparison of average Nusselt number with different interval sizes. Same conclusion can be drawn for the case of average heat transfer coefficient and average Nusselt number.

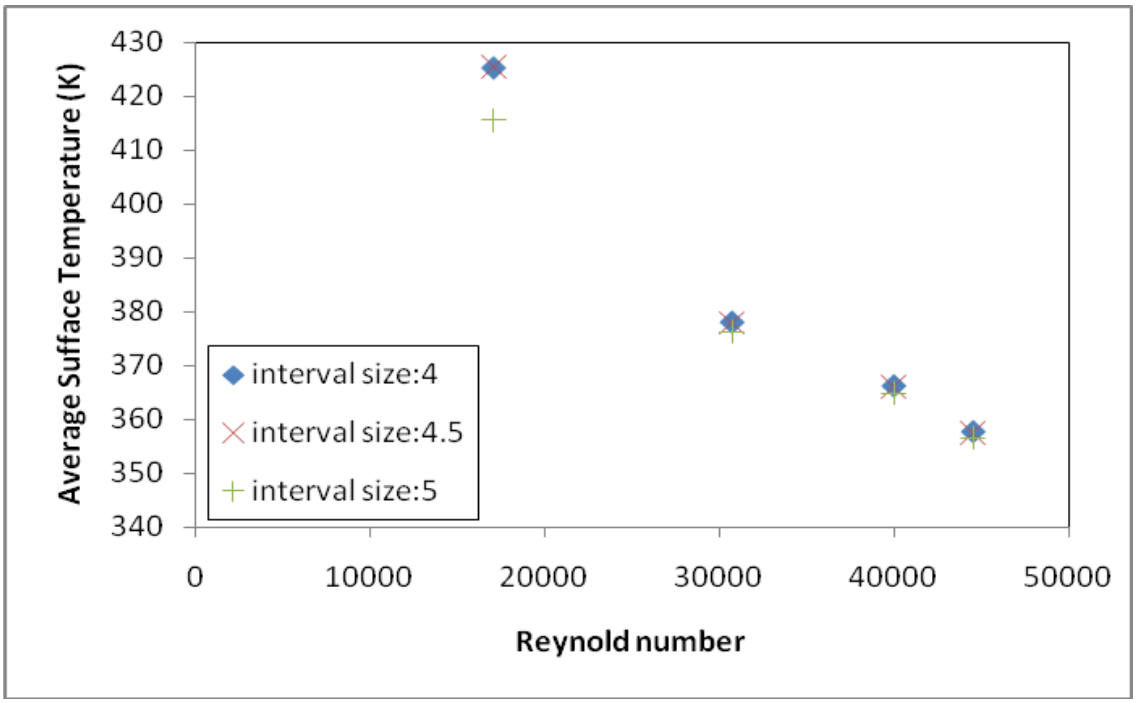

Figure 4.14: Comparison of average temperature over various Reynolds numbers at s=18.5 mm and q=2098 W/m^2.

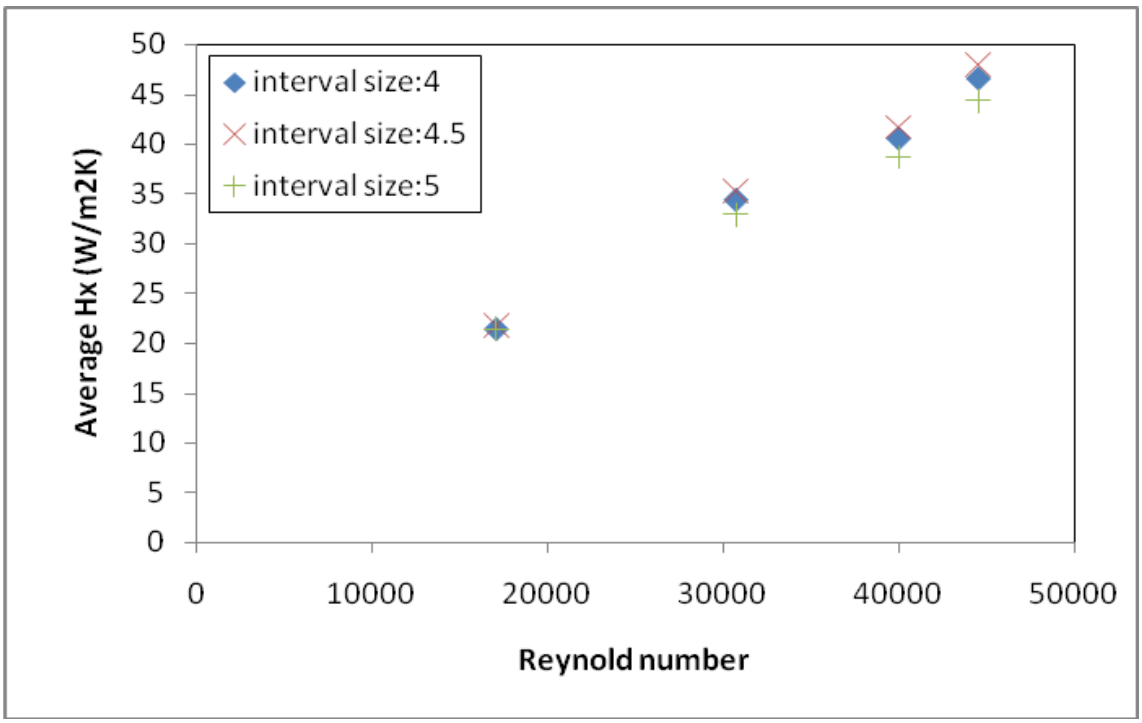

Figure 4.15: Comparison of average heat transfer coefficient over various Reynolds numbers at s=18.5 mm and q=2098 W/m^2.

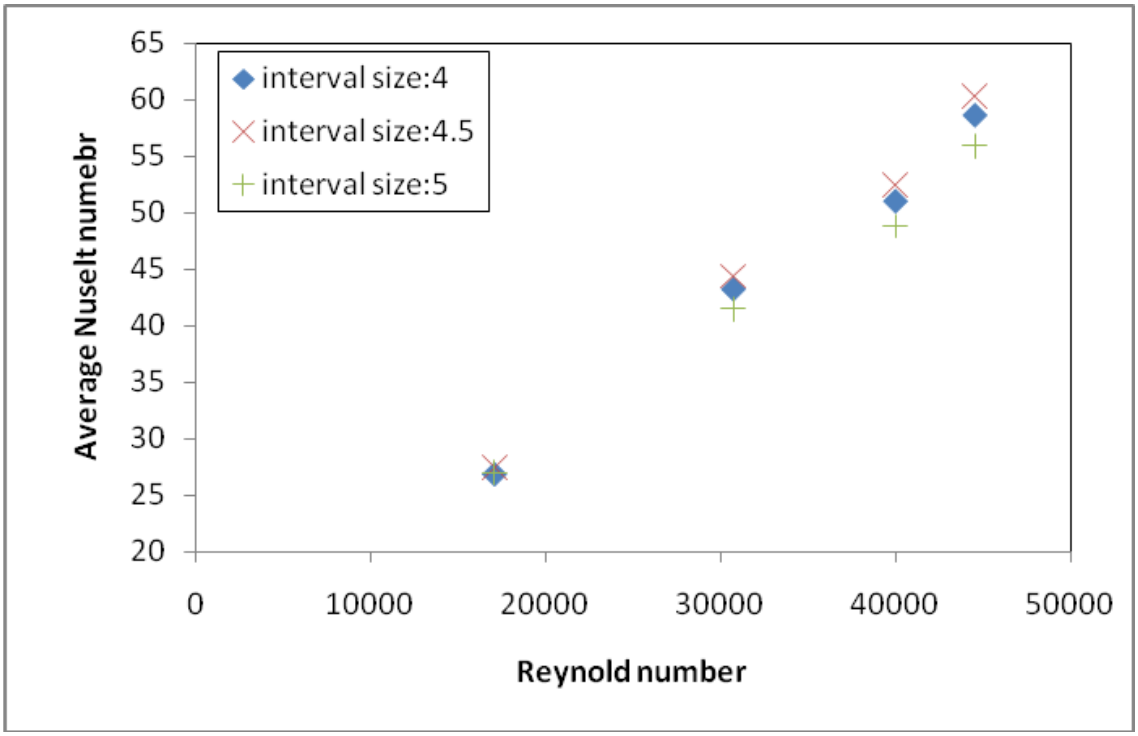

Figure 4.16: Comparison of average Nusselt number over various Reynolds numbers at s=18.5 mm and q=2098 W/m^2.

4.1.2 Surface Roughness

In the simulation process, the temperature behavior shows negligible influence by the different surface roughness. Figure 4.17 show no difference in the themperature distubution of the four different roughness heights of 0.25 µm to 2.9 µm. Figure 4.18 also shows that the increase in surface roughness have no or neglegible effect on the average temperature in the simulations. The results show that there are no significant influence of surface roughness in the simulation results.

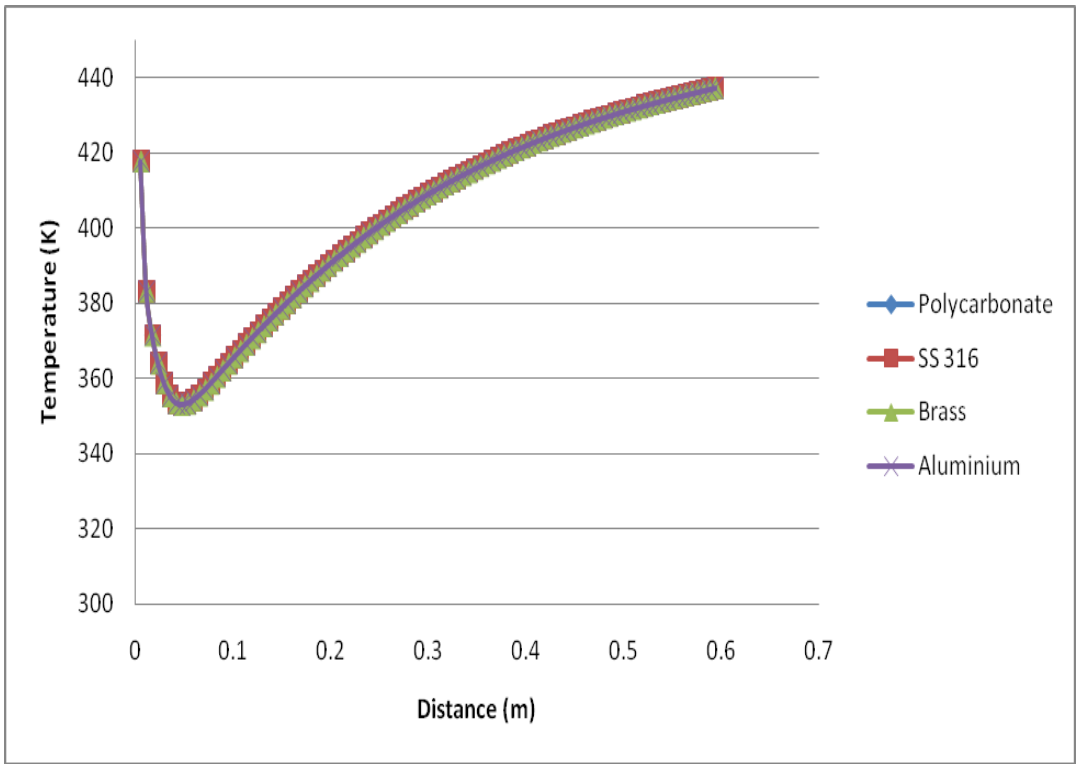

Figure 4.17: Graphical representation of temperature versus distance for various surface roughnesses.

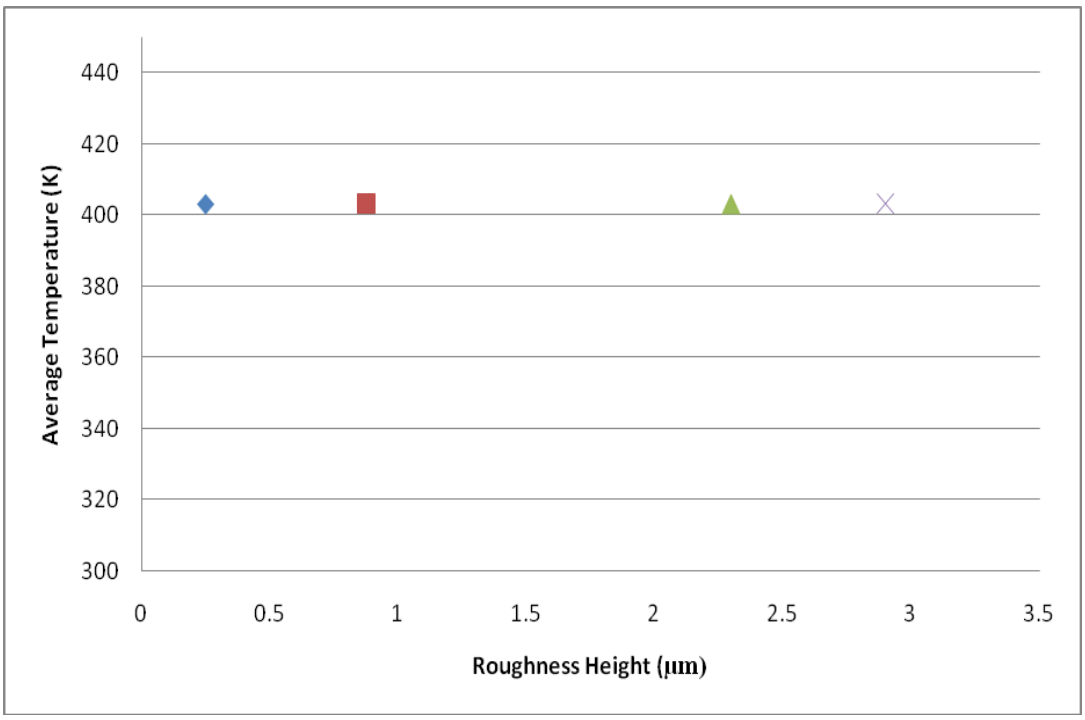

Figure 4.18: Graph of average temperature versus roughness height for different materials.

4.2 Numerical simulation of base fluid and nanofluids in an annular passage

Simulation were conducted over a straight annular passage with a different step height s = 0 and 13.5 mm maintained against expansion ratios of d/D =1 and 1.80 respectively. The test section outer tube for heat flux was constant q=49050 W/m^2. Generally, the surface temperature along the test pipe may be affected by many variables, such as concentration, heat flux, velocity and the step height of the test pipe.

4.2.1 Numerical simulation of base fluid and nanofluids for 0 step height

The temperature variations at 0 step height simulation are presented graphically in figure 4.19. There is no separation observed in the present case, after the fully developed flow reached the heat wall, surface temperature increases along the pipe.

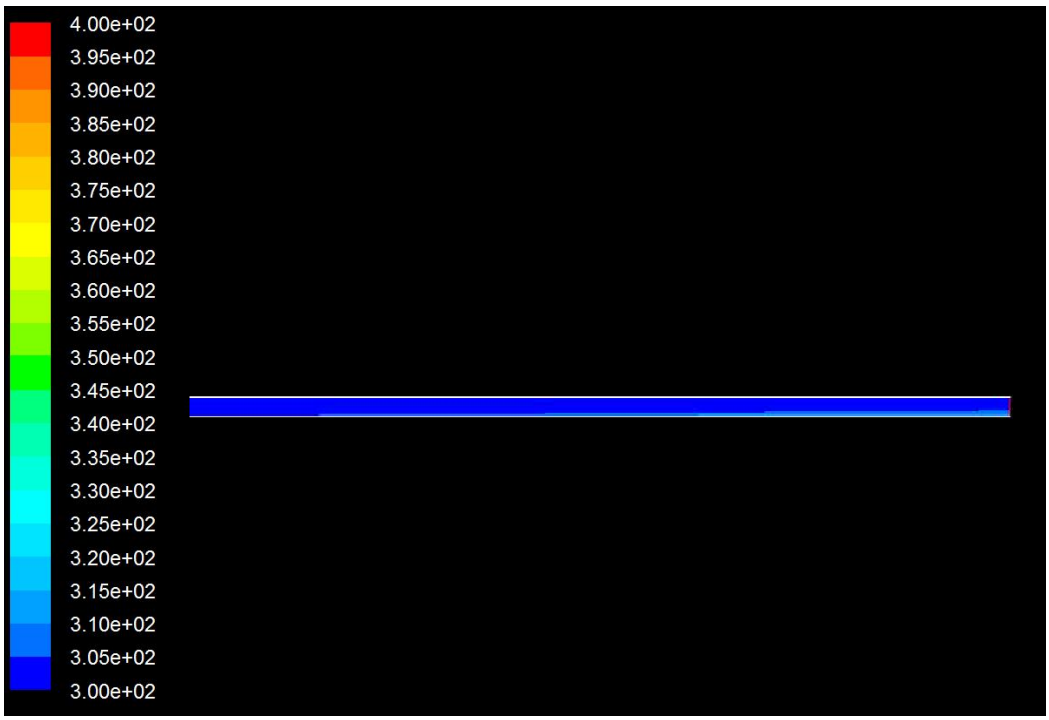

Figure 4.19: Temperature variation along the test section with wall heat flux of 49 050 W/m^2 (0 step height).

Figure 4.20 shows the variation of the surface temperature along the test section for 0 step height with various Reynolds number of 17050, 30720, 39992 and 44545 at heat flux of 49050 W/m^2. The general shape shows increment of surface temperature following the same pattern. The minimum magnitude of temperature is obtained at a zero distance where the flow reattaches the heated surface. Then the temperature undergoes sharp increment and gradually increases along the pipe.

Figure 4.21 shows the distribution of the local heat transfer coefficient at 0 step height and constant heat flux of q=49050 W/m^2 for different Reynolds numbers. It shows the effect of the different Reynolds number on the heat transfer coefficient. It is observed that with high heat transfer coefficient decreases sharply at 0 to 0.2 m then reduces gradually along the test section. Figure 4.22 shows the distribution of Nusselt numbers versus distance at different Reynolds numbers, constant heat flux q=49050 and step height=0. The trends of Nusselt number are found similar to that of heat transfer coefficient.

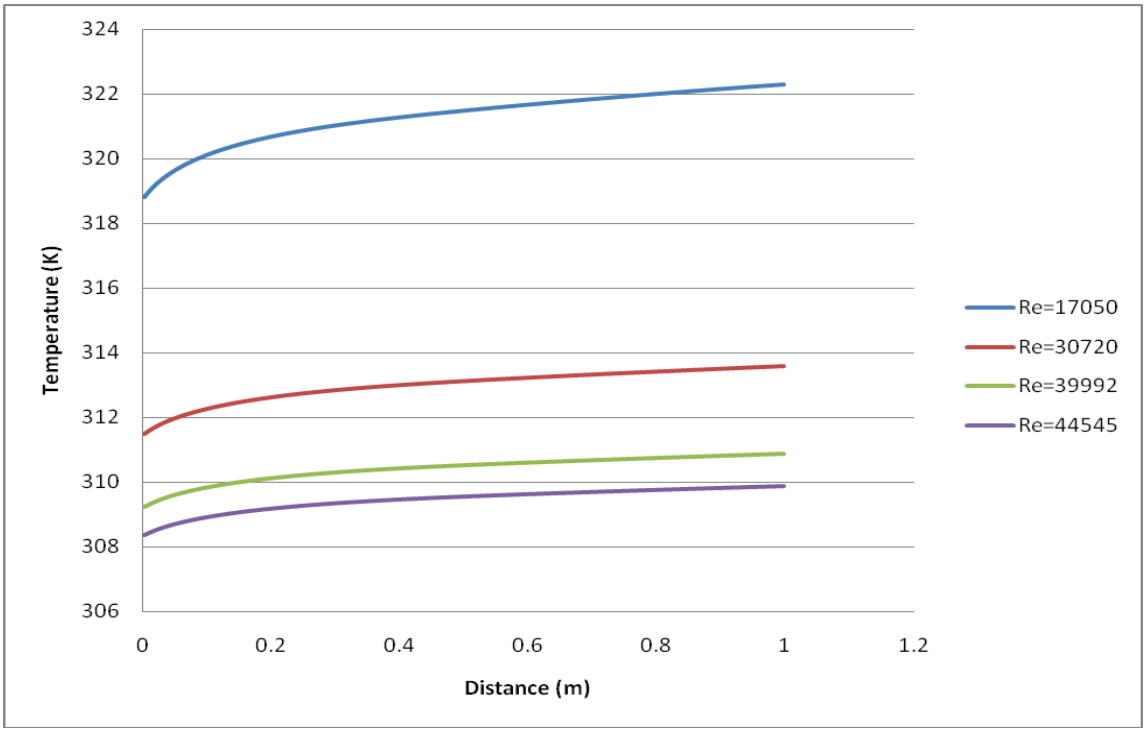

Figure 4.20: Graph of temperature versus distance for water at various Reynolds numbers (at heat flux=49050 and step height=0).

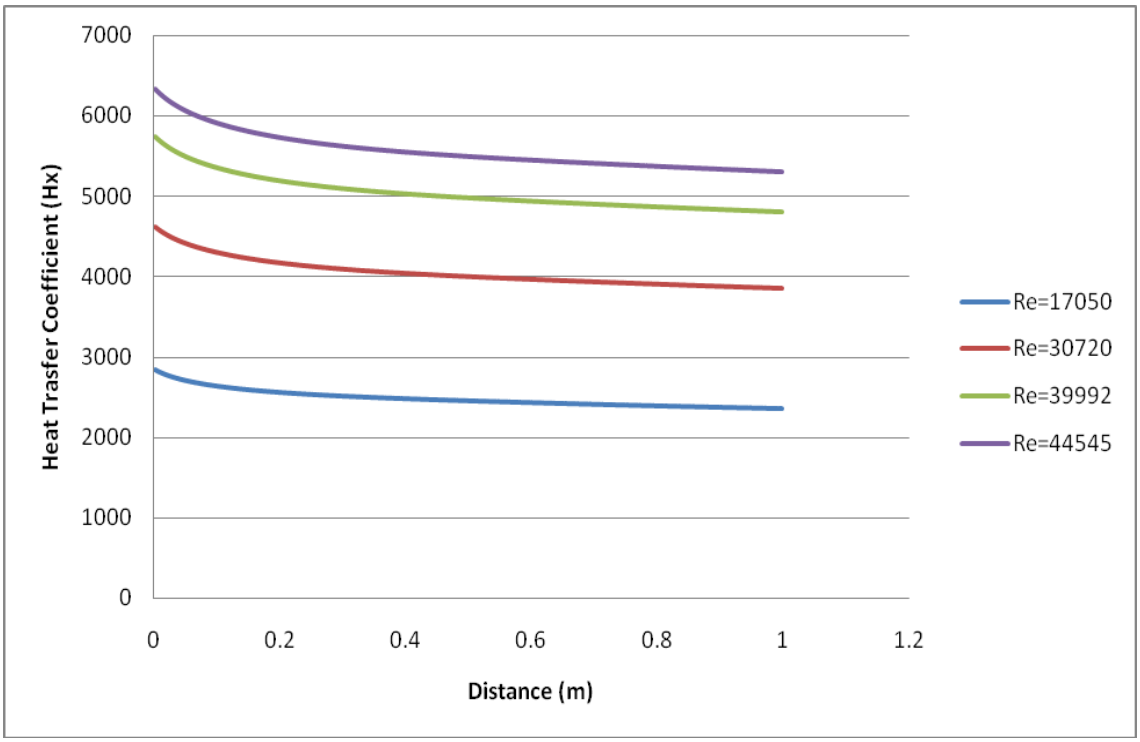

Figure 4.21: Graph of heat transfer coefficeint versus distance for water at various Reynolds numbers (at heat flux=49050 and step height=0).

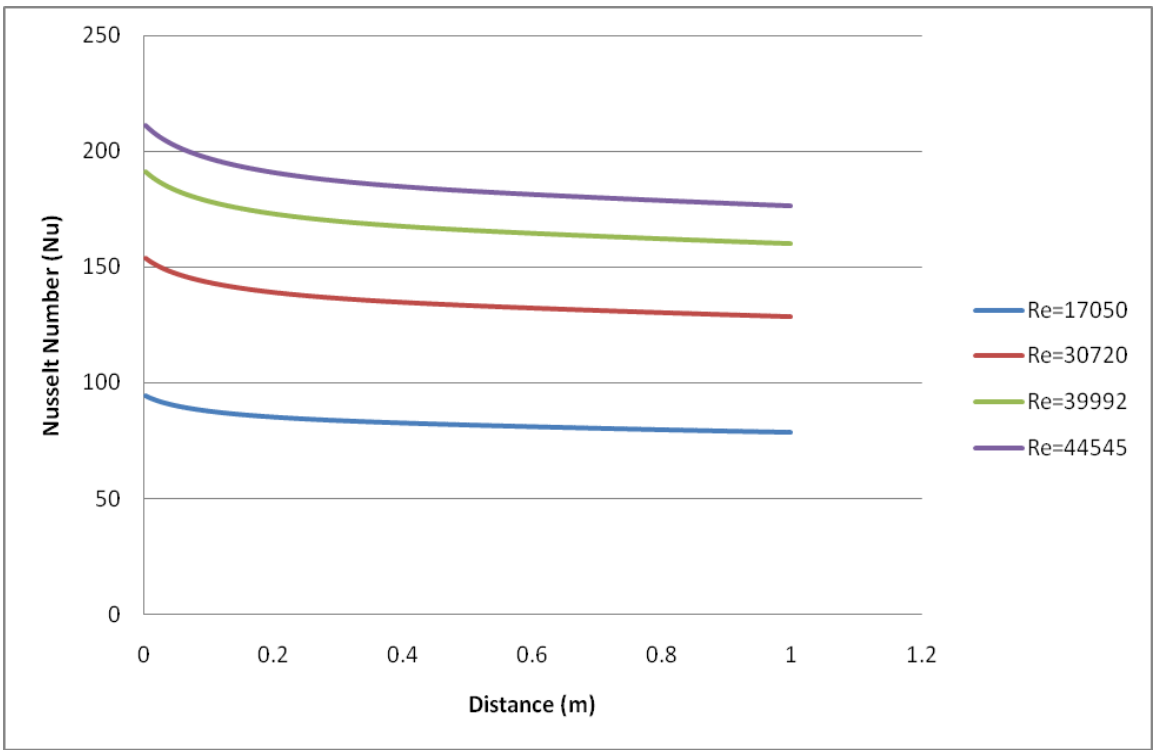

Figure 4.22: Graph of Nusselt number versus distance for water at various Reynolds numbers (at heat flux=49050 and step height=0).

Further, the simulations were carried out by employing the single phase model for volume concentrations of φ = 1%, 2%, 3% and 4%, Reynolds number, Re = 17050, heat flux, q = 49050 W/m^2 and at 0 step height. Figure 4.23 presents comparison of temperature variations at different Al_2O_3 concentrations of nanofluids. It is observed in figure 4.23 that the temperature increases with the increase of φ. The curves show similar pattern for all the concentrations. Figure 4.24 shows the heat transfer coefficient versus distance for the same concentration parameters. The highest heat transfer coefficient is obtained at the concentration φ=1% of Al_2O_3. The heat transfer coefficient curve decreases when the concentration increases from 1% to 4 %. Figure 4.25 shows the Nusselt number versus distance for the same oncentration parameters. Again, the 1% concentration shows the highest Nusselt number. Then, the Nusselt number decreases when the concentration increases. Both heat transfer coefficient and Nusselt number shows the similar trend because both temperature different and thermal conductivity increases with the increase of nano particle concentration in the suspension. Thus

overall heat transfer increases with the increase of particle concentration in the nanofluid.

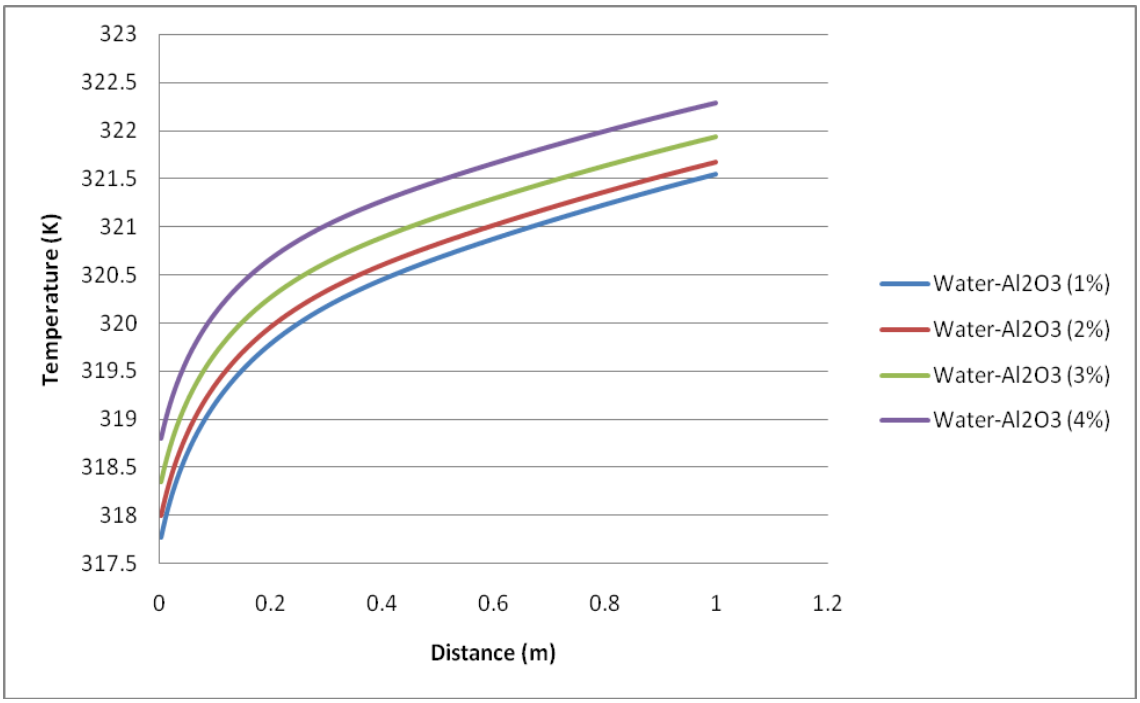

Figure 4.23: Graph of Temperature versus distance for water Al_2O_3 nanofluids with different concentrations (at heat flux of 49050W/m2 and step height=0).

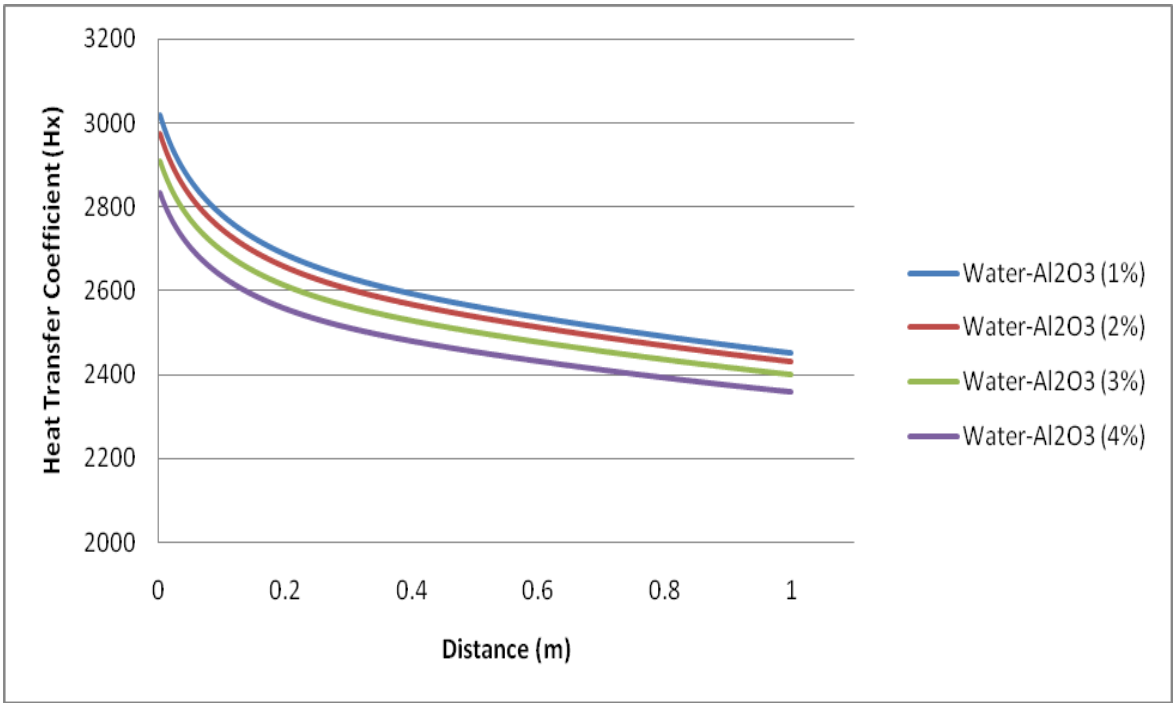

Figure 4.24: Graph of heat transfer coefficient versus distance for water Al_2O_3 nanofluids with different concentration (heat flux of 49050W/m2, step height=0).

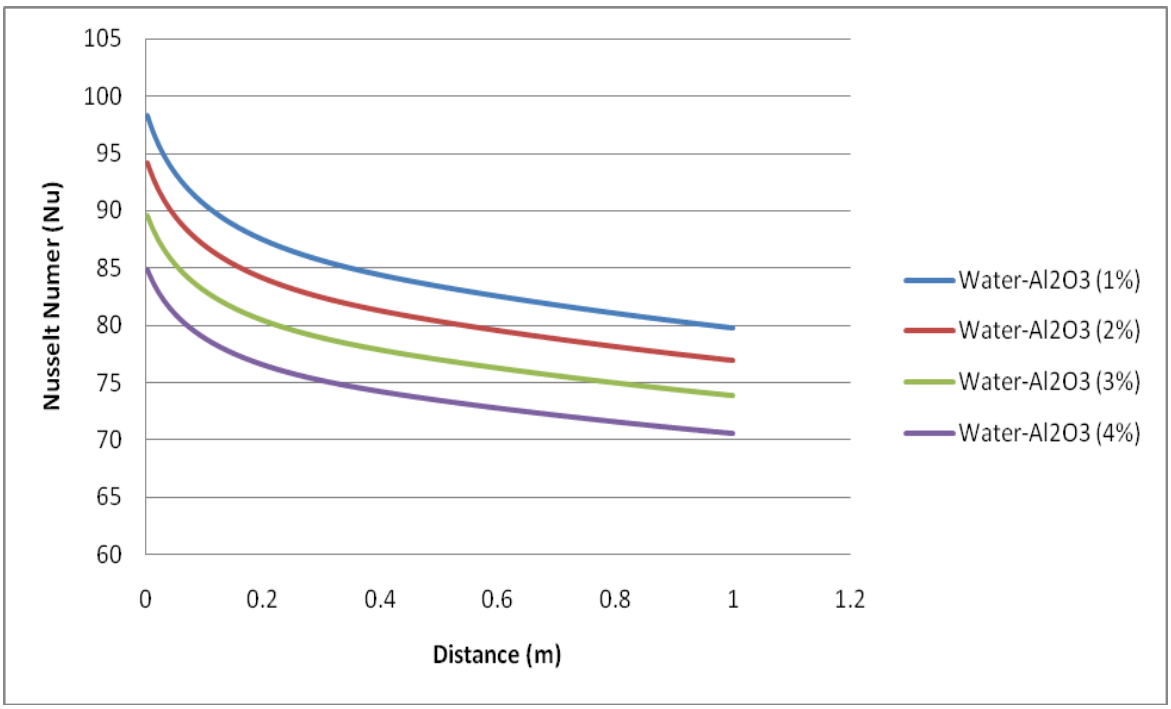

Figure 4.25: Graph of nusselt number versus distance for water Al_2O_3 nanofluids with different concentrations (at heat flux of 49050W/m2 and step height=0).

4.2.2 Numerical simulation of base fluid and nanofluids at 13.5 mm step height

The temperature variations at 13.5 mm step height simulation are presented graphically in figure 4.26.

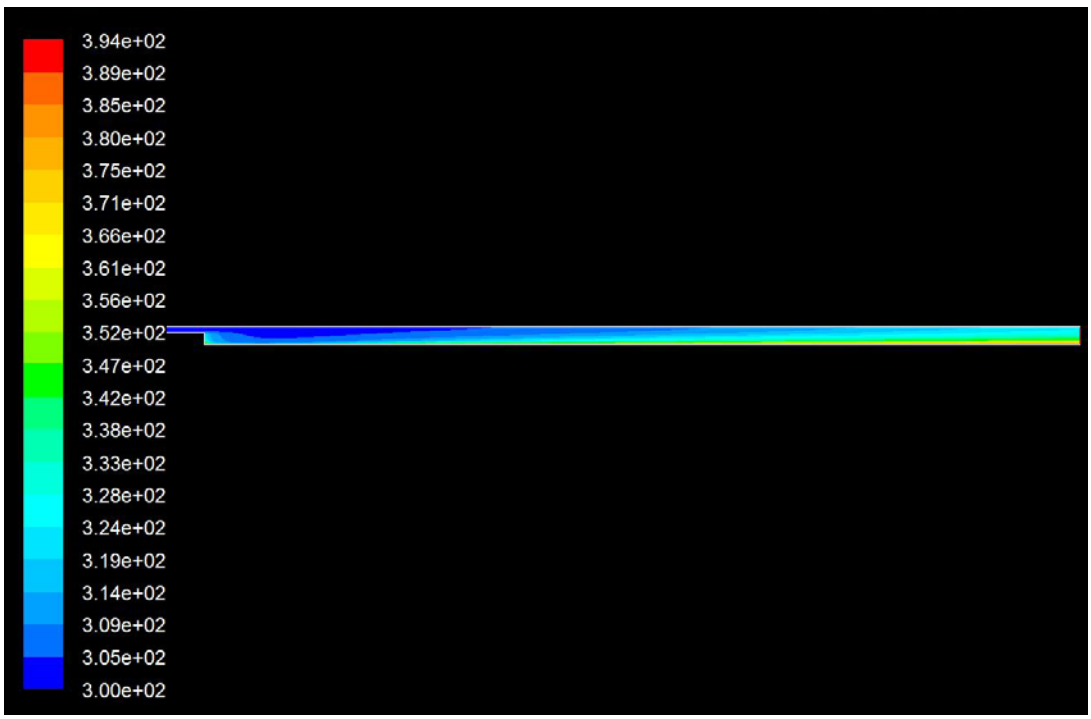

Figure 4.26: Temperature variation along the test section with wall heat flux of 49 050 W/m^2 (at 13.5 mm step height).

Figure 4.26, shows the variation of the surface temperature along the test section at 13.5 mm step height with various Reynolds numbers of 17050, 30720, 39992 and 44545 with heat flux of 49050 W/m^2. The general shape shows increment of surface temperature of the same pattern. The minimum magnitude of temperature is obtained at 0.05 m from step where the flow reattachment happens. Then the temperature decreases to a minimum point then gradually increases along the pipe. Reynolds number of 17050 shows the highest temperature and decreases as the Reynolds number increases due to augmentation of heat transfer with increase of Reynolds number. The region of heat transfer augmentations is found to be the distance of ten times diameter of outer diameter from the expansion.

Figure 4.28 shows the distribution of the local heat transfer coefficient at 13.5 mm step height and constant heat flux of q=49050 W/m^2 for different Reynolds numbers. It shows the effect of the different Reynolds numbers on the heat transfer coefficient. It started with high heat transfer coefficient and decreases sharply before 0.05 m from the expansion then increases gradually along the test tube. Reynolds number of 44545 shows the highest heat transfer coefficient which decreases with the increase of Reynolds number. The heat transfer coefficient increase at 0.1 m from the expansion is an intervallic vortex shedding followed by the reattachment at the corner area of the recirculation zone. Also, the process of fresh fluid intervallic “filling” and “emptying” the recirculation zone may contribute to the dramatic increase in local Nusselt number. Figure 4.29 shows the distribution of Nusselt numbers versus distance at different Reynolds numbers at constant heat flux q=49050 and step height=13.5 mm. The trends of Nusselt number variations are found to be similar to those of heat transfer coefficient.

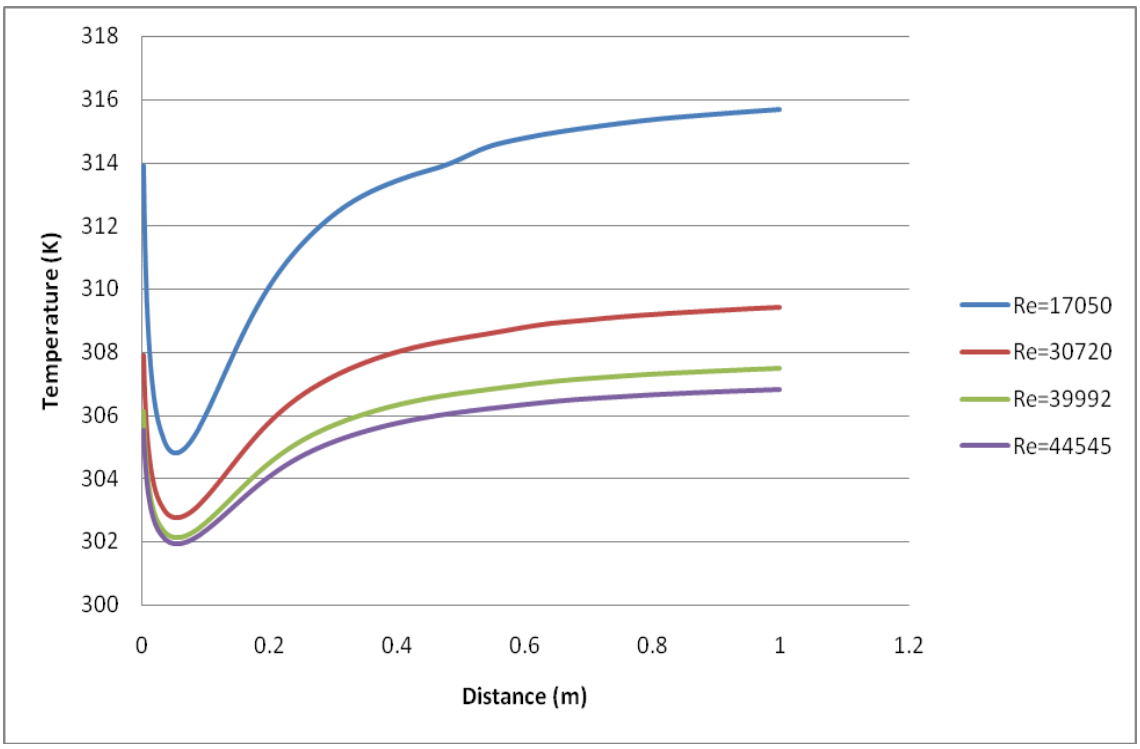

Figure 4.27: Graphical representation of temperature versus distance for water at various Reynolds numbers (at heat flux=49050).

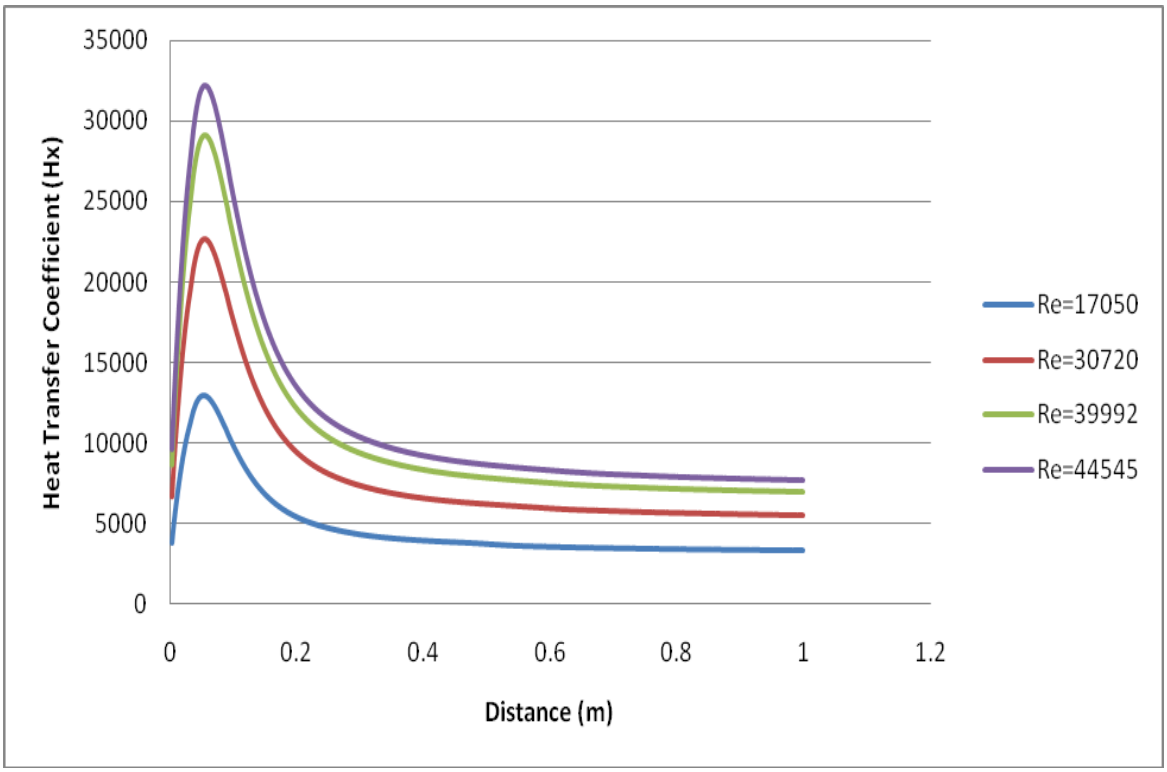

Figure 4.28: Graphical representation of Heat Transfer Coefficient versus distance at different Reynolds numbers at heat flux of 49050 W/m^2.

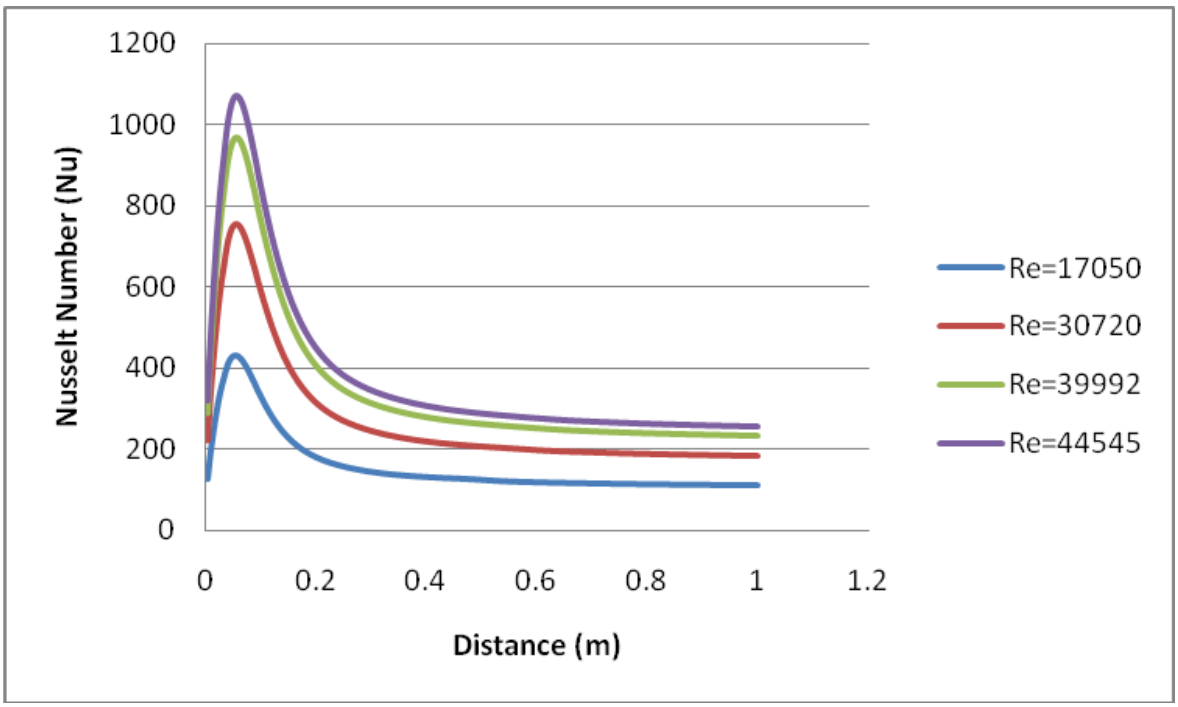

Figure 4.29: Variation of Nusselt Number as a function of distance at different Reynolds numbers at heat flux of 49050 W/m^2.

Subsequently, the simulations were carried out by employing the single phase model for volume concentrations, φ of 1%, 2%, 3% and 4%, Reynolds number, Re = 17050, heat flux, q = 49050 W/m^2 and 13.5 mm step height. Figure 4.30 represents the comparison of temperatures corresponding to the concentrations. It was observed figure 4.30 that the temperature increases with the increase of the concentration, φ. The curves show similar pattern for all the concentrations. Figure 4.31 shows the heat transfer coefficient versus distance for the same parameters as presented in Figure 4.30. The highest heat transfer coefficient is obtained at concentration, φ of 1% of Al_2O_3. The temperature decreases with the increase of concentration from 1% to 4 %. This is due to the presence of nanoparticles enhances thermal conduction under macroscopically static conditions. Figure 4.32 shows the Nusselt number versus distance for the same parameters as in Figure 4.30. Again, at 1% concentration the highest Nusselt number is obtained. Then, the Nusselt number decreases with the increase of concentration of both the heat transfer coefficient and the Nusselt number which show the similar trend.

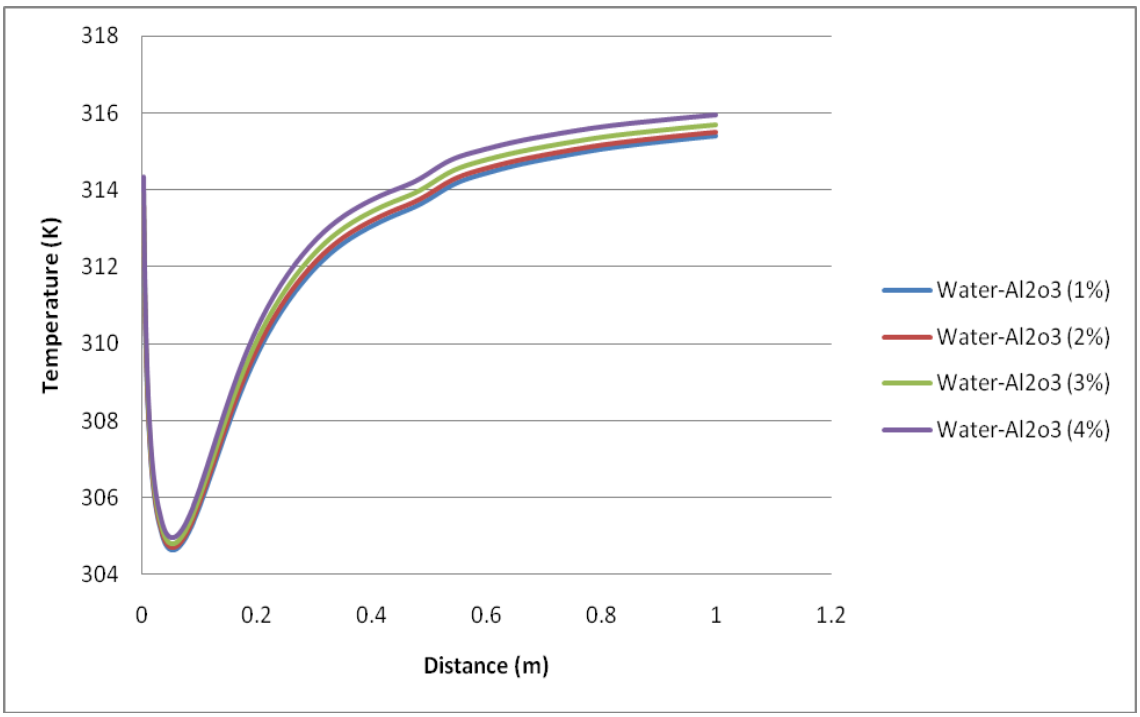

Figure 4.30: Temperature variation as a function of versus distance for water Al_2O_3 nanofluids at different concentrations and at heat flux of 49050W/m^2.

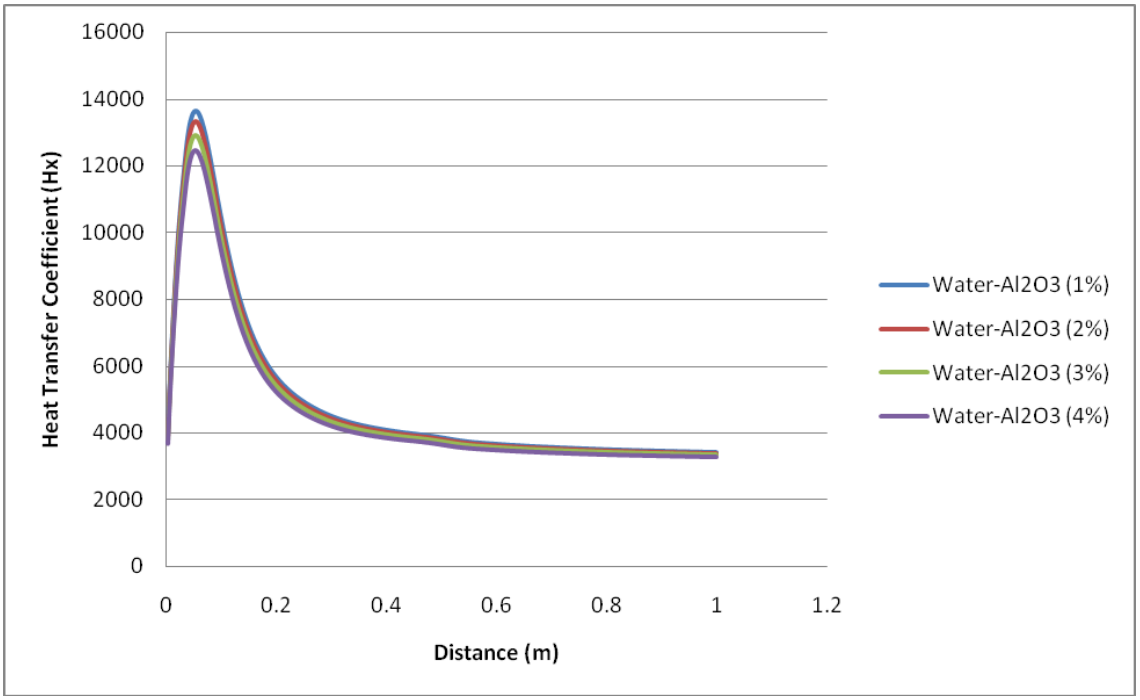

Figure 4.31: Graphical representation of Heat Transfer Coefficient as a function of distance for water Al_2O_3 nanofluids at different concentrations and at heat flux of 49050W/m^2.

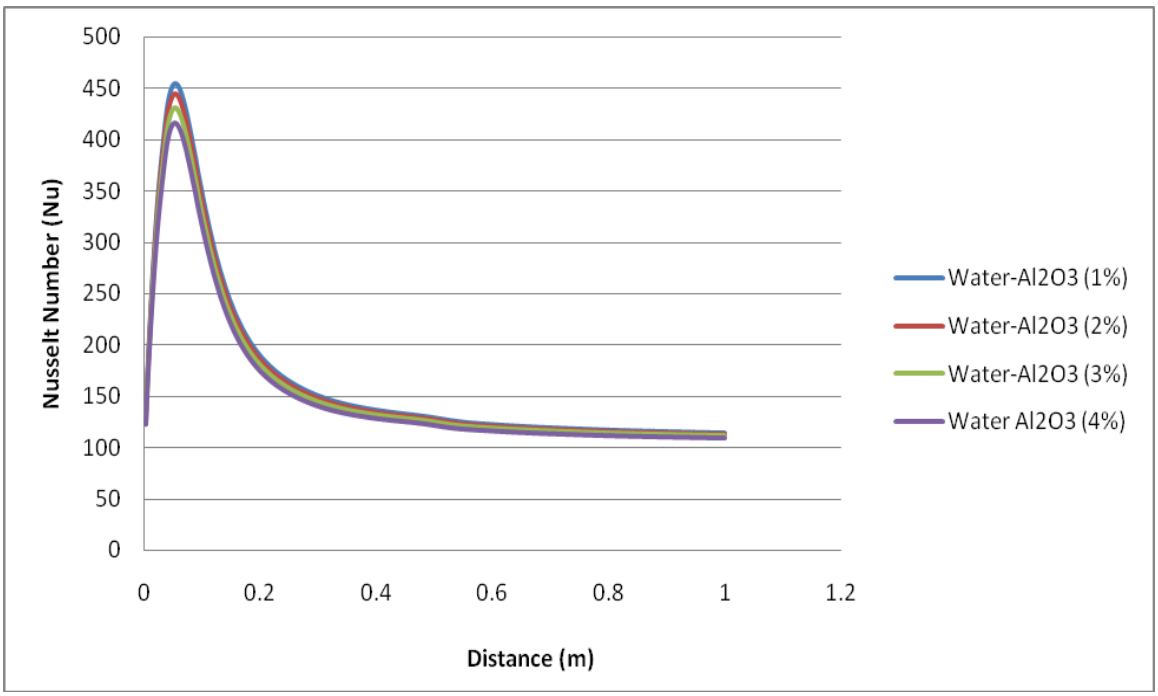

Figure 4.32: Nusselt Number variation with distance for water Al_2O_3 nanofluids at different concentrations and at heat flux of 49050W/m^2.

Average Nusselt number (Nu_{avg}) as function of Reynolds number along the test section for different step heights are shown in figure 4.33. The result represents increase of Nusselt number following the dimensions of different step heights. By increasing the Reynolds number, higher value of average Nusselt number was obtained. The increase of step height also induces higher average Nusselt number.

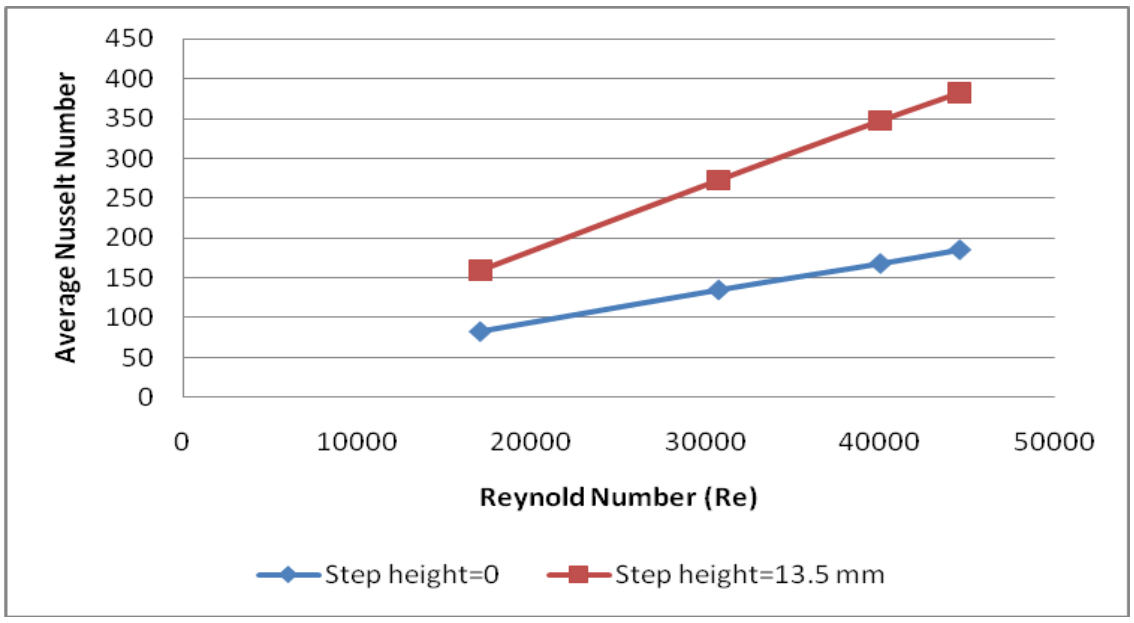

Figure 4.33: Average Nusselt number as a function of Reynolds number at different step heights.

Figure 4.34 shows the variation of the surface temperature along the test section for different types of nanofluids at a specific Re = 44545 and q = 49050 w/m^2. The common curve shows a reduction of surface temperature to a specific point and then increases though out the pipe. The minimum magnitude of temperature is obtained at a specific distance where the flow reattachment appears. The reattachment point also marked as the onset of augmentation of heat transsfer. Al_2O_3 shows lower average temperature compared to other nanofluids due to lower thermal conductivity of Aluminium in comparison to other considered metals.

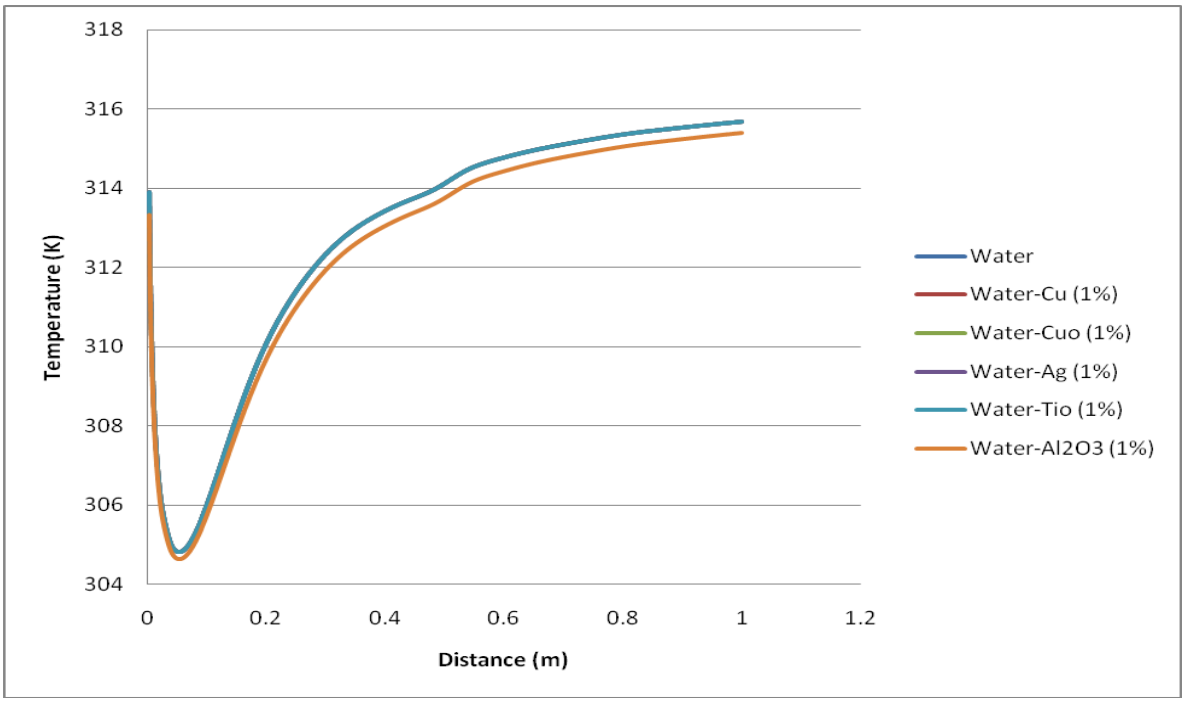

Figure 4.34: Graphical presentation of temperature versus distance for different types of nanofluids at 1% nano particles concentration (at heat flux of 49050 W/m^2).

Attention to nanofluids as advanced heat transfer fluids was initially based on the increased thermal conductivity of nanoparticle suspensions. It is not always realized that the thermal conductivity is not the only property that determines the efficiency of heat transfer fluid in practical applications. In the forced flow systems the coolant is pumped through the pipes of a heat exchanger, introducing convective heat transfer mechanisms and pumping power penalties. Therefore the convective heat transfer

coefficient becomes more important than the thermal conductivity value. Evaluation of cooling efficiency, i.e. ability of the heat transfer fluid to remove heat from the heat source depends on the flow regime and includes assessment of contributions from thermal conductivity, viscosity, specific heat, and density of the fluid and can be estimated from the fluid dynamics equations in assumption of a single phase flow. High viscosity of nanofluids compared to base fluid increases the power required to pump the fluid through the system. When the benefit of the increased heat transfer is larger than the penalty of the increased pumping power, the nanofluid has the potential for commercial viability. In turbulent flow regime the heat transfer rate (based on the Dittus-Boelter equation for heating applications) is dependent not only upon the thermal conductivity (k), but also on the density (ρ), specific heat (cp), viscosity (μ) and flow velocity (V). Introduction of nanoparticles to the fluid affects all of thermo-physical properties and should be accounted for in the nanofluid evaluations. Density and specific heat are proportional to the volume ratio of solid and liquid in the system, generally with density increasing and specific heat decreasing with addition of solid nanoparticles to the fluid. The increase in density, specific heat and thermal conductivity of nanofluids favors the heat transfer coefficient; however the well described increase in the viscosity of nanoparticle suspensions is not beneficial for heat transfer. The velocity term also represents the pumping power penalties resulting from the increased viscosity of nanofluids. It is obvious that nanofluids are multivariable systems, with each thermo-physical property dependent on several parameters including nanoparticle material, concentration, size, and shape, properties of the base fluid, and presence of additives, surfactants, electrolyte strength, and pH. Thus, the challenge in the development of nanofluids for heat transfer applications is in understanding of how micro- and macro-scale interactions between the nanoparticles and the fluid affect the properties of the suspensions.

CHAPTER 5: Conclusions

Numerical simulations were conducted for expansion ratios of d/D = 1, 1.16, 1.53 and 1.80. The parameters varied are heat flux, q=719 W/m^2, 968 W/m^2, 1458 W/m^2, and 2098 W/m^2 and also Reynolds number, Re=17050, 30720, 39992, and 44545.

The mesh interval size of 6 is suitable for the specific dimension of the pipe as it is capable of determining heat transfer coefficient and Nusselt number. Mesh interval size of 6 shows good agreement in achieving surface temperature along the test pipe with 8.99 % error. Standard k–ε model is suitable for the investigation as it offers better result in calculating the surface temperatures compared to RNG and realizable models. Standard k–ε is able to predict position of reattachment point and surface temperature more accurately. Thus, the standard k–ε model is suitable for investigating turbulent flow in sudden expansion annular passage in the present case of simple and axisymmetric geometry.

The increase of flow reduces the surface temperature along the pipe to a minimum point then increases through the rest of the pipe. The minimum surface temperature is obtained at flow reattachment point. The position of the minimum temperature point is dependent on the flow velocity over sudden expansion. Generally, the local Nusselt number (Nu) increases with the increase of the Reynolds number.

Simulations were conducted for an annular passage with different step heights and expansion ratios. Generally, the surface temperature along the test pipe may be

affected by many variables, such as concentration, heat flux, velocity and the step height of the test pipe.

Numerically the effect of backward facing step in an annular passage flow separation on heat transfer for the two dimensional axisymmetric turbulent flow is studied. Then the influence of variable parameters such as wall heat flux, fluid flow velocity, separation step height and various fluids on heat transfer characteristic is determined. The augmentation of heat transfer in the distance of 4 diameters in air and 10 diameters in water after expansion is suggested to increase the performance of heat exchangers based on the simulation design and parameters.

Heat transfer coefficient of nanofluids increases with increase in the volume concentration of nanofluids and Reynolds number. Higher temperature operation of the nanofluids yields higher percentage increase in heat transfer rate. Increase of velocity and step height causes the surface temperature reduction up to a specific point (lowest temperature) along the test section and then increases. This lowest temperature represents the flow reattachment point. The position of this lowest temperature is mainly a function of step height.

The local heat transfer coefficient (hx) increases with increase of the Reynolds number for all cases of step heights. In the separation region (recirculation zone) the local heat transfer coefficient improves until it reaches a maximum value at the reattachment point. Average Nusselt number decrease with increase of the concentration of nanofluids due to increase of thermal conductivity of the suspension. Nusselt number increases with the increase of Reynolds number for all concentrations. Finally, with the

advent of computational fluid dynamic software (Fluent), it could provide fair and agreeable results for the present research.

List of Publications and Awards

Academic Journals

1. Numerical Simulation of Heat Transfer to Separation Air Flow in an Annular Pipe. International Communications in Heat and Mass Transfer. 2012 (Published; ISI-Cited Publication, Q1)

2. Performance investigation of a power augmented vertical axis wind turbine for urban high-rise application. Renewable Energy. 2013 (Published; ISI-Cited Publication, Q2)

3. Exhaust Air and Wind Energy Recovery System for Clean Energy Generation, International Journal of Environmental Sciences and Development. 2011 (Published, ISI-Cited Publication)

Proceedings

1. A Computational Simulation of Heat Transfer to Separation Air Flow in a Concentric Pipe. International Conference on Applications and Design in Mechanical Engineering (ICADME). Penang. 27-28 February 2012. (Published; ISI-Cited Publication)

2. Vertical axis wind turbine with omni-directional-guide-vane for urban high rise application. International Conference of WREC-Asia & SuDBE2011, Chongqing, China 28-31 October 2011 (Published, ISI-Cited Publication)

3. Exhaust Air and Wind Energy Recovery system for Clean Energy Generation. Proceedings of International Conference on Environment and Industrial Innovation (ISI Proceedings). Kuala Lumpur. 4-5 June 2011. (Published, ISI/SCOPUS Cited Publication)

Award

1. Malaysia Technology Expo Gold Medal award. (Exhaust Air / Wind Energy Recovery System) 17-19 February 2011, Kuala Lumpur.

References

ABBASSI, H. & BEN NASSRALLAH, S. 2007. MHD flow and heat transfer in a backward-facing step. *International Communications in Heat and Mass Transfer,* 34**,** 231-237.

ABE, K., KONDOH, T. & NAGANO, Y. 1994. A new turbulence model for predicting fluid flow and heat transfer in separating and reattaching flows—I. Flow field calculations. *International Journal of Heat and Mass Transfer,* 37**,** 139-151.

ABE, K., KONDOH, T. & NAGANO, Y. 1995. A new turbulence model for predicting fluid flow and heat transfer in separating and reattaching flows—II. Thermal field calculations. *International Journal of Heat and Mass Transfer,* 38**,** 1467-1481.

ABU-MULAWEH, H. I. 2003. A review of research on laminar mixed convection flow over backward- and forward-facing steps. *International Journal of Thermal Sciences,* 42**,** 897-909.

ABU-NADA, E. 2008. Application of nanofluids for heat transfer enhancement of separated flows encountered in a backward facing step. *International Journal of Heat and Fluid Flow,* 29**,** 242-249.

AHN, J. W., PARK, T. S. & SUNG, H. J. 1997. Application of a near-wall turbulence model to the flows over a step with inclined wall. *International Journal of Heat and Fluid Flow,* 18**,** 209-217.

AL-ASWADI, A. A., MOHAMMED, H. A., SHUAIB, N. H. & CAMPO, A. 2010. Laminar forced convection flow over a backward facing step using nanofluids. *International Communications in Heat and Mass Transfer,* 37**,** 950-957.

ARMALY, B. F., DURST, F., PEREIRA, J. C. F. & SCHOENUNG, B. 1983a. EXPERIMENTAL AND THEORETICAL INVESTIGATION OF BACKWARD-FACING STEP FLOW. *Journal of Fluid Mechanics,* 127**,** 473-496.

ARMALY, B. F., DURST, F., PEREIRA, J. C. F. & SCHÖNUNG, B. 1983b. Experimental and theoretical investigation of backward-facing step flow. *Journal of Fluid Mechanics,* 127**,** 473-496.

AUNG, W., BARON, A. & TSOU, F. K. 1985. WALL INDEPENDENCY AND EFFECT OF INITIAL SHEAR-LAYER THICKNESS IN SEPARATED FLOW AND HEAT-TRANSFER. *International Journal of Heat and Mass Transfer,* 28**,** 1757-1771.

BARTON, I. E. 1997. Laminar flow over a backward-facing step with a stream of hot particles. *International Journal of Heat and Fluid Flow,* 18**,** 400-410.

BIANCO, V., CHIACCHIO, F., MANCA, O. & NARDINI, S. 2009. Numerical investigation of nanofluids forced convection in circular tubes. *Applied Thermal Engineering,* 29**,** 3632-3642.

BIANCO, V., MANCA, O. & NARDINI, S. 2011. Numerical investigation on nanofluids turbulent convection heat transfer inside a circular tube. *International Journal of Thermal Sciences,* 50**,** 341-349.

BRINKMAN, H. C. 1952. The Viscosity of Concentrated Suspensions and Solutions. *Journal of Chemical Physics,* 20**,** 571-581.

BSEBSU, F. M. & BEDE, G. 2002. Theoretical study in single-phase forced-convection heat transfer characteristics for narrow annuli fuel coolant channels. *periodica polytechnica ser. Mech. Eng* 46**,** 15–27.

CHEN, C.-K., YEN, T.-S. & YANG, Y.-T. 2006a. Lattice Boltzmann method simulation of backward-facing step on convective heat transfer with field

synergy principle. *International Journal of Heat and Mass Transfer,* 49**,** 1195-1204.

CHEN, Y. T., NIE, J. H., HSIEH, H. T. & SUN, L. J. 2006b. Three-dimensional convection flow adjacent to inclined backward-facing step. *International Journal of Heat and Mass Transfer,* 49**,** 4795-4803.

CHOWDHURY, S. J. & AHMADI, G. 1992. A thermodynamically consistent rate-dependent model for turbulence—part II. Computational results. *International Journal of Non-Linear Mechanics,* 27**,** 705-718.

CHUN, K. B. & SUNG, H. J. 1996. Control of turbulent separated flow over a backward-facing step by local forcing. *Experiments in Fluids,* 21**,** 417-426.

D.WEN, Y. D. 2004. Experimental investigation into convective heat transfer of nanofluids at the entrance region under laminar flow conditions. *Int. J. Heat MassTransfer***,** 5181-5188.

DAS, S. K., CHOI, S. U. S. & PATEL, H. E. 2006a. Heat Transfer in Nanofluids—A Review. *Heat Transfer Engineering,* 27**,** 3-19.

DAS, S. K., CHOI, S. U. S. & PATEL, H. E. 2006b. Heat transfer in nanofluids - A review. *Heat Transfer Engineering,* 27**,** 3-19.

DUANGTHONGSUK, W. & WONGWISES, S. 2009. Heat transfer enhancement and pressure drop characteristics of TiO2-water nanofluid in a double-tube counter flow heat exchanger. *International Journal of Heat and Mass Transfer,* 52**,** 2059-2067.

EIYAD, A.-N. 2008. Application of nanofluids for heat transfer enhancement of separated flows encountered in a backward facing step. *International Journal of Heat and Fluid Flow,* 29**,** 242-249.

FURUICHI, N., HACHIGA, T. & KUMADA, M. 2004. An experimental investigation of a large-scale structure of a two-dimensional backward-facing step by using advanced multi-point LDV. *Experiments in Fluids,* 36**,** 274-281.

GOLDSTEIN, R. J., ERIKSEN, V. L., OLSON, R. M. & ECKERT, E. R. G. 1970. Laminar Separation, Reattachment, and Transition of the Flow Over a Downstream-Facing Step. *Journal of Basic Engineering,* 92**,** 732-739.

HSU, C.-H. & CHOU, T.-Y. 1997. Unsteady flow of a second-grade fluid past a backward-facing step. *International Journal of Non-Linear Mechanics,* 32**,** 947-960.

HWANG, K. S., JANG, S. P. & CHOI, S. U. S. 2009. Flow and convective heat transfer characteristics of water-based Al2O3 nanofluids in fully developed laminar flow regime. *International Journal of Heat and Mass Transfer,* 52**,** 193-199.

IWAI, H., NAKABE, K. & SUZUKI, K. 2000. Flow and heat transfer characteristics of backward-facing step laminar flow in a rectangular duct. *International Journal of Heat and Mass Transfer,* 43**,** 457-471.

KAKAÇ, S. & PRAMUANJAROENKIJ, A. 2009. Review of convective heat transfer enhancement with nanofluids. *International Journal of Heat and Mass Transfer,* 52**,** 3187-3196.

KASAGI, N. & MATSUNAGA, A. 1995. Three-dimensional particle-tracking velocimetry measurement of turbulence statistics and energy budget in a backward-facing step flow. *International Journal of Heat and Fluid Flow,* 16**,** 477-485.

KAZI, S. N., DUFFY, G. G. & CHEN, X. D. 2010. Mineral scale formation and mitigation on metals and a polymeric heat exchanger surface. *Applied Thermal Engineering,* 30**,** 2236-2242.

KEBLINSKI, P., PHILLPOT, S. R., CHOI, S. U. S. & EASTMAN, J. A. 2002. Mechanisms of heat flow in suspensions of nano-sized particles (nanofluids). *International Journal of Heat and Mass Transfer,* 45**,** 855-863.

KHANAFER, K., VAFAI, K. & LIGHTSTONE, M. 2003. Buoyancy-driven heat transfer enhancement in a two-dimensional enclosure utilizing nanofluids. *International Journal of Heat and Mass Transfer,* 46**,** 3639-3653.

KHOEINI, D., AKHAVAN-BEHABADI, M. A. & SABOONCHI, A. 2012. Experimental study of condensation heat transfer of R-134a flow in corrugated tubes with different inclinations. *International Communications in Heat and Mass Transfer,* 39**,** 138-143.

KIM, J.-J. & BAIK, J.-J. 2004. A numerical study of the effects of ambient wind direction on flow and dispersion in urban street canyons using the RNG k–ε turbulence model. *Atmospheric Environment,* 38**,** 3039-3048.

KIM, W. S., TALBOT, C., CHUNG, B. J. & JACKSON, J. D. 2002. Variable Property Mixed Convection Heat Transfer to Air Flowing Through a Vertical Passage of Annular Cross Section: Part 1. *Chemical Engineering Research and Design,* 80**,** 239-245.

KO, S. 1999. A near-wall reynolds stress model for backward-facing step flows. *Journal of Mechanical Science and Technology,* 13**,** 200-210.

KOLACZKOWSKI, S. T., CHAO, R., AWDRY, S. & SMITH, A. 2007. Application of a CFD Code (FLUENT) to Formulate Models of Catalytic Gas Phase Reactions in Porous Catalyst Pellets. *Chemical Engineering Research and Design,* 85**,** 1539-1552.

KOUTMOS, P. & MAVRIDIS, C. 1997. A computational investigation of unsteady separated flows. *International Journal of Heat and Fluid Flow,* 18**,** 297-306.

KREITH, F. & BOHN, M. S. 2001. *Principles of Heat Transfer,* Colorado, Cengage Learning.

KUMAR, A. & DHIMAN, A. K. 2012. Effect of a circular cylinder on separated forced convection at a backward-facing step. *International Journal of Thermal Sciences,* 52**,** 176-185.

KURTBAŞ, İ. 2008. The effect of different inlet conditions of air in a rectangular channel on convection heat transfer: Turbulence flow. *Experimental Thermal and Fluid Science,* 33**,** 140-152.

LAUNDER, B. E. & RODI, W. 1983. THE TURBULENT WALL JET - MEASUREMENTS AND MODELING. *Annual Review of Fluid Mechanics,* 15**,** 429-459.

LEE, D., LEE, J., PARK, H. & KIM, M. 2011. Experimental and numerical study of heat transfer downstream of an axisymmetric abrupt expansion and in a cavity of a circular tube. *Journal of Mechanical Science and Technology,* 25**,** 395-401.

MISSIRLIS, D., YAKINTHOS, K., PALIKARAS, A., KATHEDER, K. & GOULAS, A. 2005. Experimental and numerical investigation of the flow field through a heat exchanger for aero-engine applications. *International Journal of Heat and Fluid Flow,* 26**,** 440-458.

MOHAMMED, H. A., GUNNASEGARAN, P. & SHUAIB, N. H. 2011. Influence of channel shape on the thermal and hydraulic performance of microchannel heat sink. *International Communications in Heat and Mass Transfer,* 38**,** 474-480.

MURATA, A. & IWAMOTO, K. 2011. Heat and fluid flow in cylindrical and conical annular flow-passages with through flow and inner-wall rotation. *International Journal of Heat and Fluid Flow,* 32**,** 378-391.

MURSHED, S. M. S., LEONG, K. C. & YANG, C. 2008. Thermophysical and electrokinetic properties of nanofluids – A critical review. *Applied Thermal Engineering,* 28**,** 2109-2125.

NAIT BOUDA, N., SCHIESTEL, R., AMIELH, M., REY, C. & BENABID, T. 2008. Experimental approach and numerical prediction of a turbulent wall jet over a

backward facing step. *International Journal of Heat and Fluid Flow,* 29**,** 927-944.

OON, C. S., TOGUN, H., KAZI, S. N., BADARUDIN, A., ZUBIR, M. N. M. & SADEGHINEZHAD, E. 2012. Numerical simulation of heat transfer to separation air flow in an annular pipe. *International Communications in Heat and Mass Transfer,* 39**,** 1176-1180.

OTA, T. & KON, N. 1979. Heat transfer in the separated and reattached flow over blunt flat plates —Effects of nose shape. *International Journal of Heat and Mass Transfer,* 22**,** 197-206.

PAK, B. C. & CHO, Y. I. 1998. Hydrodynamic and heat transfer study of dispersed fluids with submicron metallic oxide particles. *Experimental Heat Transfer,* 11**,** 151-170.

Q.LI, Y. X., PROC. 2002. Convective heat transfer performances of fluids with nano - particles. *Int.Heat Transfer Conference,Grenoble,France***,** 483-488.

R.BENMANSOUR, N. G., C.T.NGUYEN 2009. Developing laminar mixed convection of nanofluids in an inclined tube with uniform wall heatflux. *Int.J.Num.Meth. Heat Fluid Flow,* 19**,** 146-164.

RAHGOSHAY, M., RANJBAR, A. A. & RAMIAR, A. 2012. Laminar pulsating flow of nanofluids in a circular tube with isothermal wall. *International Communications in Heat and Mass Transfer,* 39**,** 463-469.

RAJESH KANNA, P. & MANAB KUMAR, D. 2006. Conjugate heat transfer study of backward-facing step flow – A benchmark problem. *International Journal of Heat and Mass Transfer,* 49**,** 3929-3941.

REA, U., MCKRELL, T., HU, L. W. & BUONGIORNO, J. 2009. Laminar convective heat transfer and viscous pressure loss of alumina-water and zirconia-water nanofluids. *International Journal of Heat and Mass Transfer,* 52**,** 2042-2048.

ROUIZI, Y., FAVENNEC, Y., VENTURA, J. & PETIT, D. 2009. Numerical model reduction of 2D steady incompressible laminar flows: Application on the flow over a backward-facing step. *Journal of Computational Physics,* 228**,** 2239-2255.

S.Z.HERIS, S. G. E., M.N.ESFAHANY, 2006. Exprimental invistegation of oxide nanofluids laminar flow convective heat transfer. *Int.Commun.Heat Mass Transfer***,** 529-535.

TEREKHOV, V. I. & PAKHOMOV, M. A. 2009. Predictions of turbulent flow and heat transfer in gas–droplets flow downstream of a sudden pipe expansion. *International Journal of Heat and Mass Transfer,* 52**,** 4711-4721.

TIHON, J., PĚNKAVOVÁ, V., HAVLICA, J. & ŠIMČÍK, M. The transitional backward-facing step flow in a water channel with variable expansion geometry. *Experimental Thermal and Fluid Science*.

TOGUN, H., SALMAN, Y. K., SULTAN ALJIBORI, H. S. & KAZI, S. N. 2011. An experimental study of heat transfer to turbulent separation fluid flow in an annular passage. *International Journal of Heat and Mass Transfer,* 54**,** 766-773.

TOTA, P. V. 2009. *Turbulent Flow Over a Backward-Facing Step Using the RNG k-ε Model* [Online]. Available: www.flow3d.com/pdfs/tn/FloSci-TN81.pdf [Accessed].

URUBA, V., JONÁŠ, P. & MAZUR, O. 2007. Control of a channel-flow behind a backward-facing step by suction/blowing. *International Journal of Heat and Fluid Flow,* 28**,** 665-672.

WASP, E. J., KENNY, J. P. & GANDHI, R. L. 1977. *Solid-liquid flow slurry pipeline transportation,* Clausthal, Germany, Trans Tech Publications.

WEN, D. & DING, Y. 2004. Experimental investigation into convective heat transfer of nanofluids at the entrance region under laminar flow conditions. *International Journal of Heat and Mass Transfer,* 47**,** 5181-5188.

WILLIAMS, W., BUONGIORNO, J. & HU, L.-W. 2008. Experimental Investigation of Turbulent Convective Heat Transfer and Pressure Loss of Alumina/Water and Zirconia/Water Nanoparticle Colloids (Nanofluids) in Horizontal Tubes. *Journal of Heat Transfer,* 130**,** 042412-7.

WU, T.-H., XU, Z. & JACKSON, J. D. 2002. Mixed Convection Heat Transfer to Water Flowing Through a Vertical Passage of Annular Cross Section: Part 2. *Chemical Engineering Research and Design,* 80**,** 246-251.

WYGNANSKI, I., KATZ, Y. & HOREV, E. 1992. On the applicability of various scaling laws to the turbulent wall jet. *Journal of Fluid Mechanics,* 234**,** 669-690.

XUAN, Y. & LI, Q. 2003. Investigation on convective heat transfer and flow features of nanofluids. *Journal of Heat Transfer,* 125**,** 151-155.

Y.YANG, Z. G. Z., E.A.GRULKE,W.B.ANDERSON,G.WU, 2005. Heat transfer properties of nanoparticle-in-fluid dispersions (nanofluids) in laminar flow. *Int.J. Heat Mass Transfer,* 48**,** 1107-1116.

YAKHOT, V., ORSZAG, S.A., THANGAM, S., GATSKI, T.B., SPEZIALE, & C.G. 1992. Development of turbulence models for shearflows by a double expansion technique. *Physics of Fluids A4***,** 1510–1520.

YAMAMOTO, H., SEKI, N. & FUKUSAKO, S. 1979. Forced Convection Heat Transfer on Heated Bottom Surface of a Cavity. *Journal of Heat Transfer,* 101**,** 475-479.

YANG, X. D., MA, H. Y. & HUANG, Y. N. 2005. Prediction of homogeneous shear flow and a backward-facing step flow with some linear and non-linear K–ε turbulence models. *Communications in Nonlinear Science and Numerical Simulation,* 10**,** 315-328.

YıLMAZ, I. L. & ÖZTOP, H. F. 2006. Turbulence forced convection heat transfer over double forward facing step flow. *International Communications in Heat and Mass Transfer,* 33**,** 508-517.

ZEINALI HERIS, S., ETEMAD, S. G. & NASR ESFAHANY, M. 2006. Experimental investigation of oxide nanofluids laminar flow convective heat transfer. *International Communications in Heat and Mass Transfer,* 33**,** 529-535.

ZEINALI HERIS, S., NASR ESFAHANY, M. & ETEMAD, S. G. 2007. Experimental investigation of convective heat transfer of Al2O3/water nanofluid in circular tube. *International Journal of Heat and Fluid Flow,* 28**,** 203-210.

ZHANG, Z., & KLEINSTREUER, C. 2003. Low-Reynolds-Number Turbulent Flows in Locally Constricted Conduits : A Comparison Study Introduction. *AIAA Journal,* 41(5)**,** 831-840.

Appendices

Temperature (K)

D/x	Re=17050 (Exp.)	Re=17050	Re=30720	Re=39992	Re=44545
0.196721	383	398.625	361.007	349.036	344.587
0.393443	365	374.627	345.82	336.721	333.349
0.590164	362.1	364.896	339.677	331.743	328.809
0.786885	360.4	358.484	335.631	328.467	325.821
0.983607	359.5	354.071	332.862	326.23	323.783
1.180328		351.366	331.109	324.798	322.473
1.377049	359.1	350.404	330.392	324.185	321.904
1.57377	358	350.666	330.459	324.211	321.918
1.770492		351.665	330.999	324.621	322.284
1.967213	363.1	353.118	331.82	325.258	322.856
2.163934		354.926	332.854	326.064	323.583
2.360656		357.036	334.076	327.022	324.447
2.557377	369.5	359.36	335.457	328.116	325.434
2.754098		361.772	336.911	329.274	326.48
2.95082		364.202	338.376	330.441	327.538
3.147541		366.638	339.846	331.611	328.599
3.344262	373.1	369.083	341.322	332.787	329.666
3.540984		371.547	342.812	333.975	330.745
3.737705		374.025	344.314	335.174	331.833
3.934426		376.507	345.821	336.377	332.925
4.131148		378.98	347.321	337.576	334.014
4.327869		381.43	348.809	338.764	335.092
4.52459	386.3	383.85	350.277	339.938	336.158
4.721311		386.233	351.725	341.095	337.209
4.918033		388.577	353.149	342.233	338.243
5.114754		390.882	354.552	343.354	339.26
5.311475		393.147	355.933	344.457	340.262
5.508197		395.376	357.294	345.544	341.249
5.704918		397.568	358.636	346.616	342.223
5.901639	395.1	399.725	359.961	347.676	343.185
6.098361		401.849	361.27	348.723	344.136
6.295082		403.939	362.564	349.76	345.078
6.491803		405.997	363.843	350.786	346.01
6.688525		408.022	365.107	351.802	346.934
6.885246		410.014	366.357	352.807	347.849
7.081967		411.974	367.591	353.803	348.754
7.278689	398.5	413.899	368.811	354.788	349.651

Nusselt number

D/x	Re=17050 (Exp.)	Re=17050	Re=30720	Re=39992	Re=44545
0.196721	1398.666667	1003.528	1610.532	1998.761	2194.733
0.393443	1998.095238	1407.416	2273.023	2828.351	3108.263
0.590164	2146.29156	1681.898	2726.712	3398.534	3736.587
0.786885	2243.850267	1929.905	3139.426	3918.383	4309.999
0.983607	2299.178082	2147.885	3502.212	4375.391	4813.859
1.180328		2307.65	3778.648	4728.42	5204.987
1.377049	2324.65374	2370.354	3904.709	4897.578	5395.397
1.57377	2397.714286	2352.941	3892.574	4890.158	5390.545
1.770492		2288.831	3797.457	4776.051	5266.725
1.967213	2092.76808	2201.585	3661.431	4608.963	5084.212
2.163934		2101.888	3503.381	4413.59	4869.727
2.360656		1996.384	3333.333	4201.883	4637.233
2.557377	1804.731183	1891.794	3159.995	3983.67	4397.401
2.754098		1794.236	2995.966	3776.098	4168.902
2.95082		1705.622	2847.062	3587.705	3960.732
3.147541		1625.16	2711.821	3416.799	3771.855
3.344262	1675.0499	1551.689	2588.366	3260.675	3599.245
3.540984		1484.075	2474.64	3116.806	3440.049
3.737705	1525.818182	1421.77	2369.684	2983.928	3293.176
3.934426		1364.398	2272.961	2861.527	3157.855
4.131148		1311.66	2184.222	2749.132	3033.545
4.327869		1263.285	2102.784	2646.15	2919.769
4.52459	1325.750395	1218.882	2028.18	2551.691	2815.352
4.721311		1178.106	1959.603	2464.973	2719.466
4.918033		1140.574	1896.54	2385.243	2631.298
5.114754		1105.928	1838.255	2311.591	2549.985
5.311475		1073.874	1784.279	2243.43	2474.64
5.508197		1044.093	1734.099	2180.08	2404.653
5.704918		1016.374	1687.309	2121.013	2339.364
5.901639	1163.938974	990.4987	1643.524	2065.672	2278.268
6.098361		966.2748	1602.444	2013.774	2220.928
6.295082		943.5681	1563.804	1964.879	2166.908
6.491803		922.2282	1527.401	1918.785	2115.986
6.688525		902.1522	1493.052	1875.223	2067.81
6.885246		883.2383	1460.571	1834.036	2022.217
7.081967		865.3866	1429.861	1794.965	1979.059
7.278689	1111.523179	848.5425	1400.744	1757.929	1938.061

Nu/Nu_d

D/x	Re=17050 (Exp.)	Re=17050	Re=30720	Re=39992	Re=44545
0.196721	20.5222524	14.72449	14.50104	14.69188	14.84538
0.393443	29.31750342	20.65063	20.46602	20.78977	21.02459
0.590164	31.49194741	24.67803	24.55098	24.9809	25.27463
0.786885	32.92339957	28.31697	28.26702	28.80205	29.15325
0.983607	33.73520942	31.51532	31.5335	32.16128	32.5614
1.180328		33.85952	34.0225	34.75622	35.20703
1.377049	34.10900675	34.77955	35.15753	35.99961	36.49498
1.57377	35.18100411	34.52406	35.04827	35.94507	36.46216
1.770492		33.58339	34.19185	35.10633	35.62464
1.967213	30.70661207	32.30325	32.96709	33.87815	34.3901
2.163934		30.84043	31.54403	32.44206	32.9393
2.360656		29.2924	30.01293	30.88591	31.36669
2.557377	26.48032567	27.75778	28.45222	29.28194	29.74444
2.754098		26.32633	26.97532	27.75618	28.19885
2.95082		25.02612	25.63461	26.3714	26.79078
3.147541		23.84552	24.41691	25.11516	25.51319
3.344262	24.57754778	22.76751	23.30534	23.96757	24.34564
3.540984		21.77543	22.28136	22.91006	23.26882
3.737705	22.38791171	20.86125	21.33635	21.93335	22.27536
3.934426		20.01943	20.46547	21.03363	21.36004
4.131148		19.24563	19.66647	20.20748	20.51919
4.327869		18.53583	18.93321	19.45051	19.7496
4.52459	19.45237194	17.88432	18.26149	18.75618	19.04331
4.721311		17.28602	17.64403	18.11877	18.39473
4.918033		16.73533	17.07622	17.53271	17.79836
5.114754		16.22697	16.55142	16.99133	17.24834
5.311475		15.75665	16.06544	16.49032	16.7387
5.508197		15.31969	15.61362	16.02466	16.26531
5.704918		14.91298	15.19233	15.59049	15.82368
5.901639	17.07815733	14.53332	14.7981	15.18371	15.41042
6.098361		14.17789	14.42822	14.80223	15.02257
6.295082		13.84472	14.08031	14.44283	14.65717
6.491803		13.5316	13.75254	14.10402	14.31273
6.688525		13.23703	13.44327	13.78382	13.98687
6.885246		12.95951	13.1508	13.48107	13.67847
7.081967		12.69758	12.8743	13.19388	13.38654
7.278689	16.30907475	12.45043	12.61214	12.92164	13.10923

Backward Facing Step Test Rig

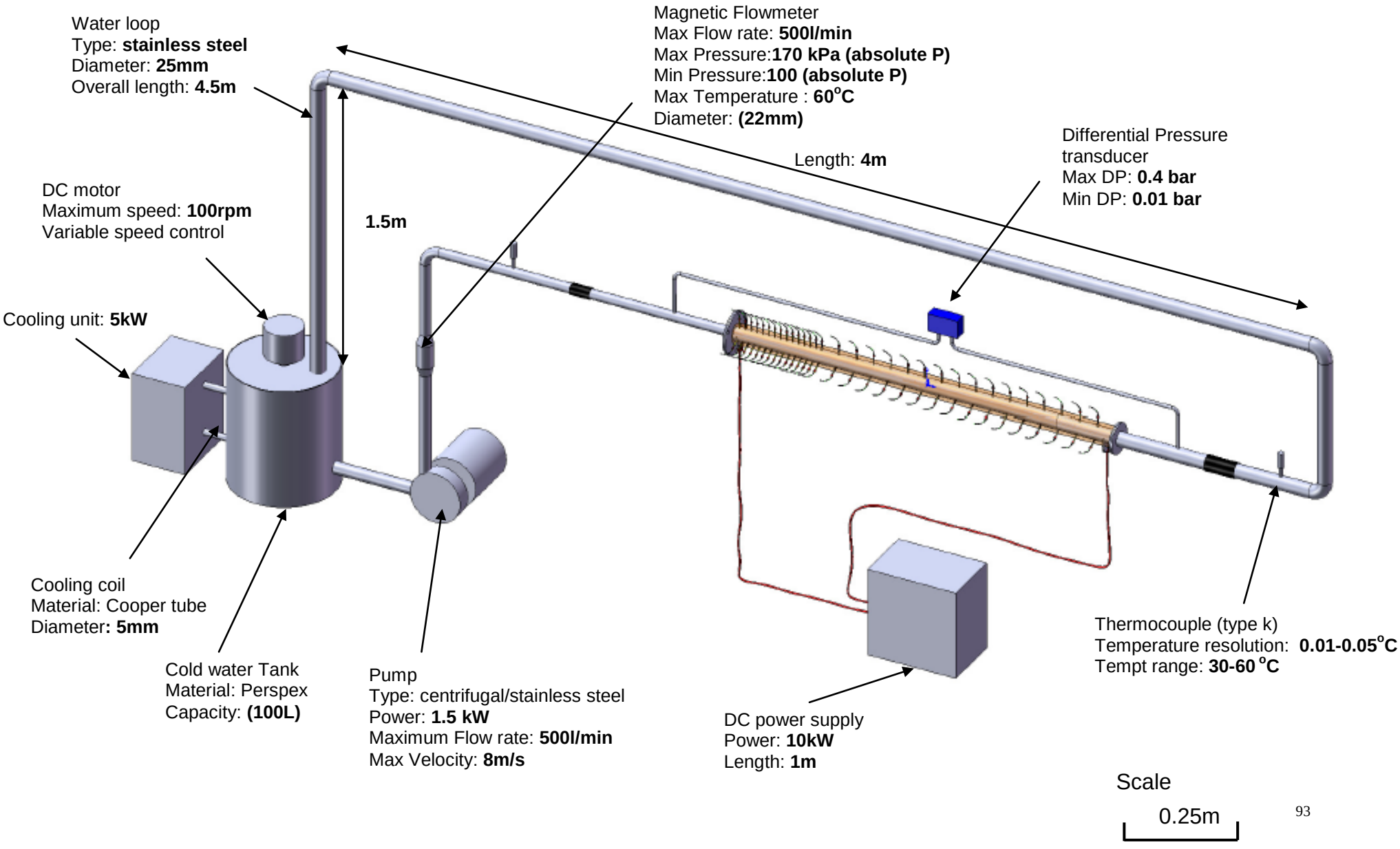

Test section

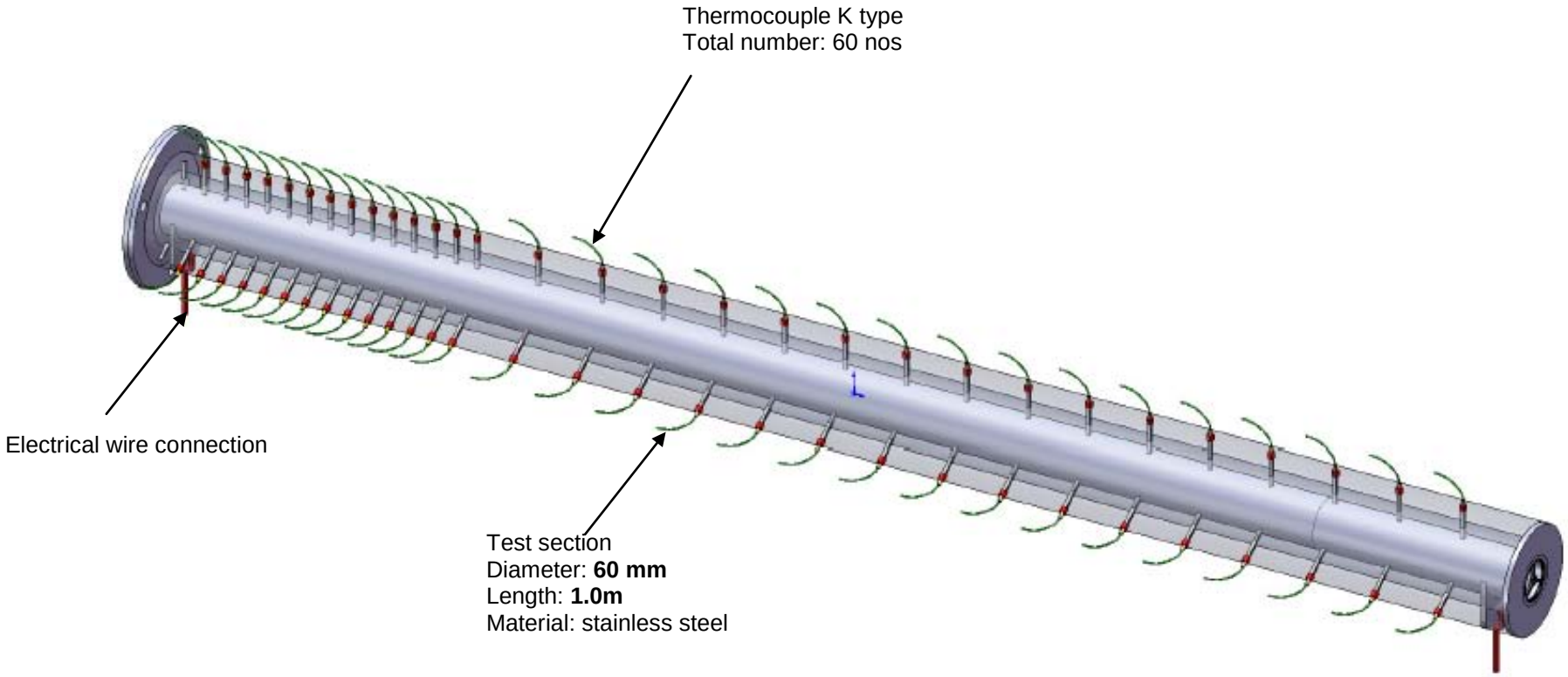

Section length: 10mm
Number of thermocouples: 30
Interval between thermocouples: 3mm
Type: k
Thermocouple Diameter: <0.5mm
Thermocouple length: 1m
Mounting type: welded with epoxy

Section length: 70mm
Number of thermocouples: 10
Interval between thermocouples: 3mm
Type: k
Thermocouple Diameter: <0.5mm
Thermocouple length: 1m
Mounting type: welded with epoxy

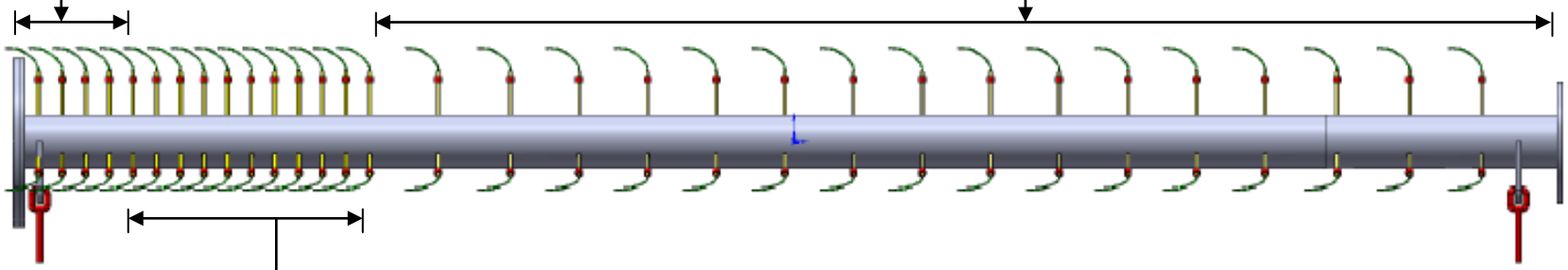

Section length: 20mm
Number of thermocouples: 20
Interval between thermocouples: 3mm
Type: k
Thermocouple Diameter: <0.5mm
Thermocouple length: 1m
Mounting type: welded with epoxy

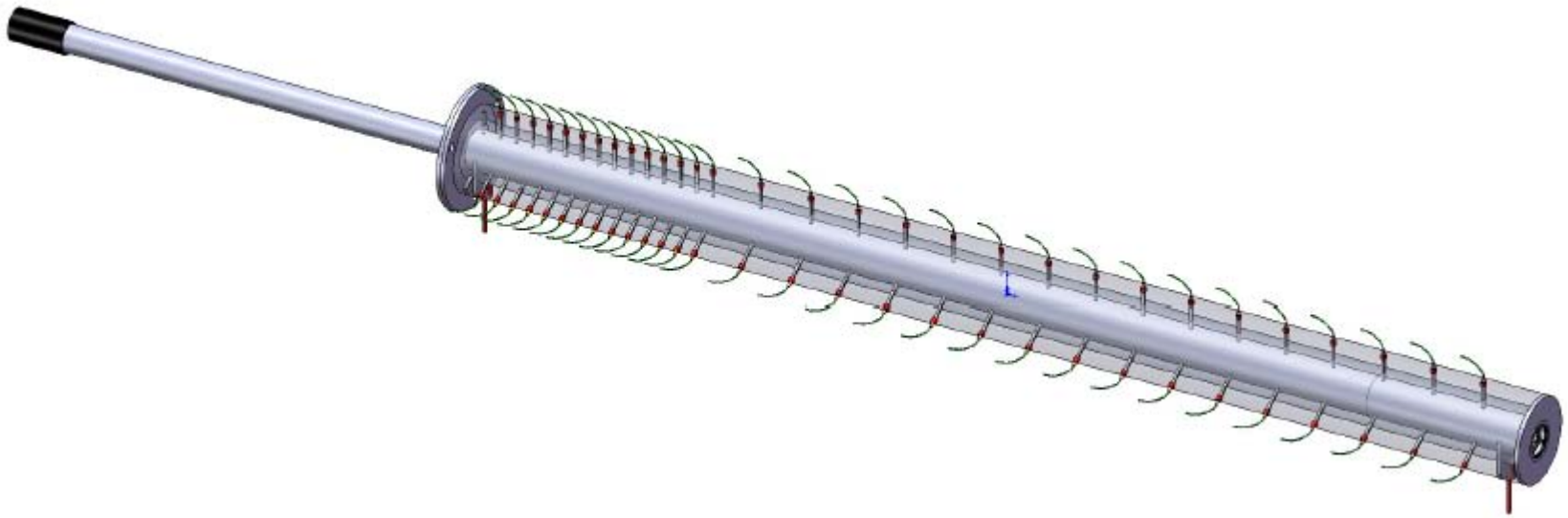

Backward facing step heat exchanger (2D diagram)

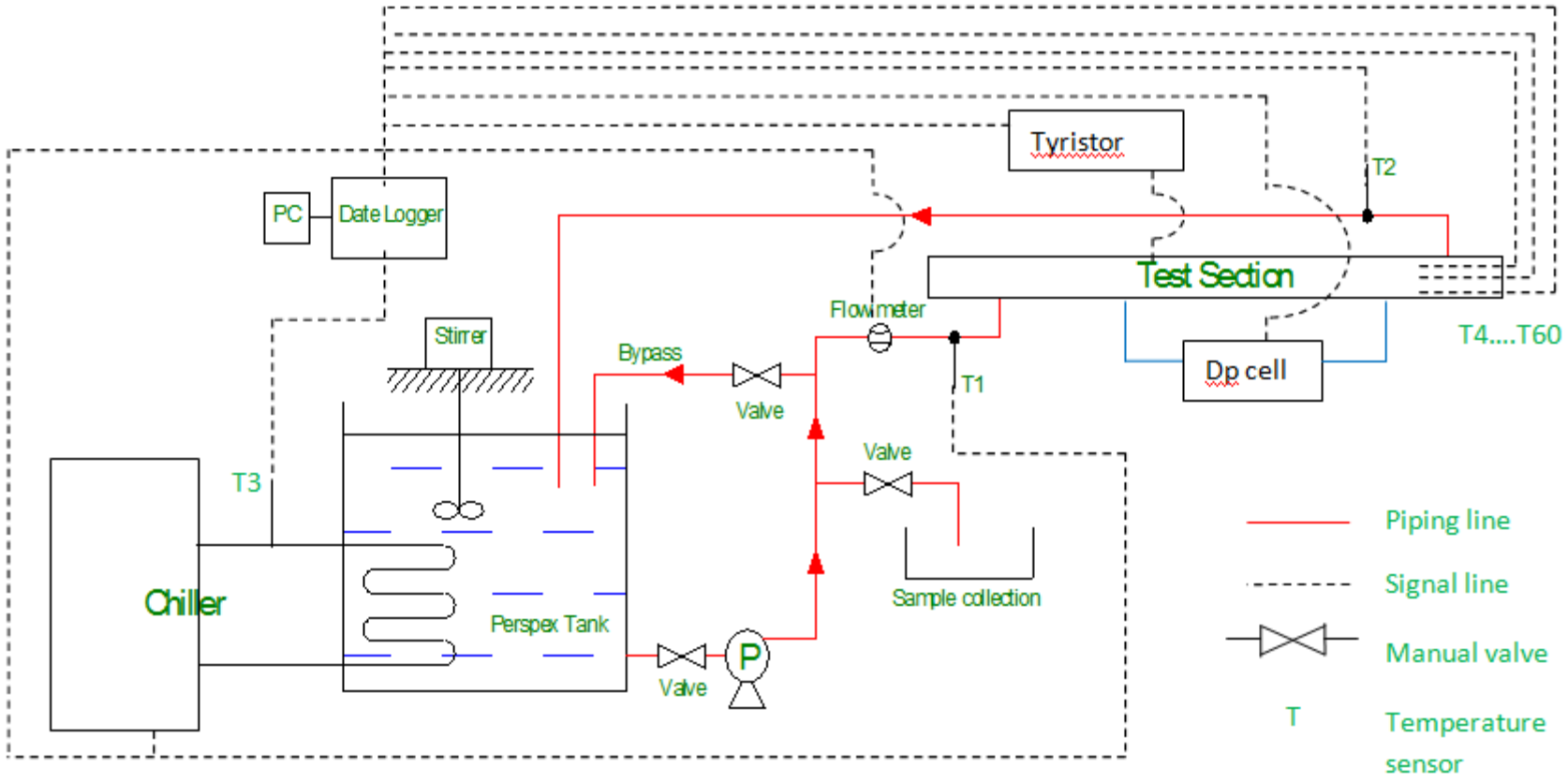

Specification

1. Liquid will be pumped to the piping line which will enter the test section and return back to the tank
2. Tank (100L in size) will be made out of Perspex or non corrosive material
3. Pump power rating (1.5kW)
4. Network pipe is 22mm in diameter
5. All signals from Dp cell, Flowmeter, pump rotation, temperature sensor, and tyristor will be sent to data logger and processor for further data manipulation
6. Heater power will be controlled by the tyristor which received output signal from the Data processing unit (DAQ)
7. Pump speed will be controlled by inverter which operate based on flowmeter signal connected to the DAQ
8. The chiller will receive temperature from the inlet line (T1) instead from the tank. The refrigerant temperature of the chiller will be automatically adjusted (by hunting method or any equivalent technique) to meet the line temperature
9. The chiller must have the capability to control the line temperature (T3) on top of the chiller line temperature (T3)
10. Three temperature sensor are attached to the rod heater which will be sent to the data logger for averaging
11. This average temperature will serve as the reference for the heater power to control the amount of power input.